Master Thesis

Degree Project in
Geology 30 hp

A 3-dimensional tectonic model of the Naxos metamorphic core complex, Greece

Henrik Linnros

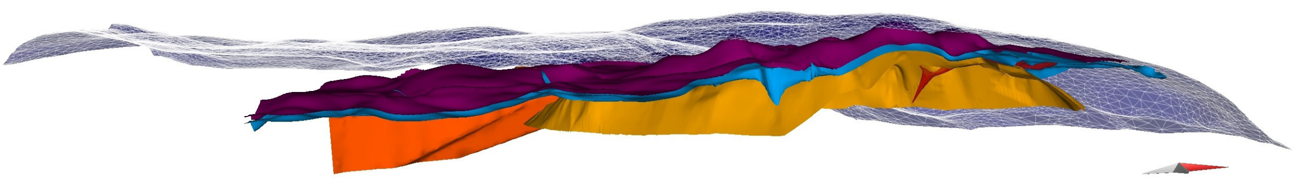

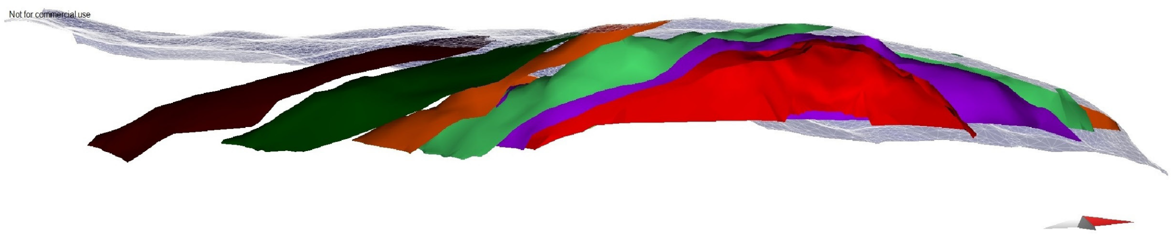

Stockholm 2016

Department of Geological Sciences
Stockholm University
SE-106 91 Stockholm
Sweden

A 3-dimensional tectonic model of the Naxos metamorphic core complex, Greece

Henrik Linnros

Abstract

3D Modeling of the island of Naxos was undertaken with data from published and own sources. A simplified, geometrically correct and geologically feasible 3D structural model of the island was produced. Special emphasis was put on constraining the geometry of the Naxos/Paros detachment, which is only sparingly exposed in the east and west, and its relation to documented metamorphic boundaries in three dimensions. N-S regional extension is estimated to ~35% and local extension associated with the Naxos/Paros detachment is calculated to ~83%, implying a local E-W shortening of ~45% is needed to maintain constant crustal volume. Regionally this E-W shortening is estimated to ~26%. From the 3D model, late E-W shortening contemporaneous with the N-S extension in the Miocene was calculated to be ~7-10%. The results show that the magnitude of E-W shortening since the early Miocene is not enough to explain the current crustal thickness. An argument for localized extension correlating with the Naxos MCC and a heterogeneous N-S stretching of the lithosphere is made on account of the extension/shortening calculated, implied mass imbalance, Moho topography and similarities with the Basin and Range province. Geometric relationships between the detachment and metamorphic isograds are presented in 2- and 3D and an attempt was made to identify and quantify fault displacement in the field to constrain the model. Possible duplexes, related to the early subduction stage and high-pressure metamorphism, were also found on the southeast coast of the island.

Sammanfattning på svenska

En geometriskt korrekt och geologiskt trovärdig 3D modell av ön Naxos berggrund gjordes utifrån egna och redan publicerade data. Det spatiala förhållandet mellan rekonstruerade geologiska strukturer såsom Naxos/Paros förkastningen, metamorf isograd och öns metamorfa komplex avgränsades i möjligaste mån. I fält gjordes försök att kvantifiera förkastningsförflyttning i syfte att förbättra modellens relevans. Med hjälp av 3D modellen uppskattades en öst- västlig veckningsförkortning på ~7-10% associerad med den nord- sydliga regionala extensionsfasen i miocen (D_2) som häri uppskattas ha sträckt Kykladerna med en faktor av ~1.35 och mer lokalt ~1.83. Antas en konstant volym för jordskorpan bör den regionala öst- västliga förkortningen således uppgå till ~26%. Dessa resultat är inte förenliga med antagandet att öst- västlig förkortning ska ha balanserat förtunning av jordskorpan i samband med ovan nämnda extensionsfas. En heterogen extensionsmodell med avseende på den Kykladiska litosfären diskuteras utifrån resultaten. Möjliga duplexstrukturer härrörande från den i kritperioden begynnande regionala subduktionsfasen (D_1) tros även ha hittats på öns sydostkust.

Keywords: 3D Modeling, Detachment faulting, MCC, Structural Geology, Naxos, Cyclades.

Table of contents

Front page. S-N profiles of the principal 3D layers of the model as seen from the east. **Top:** Reconstructed detachment surface (polygonised blue) draping over the marble (purple), schist (light blue), migmatite core (yellow), granodiorite (orange) and S-type granite (red). All horizons are extended above the topography (not shown). **Bottom:** Detachment surface (polygonised blue) cuts the reconstructed metamorphic isograds. Isograd layers are: +Corundum (brown), +Biotite (green), -Chloritoid (orange), +Sillimanite (turquoise), -Kyanite (purple) and +Melt (red). Scale is ~43x6 km, note compasses in bottom right of each model.

1. Introduction

The geology on Naxos has been intensively studied, mainly due to its metamorphic core complex (MCC) that has a textbook style migmatite dome in the center (eg. Jansen 1973, Jansen & Schuiling 1976, Lister et al. 1984). The MCC was exhumed in part by a Cycladic-wide detachment fault system (Gautier et al. 1993, Avigad 1998, Jolivet et al. 2010b), the Naxos/Paros detachment fault is exposed north of Moutsounas on the east coast, in a synclinal structure to the west of the migmatite dome and again along the westernmost tip of the island (fig. 1b). The detachment is thought to dome over the island in a north dipping arc, closely curve with the north coast and run parallel to the coast in the east (eg. Jansen & Schuiling 1976, Jansen 1977, Keay et al. 2001).

In constructing geological 3D models one can gain insight beyond what is otherwise possible of how geometric features may behave at depth. Given correct assumptions, such modeling can also extend metamorphic- and fault related boundaries in spherical space. Today little is known about the E-W shortening component believed to be synkinematic with the extensional event forming the Naxos/Paros detachment in the Miocene.

Avigad et al. (2001) concluded that E-W folding, alternating and/or coeval with the Miocene extension, somehow balanced crustal thinning. It was argued that either crust was fed from the elevated regions in the east and west or that the Aegean plate was squeezed between east- west converging plates, producing no net crustal thinning. This stands in contrast to the results in this work and the crustal thickness since early Miocene will be discussed in light of this.

1.1. Purpose of study

A true 3D model of the island of Naxos has not yet been published and stands to enhance the understanding of the interplay between N-S extension and E-W shortening as well as the architecture of the metamorphic zone boundaries with respect to the Naxos/Paros detachment. Hopefully, such a model could also be used in pinpointing the structural position and relation of rock samples gathered on the island. The underlying purpose of this work is for the author to gain proficiency with the Midland Valley software suite MOVE, construct and test a 3D model, estimate regional shortening and if possible, further the understanding of geological structures in the area with an emphasis on the detachment fault geometry.

2. Geological setting and tectonic evolution

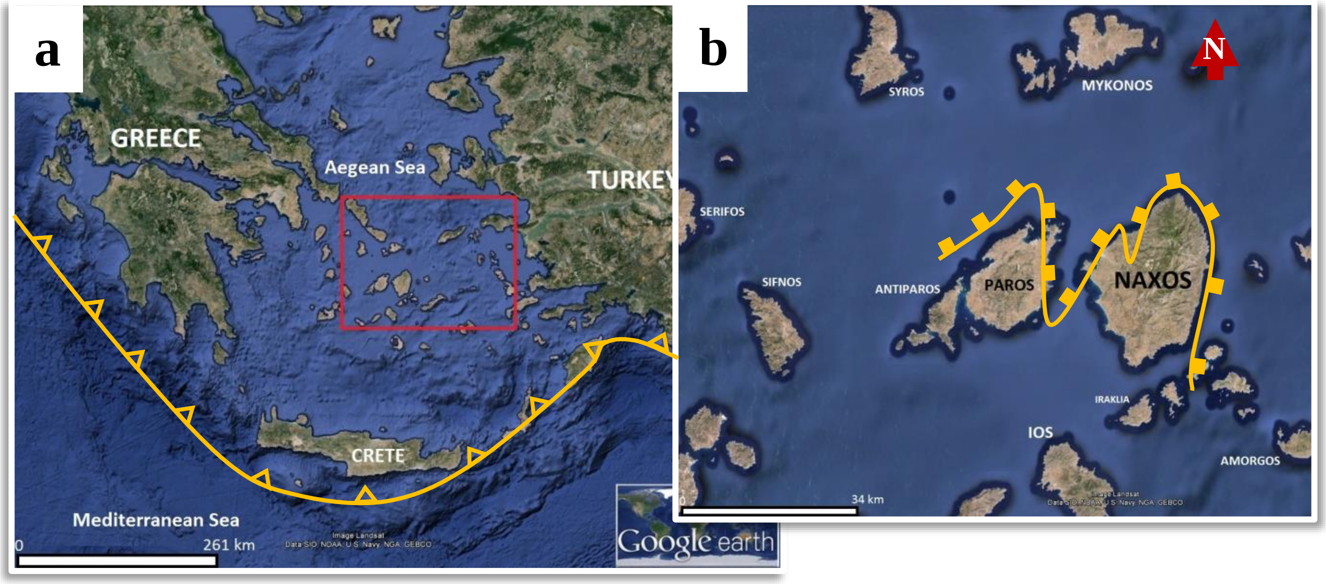

Figure 1a. Regional satellite image of the Aegean showing the Hellenic trench in yellow, subduction zone geometry is from Zhu et al. (2006). The Cyclades are boxed in red. **1b.** Satellite image of Naxos and its closest neighboring islands in the Cyclades showing the Naxos/Paros detachment in yellow, detachment geometry from Phillipon et al. (2012). Both figures were modified from images procured in Google Earth, scale in bottom left corners.

Naxos is the largest island in the Cycladic archipelago (Fig. 1a) in the Aegean Sea between Greece and Turkey. An area host to magmatic arcs and high pressure metamorphism tell of ~60 million years of southwardly retreating subduction (Ring & Layer 2003, Ring et al. 2010). The Attic-Cycladic massif (Dürr et al. 1978) is thought to be part of a fore arc accretionary system (Ring et al. 1999, Ring & Layer 2003, Huet et al. 2009, Jolivet et al. 2010) that formed in the Cenozoic as the Pindos oceanic unit was partly subducted underneath Eurasia, fused to the Aegean plate in an 'Alpine compressional phase' (Urai et al. 1990) that began in the Cretaceous (Keay et al. 2001).

This subduction gave rise to N-S folding (D_1) and HP-LT metamorphism in the subducting slab (M_1) in the Eocene (Dürr et al. 1978, Wijbrans & McDougall 1988, Buick 1990, Avigad 1998). It is believed that regionally, accretionary thrusts are responsible for the formation of the Cycladic blueschists (Ring et al. 1999, Ring & Layer 2003, Ring et al. 2003, Philippon et al. 2012). These rocks can be seen on southeastern Naxos where retrograde metamorphism associated with the Miocene M_2 event has not occurred (Avigad 1998).

Extension is thought to have commenced around 20 Ma (Lister et al. 1984, Gautier & Brun 1994), initiated due to slab retreat (Buick 1990). Increased slab pull due to subducted lithosphere draping over the 660km deep phase change discontinuity taken together with the relative increase to subduction rate as plate convergence between Africa and Eurasia was reduced (Schellart 2005, Ring et al. 2010 and sources therein) are considered major initiating factors. As the subduction zone migrated south, the Attic Cycladic massif experienced N-S extension (D_2) from 23-8 Ma with associated E-W shortening (Urai et al. 1990, Avigad et al. 2001, Jolivet et al. 2004, Brichau et al. 2006, Bolhar et al. 2010, Kruckenberg et al. 2011).

Extension caused regional detachment faulting (eg. Brun et al. 1994, Gautier & Brun 1994) and Cordilleran type core complexes (Lister et al. 1984, Avigad 1998, Keay et al. 2001) rose as thinning of the crust caused an increase in the geothermal gradient. On Naxos, partial melts concentrated in isoclinal fold hinges suggest that deformation and migmatization was simultaneously ongoing in the MCC (Gautier et al. 1993, Kruckenberg et al. 2010, 2011).

This Barrovian (MP-HT) metamorphic event (M_2), first proposed by Jansen & Schuiling (1976) reached upper amphibolite facies with partial anatexis in the Naxos dome culminating at ~16 Ma (Wijbrans & McDougall 1988, Buick 1990, Avigad 1998, Keay et al. 2001, Duchêne et al. 2006). Arc magmatism was active in the Cyclades between ~17-11 Ma (Bolhar et al. 2010) and the western part of Naxos was intruded by a granodiorite batholith at ~13-12 Ma (Wijbrans & McDougall 1988, Keay et al. 2001, Bolhar 2010). The metamorphic isograds on Naxos, described by Jansen & Schuiling (1976), froze somewhere after peak M_2 on Naxos and before the intrusion of the granodiorite (Uwe Ring pers. comm) as there is a contact metamorphic overprint in country rock M_2 assemblages from the intrusion (Jansen & Schuiling 1976). ^{40}Ar–^{39}Ar ages by Wijbrans & McDougall (1988) indicate the metamorphic isograds have been static since ~15 Ma.

Systematic fission-track thermochronology and thermal modeling by Brichau et al. (2006) have shown a slip rate of ~6-8 km/My at the Naxos/Paros detachment fault with no apparent change in slip rate through the ductile/brittle transition, aided in part by thermal softening due to the presence of arc magmatism. Movement of the detachment fault is thus believed to be no less than ~50km between ~16- to 8 Ma (Brichau et al. 2006). These results were however questioned by Seward et al. (2009), who proposed that a more complex exhumation process made the sampling criteria used inappropriate. Pseudotachylites in the granodiorite associated with extensional shearing have been dated as 9.9 Ma (Andriessen et al. 1979), setting the maximum age for the cessation of extension on Naxos.

Tectonic unroofing, aided by isostatic disequilibrium (Kruckenberg et al. 2010) exhumed the Migmatitic Core Complexes of the Aegean to the surface at ~3 Ma, since migmatitic rocks are found in upper Pliocene conglomerates in the region (Jansen 1977) or ~8 Ma according to Keay et al. (2001). Close to the Moutsounas detachment, which is the part of the Naxos/Paros detachment exposed on the east coast of Naxos, the sediments dip at an angle to the detachment fault (fig. 2b). Buick (1990) also noted that the transport direction of the tectono-sedimentary units is the same as what has been determined from mylonitic fabrics in the metamorphic pile.

Southward retreat of the magmatic arc have been estimated at ~20 km/My since ~38 Ma (Ring et al. 2010 and sources therein) and today the African plate subducts beneath the Aegean plate in a NW-SE arc underneath Crete (fig. 1a) as can be seen in Bouguer anomaly imaging (eg. Tirel et al. 2004). As a result arc magmatism is presently active south of the Cyclades.

3. Rock description

Naxos lithologically consists of three distinct units: The Metamorphic Core Complex, where a leucogneissic migmatite core is mantled by meta-sediments of platform carbonate- and pelitic marine sediment protoliths; a post-metamorphic granodiorite pluton and sediments deposited from early Miocene to recent above the Naxos detachment (Jolivet et al. 2004 and references therein). The mantling metasediments are believed to be ~7 km thick (Jansen 1977, Avigad 1998), while the migmatite core is thought to be ~4 km thick (Buick 1990) with an S-type granitic origin (Keary et al.

2001). Coevally emplaced, a large N-S trending S-type granitic body is found on the northwest island. This S-type granite is probably fractionation melt related to the migmatite (Johannes Glodny pers comm.) and show structural contacts with surrounding rocks to this effect (Gautier et al. 1993 and sources therein).

3.1. Conglomerates

Deposition has been characterized as syntectonic and was ongoing from early Miocene (Aquitanian) to early Pliocene (Gautier et al. 1993, Jolivet et al. 2010). In the west of the island, north of the granodiorite, conglomerates are clast supported with sub-angular to rounded clasts ranging from 10 cm to 1.5 m in size consisting of all lithologies present on the island (fig. 2a). The conglomerates show signs of brittle deformation and grade into unconsolidated finer grained, clayey, matrix-supported sediments. On the east- (fig. 2b), southeast- and southwest side of the island the conglomerates are poorly to well lithified, sandy, matrix-supported and bear sharp to rounded mainly marble clasts of homogenous sizes with a preferred orientation. The more poorly lithified of these younger sediments exhibit crossbedding in the southeast.

Figure 2a: Conglomerates close to the granodiorite in the west, located in the detachment hanging wall. Hammer for scale. **2b:** Conglomerates at an angle (dashed red lines) toward the E-dipping Moutsounas detachment fault (west of the arrow, attitude indicated by the dashed black line), on the east coast of Naxos.

3.2. Granodiorite

A coarse- to medium grained, almost plagioclase porphyric granodiorite (fig. 3) with preferred mineral lineation, cataclasites, shearing and brittle faulting present.

Figure 3. Granodiorite with a cataclasitc zone and crosscutting quartz veins, pen for scale.

3.3. Marble

Massive marble of varying purity is a conspicuous presence on Naxos. There are a number of quarries, all located in N-S trending synforms, where huge sections can be seen in unweathered condition (Fig. 4). The marble is coarse grained near the migmatite with grain size generally decreasing with decreasing metamorphic grade (Urai et al. 1990). Impurities range from intensely folded or boudinaged laminae to layers meters across. Dürr et al. (1978) described the presence of Triassic algae in these marbles. Thinner horizons have been observed interbedded with schist and vice versa. In the center of the migmatitic dome and on its northeastern side marble and migmatite are in direct contact.

Figure 4. Subvertical, N-S striking intensely folded marble at a quarry in the central dome area. Note the truck (bottom right) for scale.

3.4. Schist

Metasediments of pelitic marine origin (Gautier et al. 1993) range from low greenschist facies (fig. 5a) in the east and west to amphibolite facies toward the contact with the migmatite (fig. 5b). All schists have increasing amounts of garnet closer to the dome and biotite in some horizons in the very north, where large kyanite crystals are abundant. The schist is missing from the sequence at the contact with the migmatite in the northeast. Migmatized leucogneiss (fig. 6a) with pelites and marble rafts (Jansen 1977). The migmatite grades in texture from fine-grained foliated at the west contact with the mantling rocks to wispy flow patterns in biotite where anatexis has affected the rock in the central dome (fig. 6b). Transition from ductile to brittle deformation has resulted in mylonitic shear zones (Buick 1990, Urai et al. 1990, Gautier et al. 1993) sometimes mesoscopically visible trending N-S.

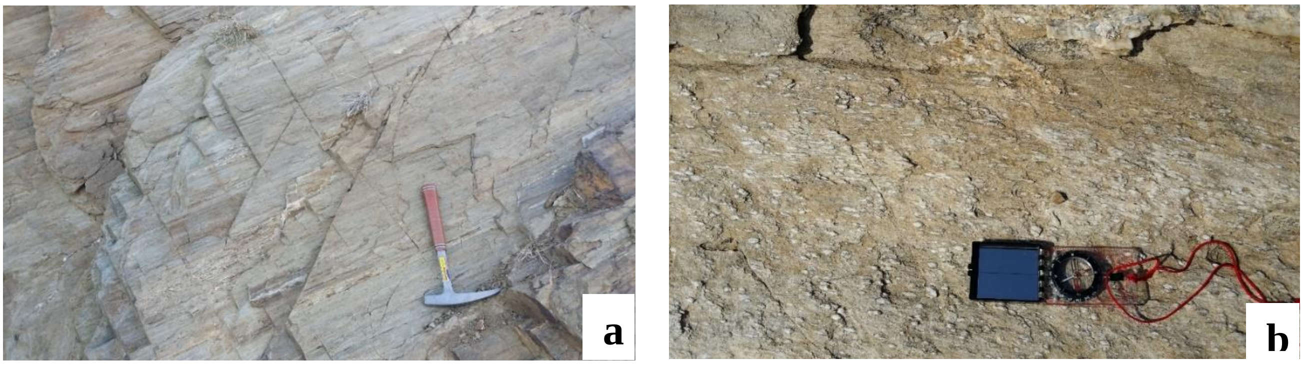

Figure 5a: Greenschist facies mica schist in road cut on the northwestern coast of Naxos, hammer for scale. **5b:** Kyanite bearing amphibolite on the northern tip of the island, compass for scale.

3.5. Migmatite

Migmatized leucogneiss (fig. 6a) with pelites and marble rafts (Jansen 1977). The migmatite grades in texture from fine-grained foliated at the west contact with the mantling rocks to wispy flow patterns in biotite where anatexis has affected the rock in the central dome (fig. 6b). Transition from a ductile to brittle deformation has resulted in mylonitic shear zones (Buick 1990, Urai et al. 1990, Gautier et al. 1993) sometimes mesoscopically visible trending N-S.

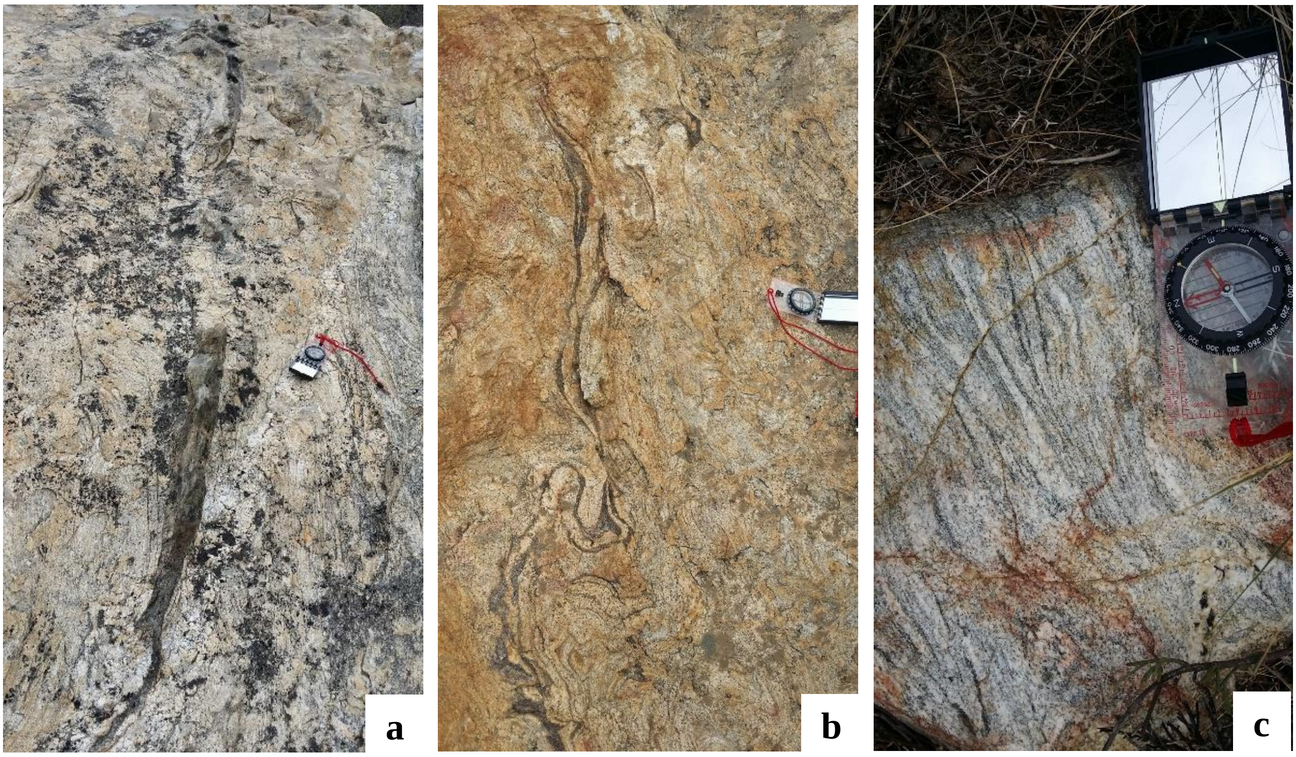

Figure 6. Migamtites from the southernmost subdome. **6a**: N-S trending boudinaged raft. **6b**: flow patterns in biotite. **6c**: unweathered surface. Note compasses for scale.

3.6. S-type Granite

Granitoid body (Jansen & Schuiling 1976) with microstructural indications of subsolidus deformation at high temperatures (Urai et al. 1990 and sources therein) found mainly on the northwestern side of the migmatitic dome. Granitic dykes crosscut the mantling metamorphics containing large plagioclase crystals with no mesoscopic sign of internal deformation (fig. 7). Some ductile deformation in metasediments at contact surfaces and brittle faulting can be seen.

Figure 7. Granitic dike with large grained plagioclase, brittle deformation crosscutting both the dike and surrounding schist. Hammer for scale.

4. Methods and software

4.1. Digitization of data and 2D sections

Dip data from existing geological maps, structural studies (eg. Jansen & Schuiling 1976, Jansen 1977, Urai et al. 1990, Kruckenberg et al. 2010, 2011) and own field mapping were digitized in Midland Valleys software suite MOVE and projected on a Digital Elevation Model (DEM) obtained from USGS. Section construction was done with dip data projected onto the section within a 150-200 meter lateral limit. In the migmatite dome this limit was set to 50-100 meter taking into account the relative abundance of data. Surface intersections were mainly based on the geological map in Cao et al. (2013), an adaptation of the Jansen & Schuiling (1976) map. The higher resolution of other maps (eg. Vanderhaeghe 2004, Kruckenberg et al. 2010, 2011) was deemed too complicated for consistent modeling without extensive additional surface- and/or drill core data. All geological maps and satellite images were georeferenced with the Global Mapper software.

Vertical images aiding in section construction were digitized from Kruckenberg et al. (2011) and Cao et al. (2013). Both works were influenced by Vanderhaeghe (2004) and Siebenaller (2008). Vertical images were adhered to where geometrically sound and not conflicting with dip-, horizon data or the surface trace generated by the DEM. The horizon data in Kruckenberg et al. (2010, 2011) was occasionally cross-referenced since these maps differ from those of other authors and most of the sections were based on interpretations therein. The metamorphic pile was laterally constrained by the detachment zone to the north and east as well as the granodiorite intrusion in the west. The presence of meta-limestone and meta-sediment sequences indicate a contrast in rock competence. Based on this a constant bed length and bed thickness as well as layer parallel slip were assumed in the section balancing (eg. Ramsay & Huber 1987, Allmendiger et al. 2013). The sections were not oriented parallel to the stretching lineation, influencing the balancing equations. The D_2 syntectonic to recent conglomerates were not modeled as the later sediments were deemed unnecessary for the objectives of this work and the model resolution did not allow differentiation between early and late sediments.

Two distinctly different interpretations of the mantling sequences folding geometry arose from the data available on the eastern side of the migmatite dome, both geometrically possible (appendix 1-2). Previously, no west verging thrusts have been described on Naxos but judging from the structural pattern on the geological map (eg. Cao et al. 2013) it was not an impossible prospect. Further analysis in the field was required to eliminate one of the interpretations before 3D modeling could commence. Sections A-‘A and C-‘C were shortened in the west (appendix 3) to where the W-dipping detachment plane is separating the mantling rocks from the granodiorite, in the N-S trending synclinal structure of the detachment surface. This synclinal structure will henceforth be called ‘the detachment syncline’. This was done before balancing as neither the late sediments nor the granodiorite were subjected to the balancing operation, therefore the mantling sequence past this point in sections A-‘A and C-‘C is purely speculative. Figure 8 shows the general workflow of 2D section construction in this work using section B-‘B as a template.

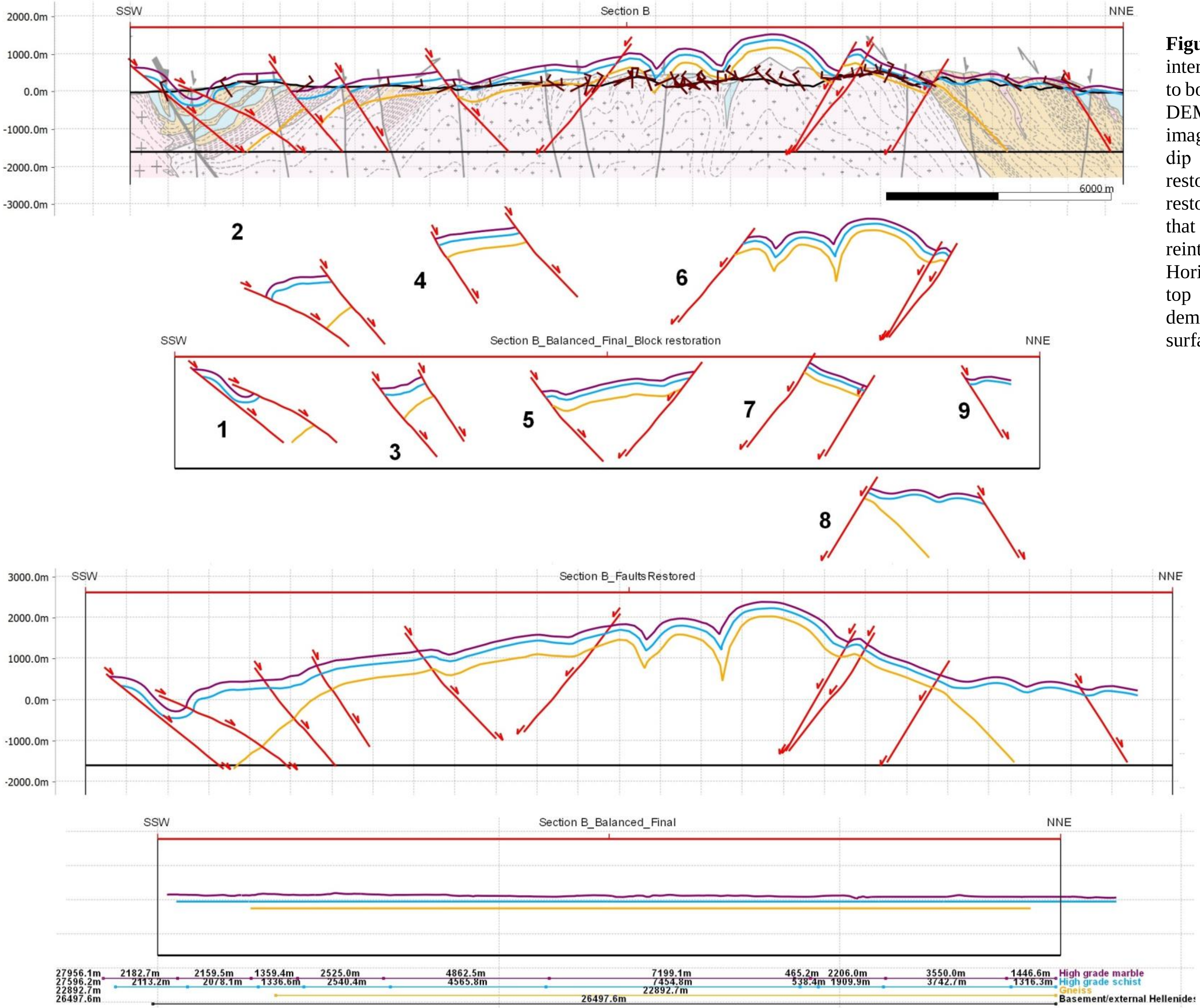

Figure 8. Workflow of 2D profile interpretation in MOVE. From top to bottom; Initial interpretation from DEM surface (black line), vertical images (visual interpretation) and dip data (inclined L's); Block restoration and resulting fault restoration; line length balancing that may or may not result in reinterpretation and reiteration. Horizon data is not shown but the top contact of a layer would be demarcated by an X on the DEM surface in color code.

4.2. Faults

Brittle faults were digitized from the geologic map of Kruckenberg et al. (2010), adapted from the work of Jansen (1973), Vanderhaeghe (2004) and Siebenaller (2008), since it provided the highest resolution and recorded kinematics. Fault interpretations in the vertical images were mostly sub vertical, even the normal faults, sometimes showing opposite sense of shear to what was described in the geological map. This led to the introduction of major normal faults with a generic 60° fault angle in 3D, projected onto the sections as a means of getting probable fault angles. Where no indication of fault surface strike direction was present faults were modeled as vertical, assuming a pure strike slip component. The difficulty in balancing faults with a strike slip component in 2D led to the exemption of faults believed not to have a normal component in the section balancing and the interpretation of no visible displacement on these faults in 2D.

4.3. 3D surfaces

Metamorphic isograds were traced from Jansen & Schuiling (1976) and modified from interpretations in Gautier et al. (1993) drawn from the work of Jansen (1973) and Jansen & Schuiling (1976). Topographic traces were combined with dip data and the general geometry of the migmatite to constrain the 3D construction of the isograds, which extend to 1500 meters below sea level. Tracing of the detachment fault was done from Gautier et al. (1993), Kruckenberg et al. (2010) and Cao et al. (2013) influenced by interpretations in Keay et al. (2001) and Brichau et al. (2006). Dip angles of 30° are reasonable according to the fault slip modeling of Brichau et al. (2006) and a gradual increase to 35° on the northern face of the detachment was modeled in accordance with Gautier et al. (1993), not exceeding their calculated values of ~53° at depth. The Moutsounas shear zone (eastern constraint for the detachment surface) was constructed with a 20° dip after own field data. The 3D detachment surface was edited to follow the structural NNE-SSW trend of the other layers as it drapes in a N-dipping anticline over the MCC. Prof. The detachment surface extends to ~3500 meters below sea level.

The granodiorite was constructed from the surface exposure in Kruckenberg et al. (2010) and its subsurface shape is loosely based on an interpretation in Gautier et al. (1993) constrained only in the east where it cuts the MCC layers with the same plunge as the E-dipping detachment. The intrusive body was interpreted as rootless beneath Naxos, on the grounds of poorly resolved regional gravimetric imaging in Tirel et al. (2004). The Granodiorite was modeled to 3000 meters below sea level. The shape of the S-type granite was inspired by a N-S profile interpretation in Keay et al. (2001) and its surface trace in Cao et al. (2013).

The 3D structural models principal rock layers (migmatite dome, schist and marble) extends no further than 1500 meters below sea-level due to the lack of subsurface data (eg. seismic and bore hole). Adjustments were made to the finished surfaces in order to honor the section lines where applicable and geologically reasonable in three dimensional space. Examination of surface structures and section traces generally produced a N-S trending synform where marble is visible and an antiform where schist is denoted on the map (eg. Cao et al. 2013). Island wide dip data (N = 560) was largely honored. Some measurements, which had been projected onto sections from close to the maximum lateral limit, were sometimes not deemed reliable enough.

All fault surfaces were extended to cut the layers of the model and manually edited for offset. Since the offset is primarily not based on field data but interpreted from the offsets in stratigraphy seen on the geological maps (eg. Kruckenberg et al. 2010, Cao et al. 2013) the net slip of oblique faults is unknown and only the pure dip slip minimum heave can be quantified. Restoring fault displacement in 3D resulted in erroneous geometries while backward-modeling (balancing) and was problematic due to a lack of constraints on the strike slip component. Calculation of E-W shortening was done in Microsoft Excel using the formula below:

$$Extension/shortening\ (\pm\%) = \frac{(L_f - L_0)}{L_0} * 100$$

Where L_f is the deformed, final length of strata and L_0 the initial average line length after fault restoration and unfolding of strata. $L_0 = \frac{(L_m + L_s)}{2}$, where L_m is marble layer length and L_s is schist. Because both schist- and marble horizons are presumed to have been deformed in the same way and have been observed in the field to adhere to this, an average line length for L_0 was used in the calculations. This average should remove some amount of interpretational error. It is important however, to point out that this equation assumes a sedimentary sequence deposited horizontally and deformed within the same kinematic field. Assuming plane-strain and volume-constant deformation, extension/shortening due to differences in crustal thickness is solved using:

$$S\ (shortening) = \left(1 - \frac{C_c}{C_i}\right) * 100 \quad \text{and} \quad E\ (extension) = \frac{1}{\left(\frac{C_c}{C_i}\right)}$$

Where C_c is current crustal thickness, C_i is the initial thickness, *S* is the shortening in % and *E* is the factor of extension.

4.4. Field Study

A six day field study on Naxos was conducted to get a better understanding of the geology, gather additional data and investigate the possible occurrence of an E-dipping thrust on the eastern side of the migmatite dome (fig. 9, [A]). In order to constrain the fault movement on the NE trending oblique strike slip faults and the E-W trending normal faults the study aimed to, if possible, quantify their displacement (fig. 9, [B]). The northern tip of Naxos has a collection of large scale plunging or refolded folds described by Urai et al. (1990) that was also of interest for this work. Marble/schist contacts on the SE coast were also investigated (fig. 9, [C]). All measurements were made with a ‘Silva Ranger’ Compass and coordinates for outcrops recorded with either the ‘GPS Status’ or ‘Rangefinder GPS’ Apps for smartphones. All measurements were imported into MOVE and subsequently used to update and modify the 3D models. Stereonet9 and MOVE was used to analyze and visualize aspects of the data in Stereonet plots. Details on the algorithms behind Stereonet9 can be found in Allmendinger et al. (2013) and Cardozo & Allmendinger (2013).

A model is only as good as the data it is based on. No GPS data was available for any of the measurements outside of this authors own field survey. Since the published geologic maps are all based on older maps that predate the days of satellite imaging and GPS the DEM does not physically match these maps. Spatial referencing in eg. ArcGIS was not done as this ran the risk of warping the geographic location of measurements marked on the maps being digitized. As a result georeferencing left an estimated maximum error of +/-200 meters. Section balancing when dealing with heterogenic metamorphic strata leave uncertainties as to how differences in response to stress affect backward modeling. How much volume is missing, redistributed to the surrounding area or compressed in the metamorphics is beyond the scope of this model. The need to simplify and scale down the resolution of all features relates to these considerations, lack of data on fault movement and the absence of any subsurface data. Lastly it should be added that as with any geological interpretation no guarantee can be given that subsequent interpretations yield exactly the same result even with the same underlying data. The differences between model one and two are excellent examples of this.

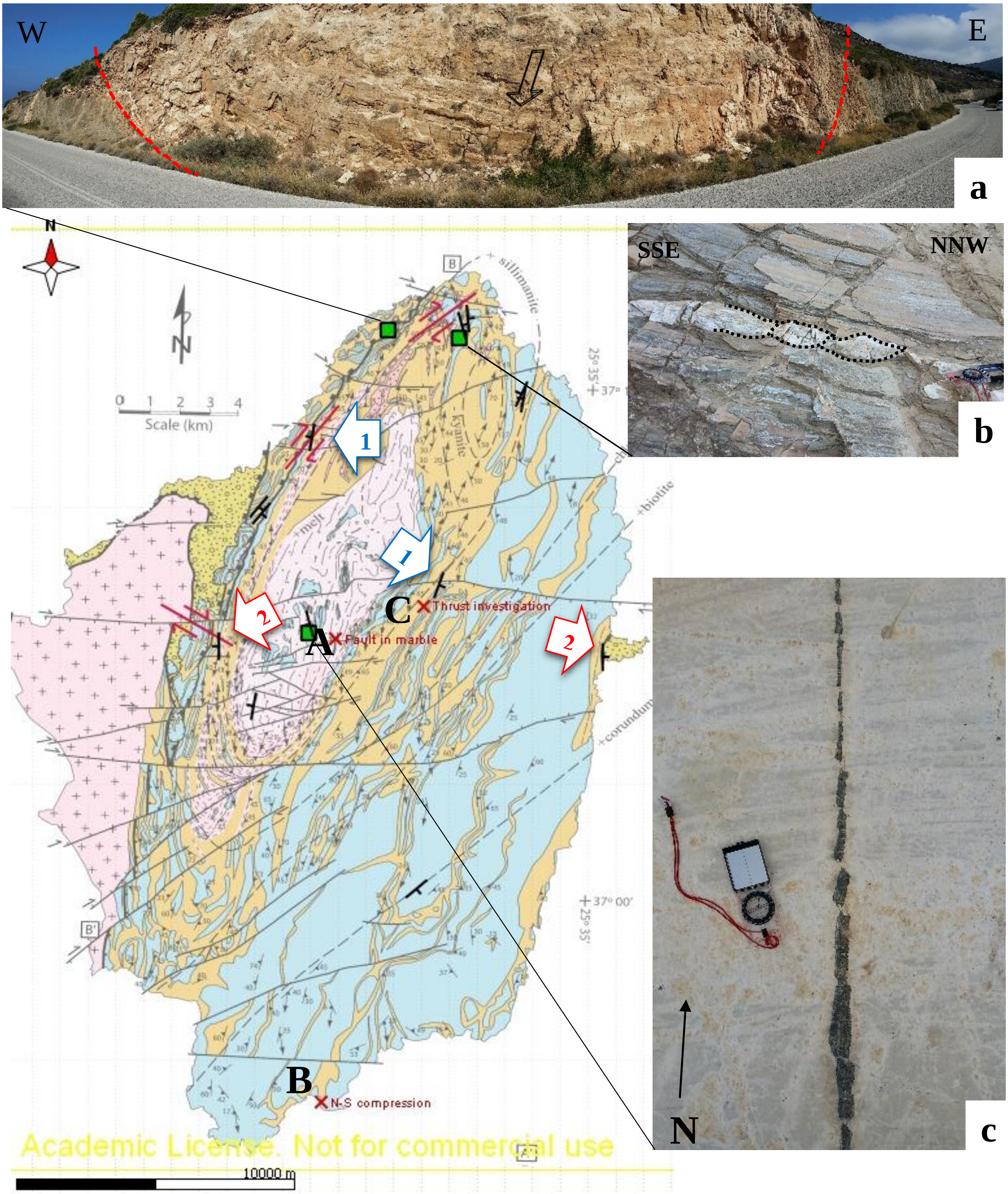

Figure 9. Geological map of Naxos modified after Kruckenberg et al. (2010) showing location of measured foliations (black dip markers) and shear zones identified in the field (red shear indicators), location of photos (green squares) and points of interest discussed below (A, B and C). Color coded numbers indicate the data subsets used in calculating the axial plane in figure 10. **9a**: N-plunging synform in marble and schist. **9b:** Marble boudinaged in schist indicating top N shear sense, note compass for scale. **9c:** Boudinage in marble showing NNE sense of shear.

5. Field Results

Dip data gathered in the field were done so based on the localities visited and accessibility. Since measurements were taken from a large area it was interesting to see if this small dataset could in any way be representative of the islands overall structure. Measured foliations were plotted in Stereonet9 (fig. 10) and they show a fold axis with ~194°/05° trend/plunge, the great circle to the planes have a strike/dip of 284°/85°. The dashed green line shows the axial plane for datasets 1 & 2, color coded with location in figure 9.

The reason for making these separate attempts at finding the axial plane was to test if the field data could give any insight as to the best attitude for cross sections in the calculation of shortening. While the resulting fold axis is not in accordance with island wide data presented below, it is interesting that this small dataset nonetheless comes very close (+002°) to what would be a suitable stretching direction orientation.

Three shear zones were observed in the field where it was possible to establish the shear sense (fig. 9, red shear indicators). They were all dextral, steeply inclined (60°-90°) and the northernmost observation included slickenlines with a 105°/20° trend/plunge. At least two of these shear zones could possibly belong to the numerous N-S extensional shear zones observed on Naxos (eg. Urai et al. 1990).

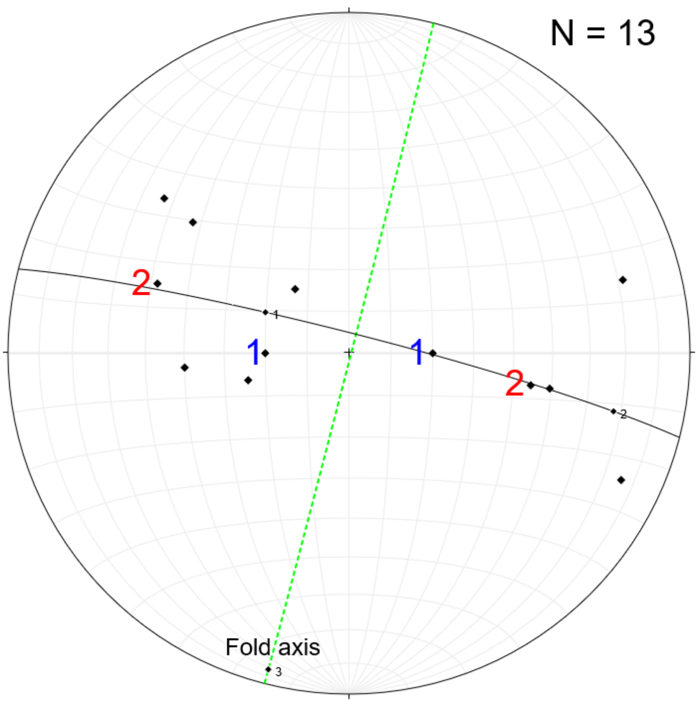

Axial plane of dataset:	1
Trend & plunge of fold axis:	194°/05°
Strike & dip of axial plane:	014°/90°E
Interlimb angle:	140°
Axial plane of dataset:	2
Trend & plunge of fold axis:	194°/05°
Strike & dip of axial plane:	014°/90°E
Interlimb angle:	81°

Figure 10. Stereonet plot of poles to foliation planes (black diamonds) and the fold axis of the complete dataset (denoted). The axial plane from dataset 1 & 2 is represented by a dashed green line. Equal area-, lower hemisphere projection. Table shows additional information on subsets 1 & 2.

5.1. Faults

An E-W striking fault exhibiting tension cracks and possible striations on the fault surface inferring a normal sense of movement with the hanging wall to the south was investigated (fig. 9, [B]), shown in figure 11 below. Despite being found in a location with known strike slip faults evidence for an oblique sense of movement could not be ascertained and the striations were too uncertain to measure with any confidence. Despite some effort, no fault data able to constrain the model could be gained in this nor in other fault localities visited.

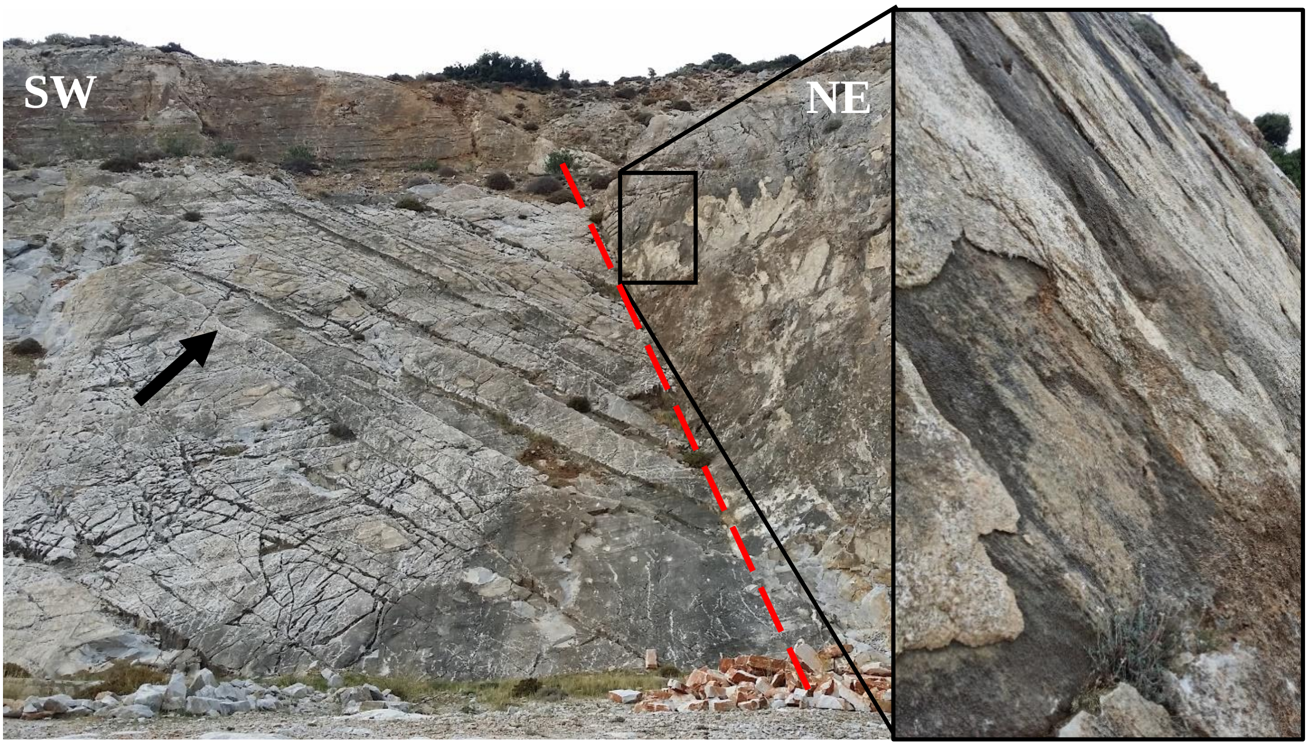

Figure 11. 'Fault in marble' (A in fig. 9) exposed by construction of a football field 400m NW of Moni. Dashed red line delineates the probable fault contact, tension cracks in the hanging wall terminate at the arrow. Inset shows what is believed to be the fault surface.

5.2. Contacts between marble and schist in SE Naxos

The southeast coast of Naxos is interesting as this part of the island has not been metamorphically overprinted by the M_2 event (Avigad 1998) and was originally intended as a site for gathering of additional dip data. The succession found here dips to the south at ~20°, consistent with data already digitized. The appearance of contacts between marble- and schist layers here demanded closer inspection. The contact zone (dashed lines, fig. 12) is highly crushed with striations on the marble contact surface, indicating northward thrusting of the upper schist layer on top of the marble. This could of course indicate extensional normal faulting as well but the low angle seems to indicate a reactivation of an earlier thrust if this is the case.

The sequence repeats further upslope to the east. What was interpreted as the same sequence can be seen on the western side of the bay in figure 13. Later E-W shortening, with a hinge zone to the west, was observed in both marble and schist on the south face of the outcrop (fig 14) 20 m east of where figure 13 was taken.

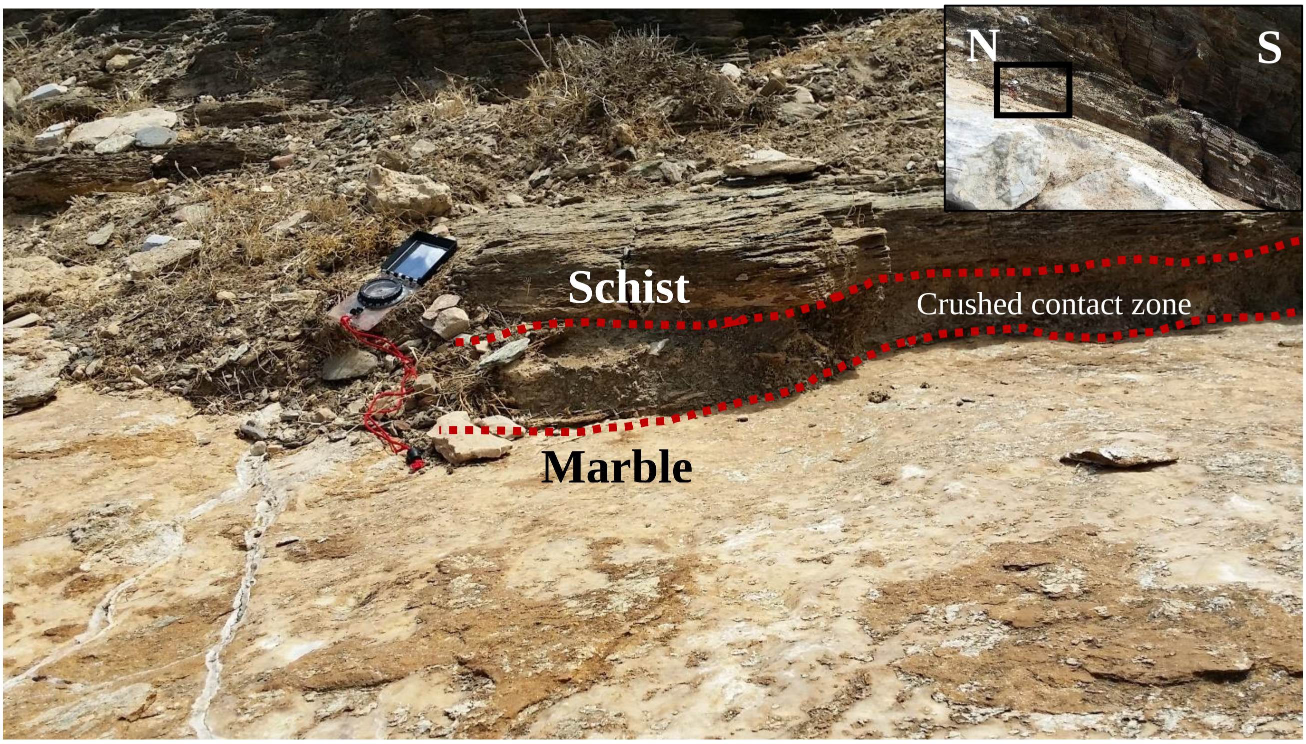

Figure 12. 'N-S compression' Shows the contact between marble and schist S of the pier in Kalantos on the SE coast of Naxos (B in fig. 9). Note the fine grained, easily eroded contact surface above the dashed line. Inset shows the attitude of the contact.

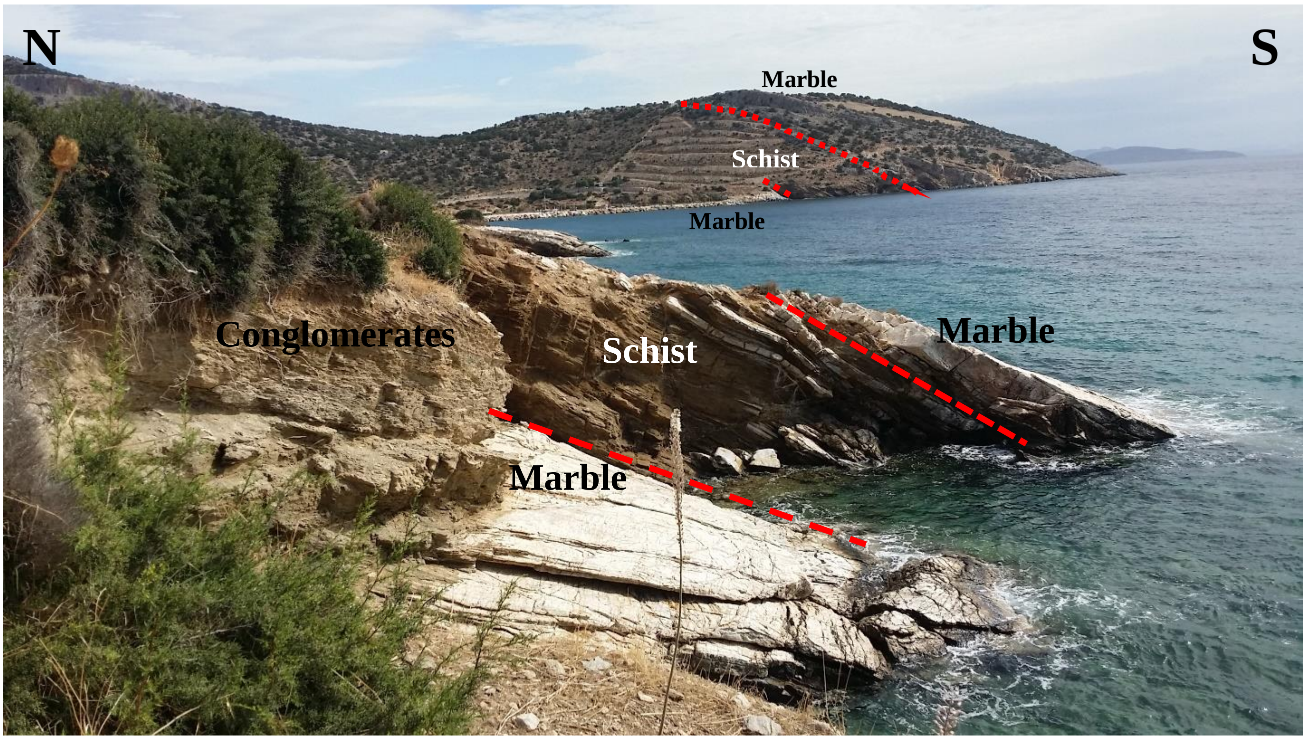

Figure 13. View from across the bay, looking east toward the pier S of Kalantos.

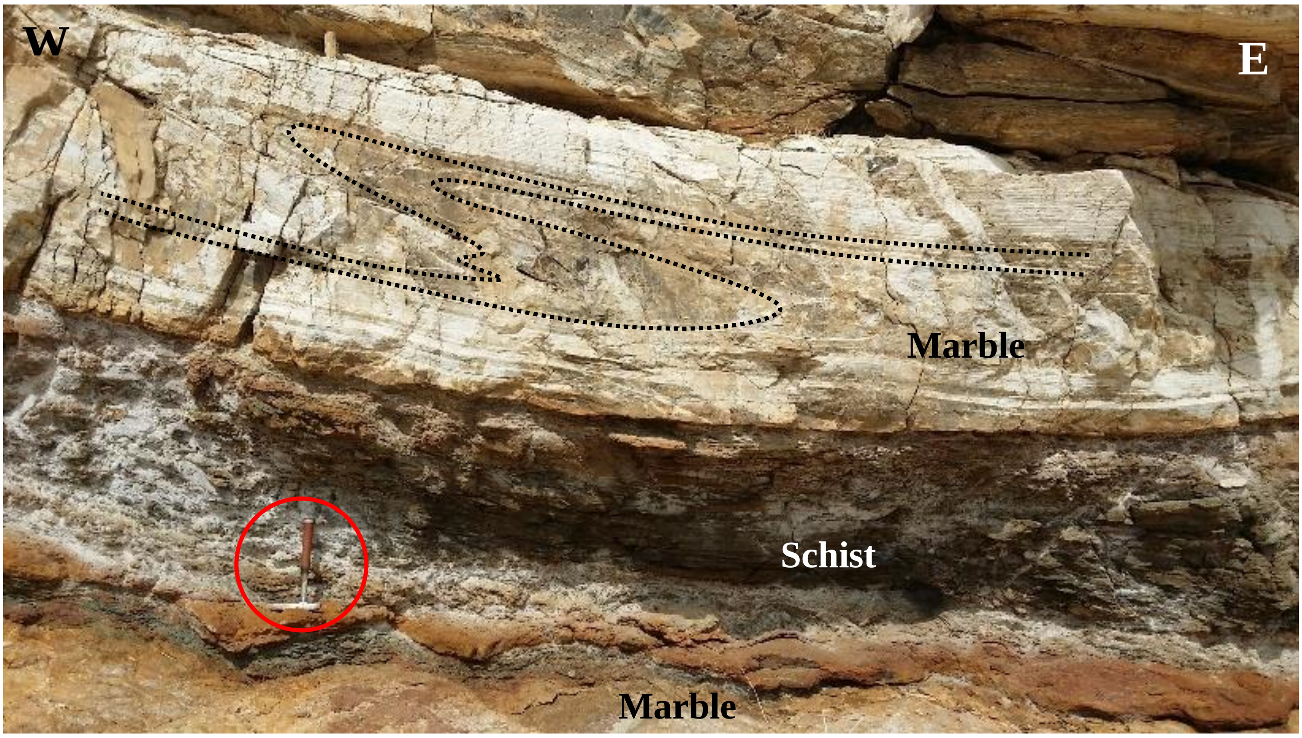

Figure 14. South face of the outcrop 20 m east of figure 13's location. Strong top E sense of shear in both marble and schist (dotted trace in figure). Hammer for scale. Note the difference in fabric at the bottom contact between schist and marble (just below the hammer).

5.3. Moutsounas detachment

Schist in contact with Moutsounas shear zone on published geological maps were reinterpreted as marble in sections A-'A, C-'C and the 3D model. Initially a photo in Cao et al. (2013) raised suspicion that a marble horizon may in fact constitute the footwall of the detachment at this location, this needed confirmation in the field (fig. 15a). The marble is very thin (~1m) which is probably why it was left out of previous interpretations. An important aspect of this locality was the rarity of the exposed detachment plane, which is highly mylonitized, and the constraints this provides for the 3D model. The measured N-trending dip of 20° coincides well with the geometry of the 3D model as seen in figure 15b (triangles are equal in angle although they have not been measured to exactly 20° and are only for visual reference).

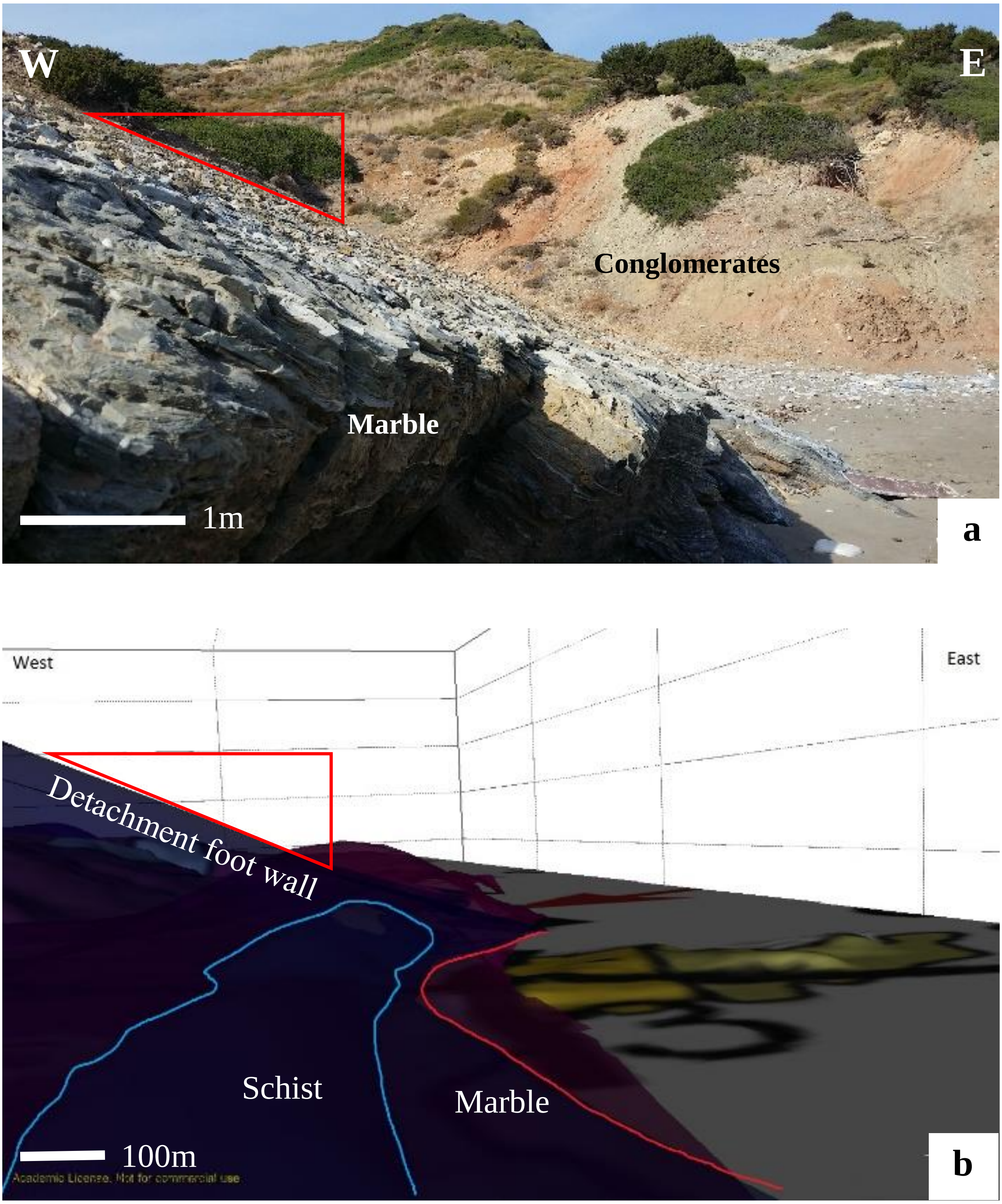

Figure 15a. Mylonitized marble on top of highly deformed schist at Moutsounas shear zone in tectonic contact with conglomerates. **15b.** Red line delineates the Moutsounas shear zone in the model, blue defines the horizontal occurrence of schist in the vicinity. Layers are superimposed on a topographic DEM of Naxos with an overlay of the geological map from Cao et al. (2013).

5.4. Thrust investigation

It was found that along strike of what was initially interpreted as a possible E-dipping thrust on the eastern slopes of the migmatite dome (fig. 16, appendix 1-2) probably is an overturned to the W fold with the axial plane (fig. 17, blue great circle) dipping E. In the schist, S-shaped parasitic folds on the south face and Z- shaped ones on the north face of the outcrops visited indicate a space problem developing toward the hinge zone. Geometry is defined by looking down the fold axis to the SSW (fig. 17, red circle). Rotated marble clasts with the same kinematics were also observed. The hinge zone is thought to be located somewhere in midair toward the northwest in figure 18.

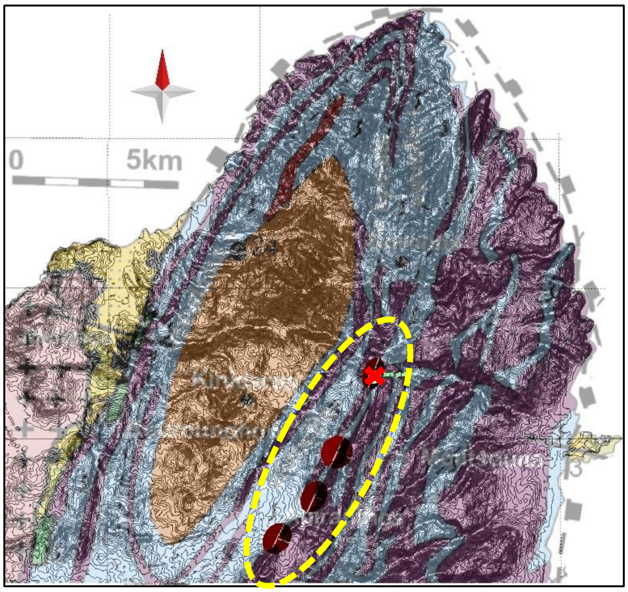

Figure 16. Geologic map modified after Cao et al. (2013) showing the general area of the possible thrust (dashed yellow line), data locations for the stereoplot in figure 17(dark red dip markers) and location of photo in figure 18 (red X).

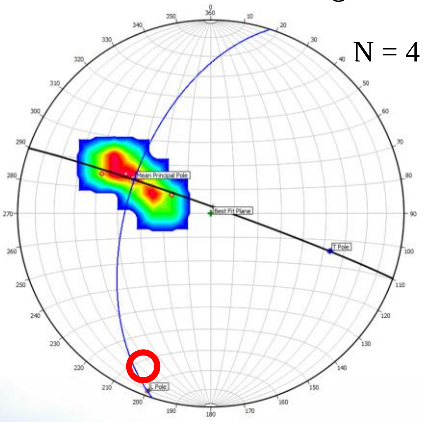

Figure 17. Equal area, lower hemisphere projection of poles to foliation for the fold seen in figures 16 and 18. Black line is the best fit great circle, blue line is the fold axial plane and the fold axis is circled in red. Data from Urai et al. (1990).

Figure 18. Several road cuts exposing the eastern limb of the fold perpendicular to fold hinge 800m northeast of Sifones on the eastern side of the migmatite dome (A in fig. 9). Red arrows indicate observed apparent sense of shear and black 3D box shows approximate attitude of hinge zone to the northwest.

6. Modeling results

6.1. 2D sections

Fourteen sections labeled A-‘A to C-‘C and j-‘j to k-‘k (appendix 3) and a-‘a to i-‘i (appendix 4-5) were constructed and balanced by line length restoration. Two 2D sections, L-‘L and M-‘M, were made to illustrate the geometrical relationship between the metamorphic isograds and the Naxos/Paros detachment fault presented in ‘7.6. Metamorphic isograds’ below. Eighteen additional sections were made from the two finished 3D models used in E-W shortening calculations, which is outlined in ‘7.7. Extension/shortening evaluation’.

Figure 19 shows section B-‘B after final balancing. The granodiorite and S-type granite were left out during balancing in order to keep it simple and because the S-type granite probably derives from the migmatite. The granodiorite is a later addition that was present only in the later stages of extension (Bolhar et al. 2010). These units are therefore added to the sections post balancing and in some cases derived entirely from the 3D interpretation projected onto the sections. Polygon creation was not utilized in the 3D construction and is only for presentation of the 2D sections. Location of all section transects can be found in appendix 6-7.

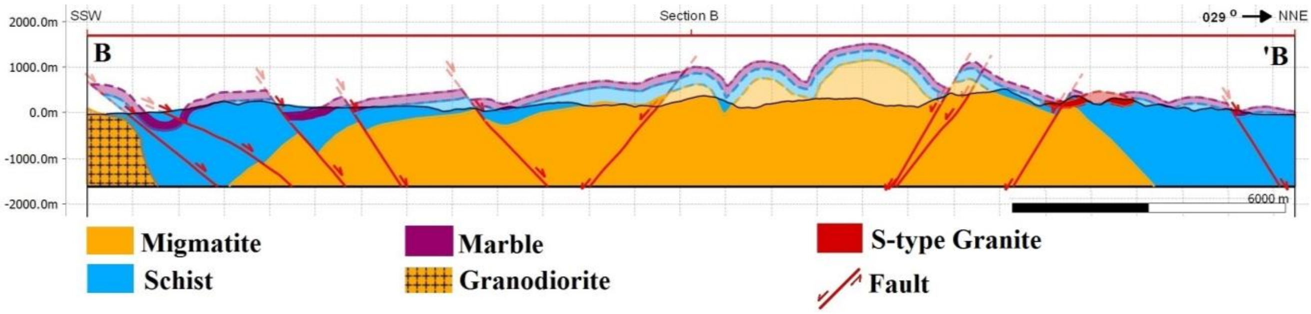

Figure 19. Section B-’B trending 029°-209°. Inspired by the profile and interpretation from Kruckenberg et al. (2011) simplified to work as a precursor to the 3D model. Transect can be found in appendix 6a.

A striking feature in all polygonised sections (A-‘A to k-‘k) is the massive amount of schist and relative lack of marble. This is due to the simplification needed for the 3D model and has no relevance for the actual thickness of the schist layer beyond its vertical extent constrained by the migmatite. The underlying assumption for this work was that the schist is chronologically older than the marble and that horizon- and dip data must be honored. As there is no practical way to constrain multiple interlayered marble/schist horizons while preserving the integrity of the 3D model on the scale of the island, a simple two layer model had to be utilized. In reality these units, apart from the start and end of the succession, are probably intermingled and have several sub-units. This is evident from observations in the field (fig. 20), as well as from looking at the complex pattern of folds exposed at the surface on any geological map of Naxos.

Figure 20. Looking east from the center of the island toward a large scale east dipping marble (lighter) and schist (darker) succession, migmatite/mantling rocks transition is west of this picture (not shown).

6.2. 3D faults

Data for the rose diagram (inset, fig. 21) and azimuth/dip plot (fig. 22) was downsampled from ~22000 to 456 data points for the presentation. The rose diagram shows the principal dip direction of the faults in the model while the dip/azimuth plot adds the dimension of fault dip angle. The diagram mixes the E-W normal- and ENE-WSW strike slip faults giving a general ~075°-255° fault strike direction perpendicular to the dotted black line in the rose diagram in fig. 21. This is perhaps reflective of how it looks in the field as it was hard to exclude oblique sense of movement on most faults encountered. This subgroup is boxed in figure 22 with a dotted black line.

Displacement on E-W trending normal faults proved hard to quantify and was therefore estimated from the 2D interpretation in the cross sections. Displacement on the NNE-SSW trending strike slip faults remains unknown and as a result these had to be restored with a pure normal sense during unfolding and backward modeling of the 3D model. Figure 21 on the next page show all faults modeled in 2D and 3D. There is some support for a normal component to the fault in figure 11 as well as a cross section drawn in Jansen & Schuiling (1976) wherein a strike slip fault is interpreted as having normal/reverse sense offset. It is hard to tell which since they have interpreted the fault as vertical. Using additional information in the geological map of Kruckenberg et al. (2010) the concerned fault is seen to have a normal component with the hanging wall to the NNW (fig. 21, dotted green line). In the area where the detachment surface forms a syncline (fig. 21, dotted yellow line), the detachment fault consisted of several low angle faults at ~30° (obscured by the granodiorite in fig. 21) for the purpose of layer unfolding in 2- and 3D. This was also how the detachment fault was expressed in the geological map of Kruckenberg et al. (2010).

The faults with a dip direction of ~280°-100° (solid black line, rose diagram in fig. 21) is interpreted as one subgroup. These faults mostly belong to the N-S striking normal faults made by the detachment in the detachment syncline between the granodiorite and the migmatite or on the east coast by Moutsounas. Looking at figure 22 this is much clearer (solid black rectangle) as this subgroup have a lower fault angle of ~40°-10°. Note how the main fault set also have low fault angles represented (dotted black rectangle), this is because they decrease in angle as they propagate toward the surface. This effect mimics what have been outlined in the literature (eg. Brun et al. 1994, Gautier & Brun 1994) with respect to the effects of detachment faulting and core complexes on extensional faults. While there is apparently fault data for Naxos in a PhD thesis by Luc Siebenaller (2008) this publication is not in English and thus unavailable to this author.

Interestingly, looking at the rose diagram in figure 21, there is a conspicuous lack of NE-SW striking fault surfaces even though this is the general stretching direction of the Cyclades (Avigad et al. 2001). Extensional normal faults would ideally be forming perpendicular to the extension (facing NE-SW) if there was no coeval horizontal shortening.

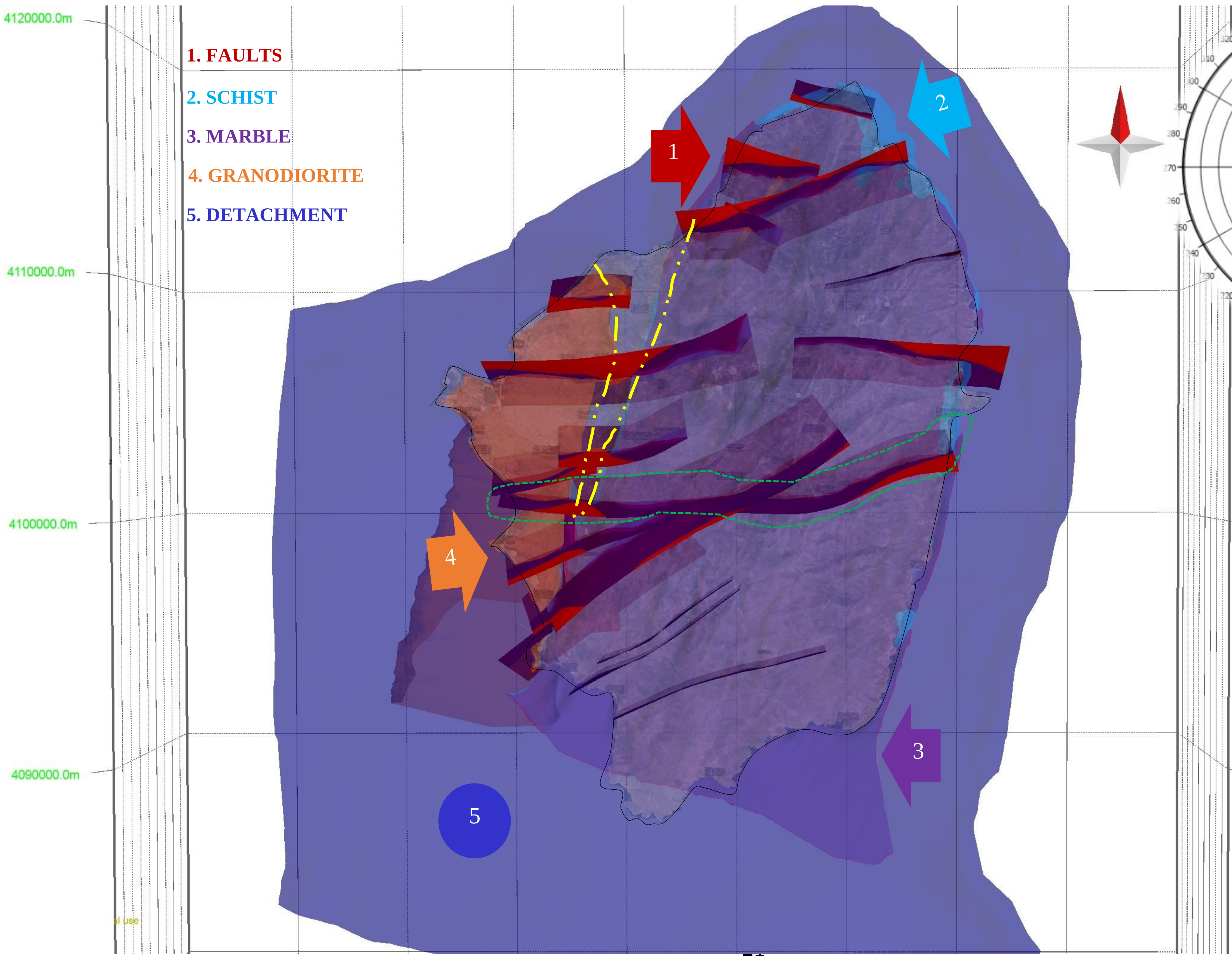

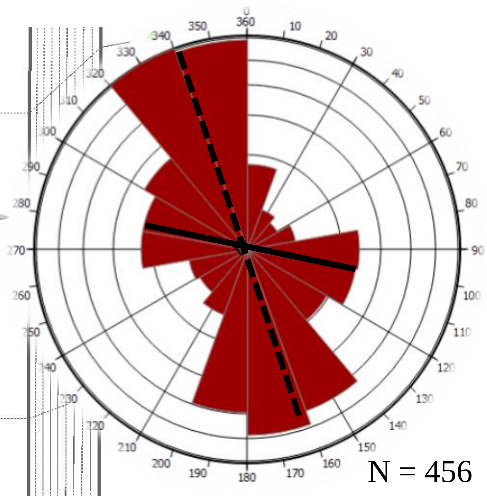

Figure 21. Major faults (1) present in the 3D model and the 2D sections superimposed on a DEM with transparent layers including schist (2), marble (3), granodiorite (4), and the detachment surface (5). Detachment syncline is demarcated by a yellow line, black line is the coast line. Fault mentioned in the text is circled with dotted green line. Bounding box is 45x35x6km. Inset shows strike of fault surfaces for all faults modeled, including the detachment, which crosscut the topography on land. Black- dotted line (~340°-160°) and solid line (~280°-100°) correlates to rectangles in figure 22 indicating fault subgroups. A more detailed trace of the dataset is available in appendix 8.

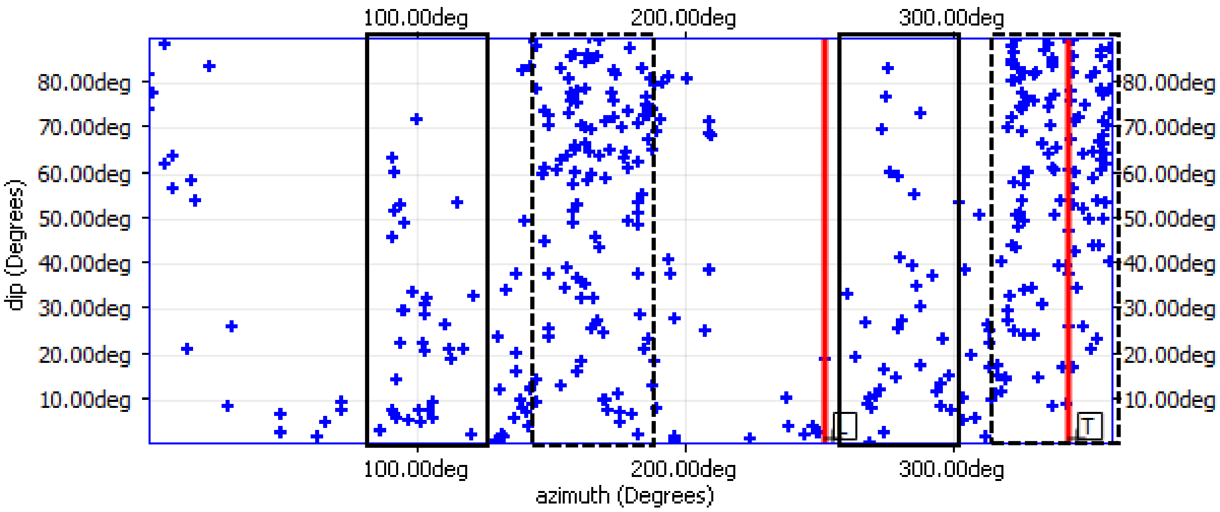

Figure 22. Diagram of dips to azimuth plotted for the faults modeled in 3D, N = 456. Dotted- and solid rectangles correlates to lines drawn on the rose plot in figure 21 indicating fault subgroups.

6.3. Determining the optimal section orientation and analysis of dip data

Rose plot diagrams of the foliation strikes used in the 3D model show a strong N-S orientation for the data from the migmatite dome (fig. 23a). The mantling sequence has similar foliation orientations (fig. 23b). Looking at these diagrams it becomes clear that the optimal section direction would lie around ~115°-285° for the principal shortening direction and ~015°-195° perpendicular to it. It is also evident that there is a difference in preferred strike orientation between the migmatite and mantling sequence but this could be due to the relative lack of data for the mantling rocks. Note that the extension direction is previously well defined by the stretching lineation data reported in many studies (eg. Buick 1990, Urai et al. 1990).

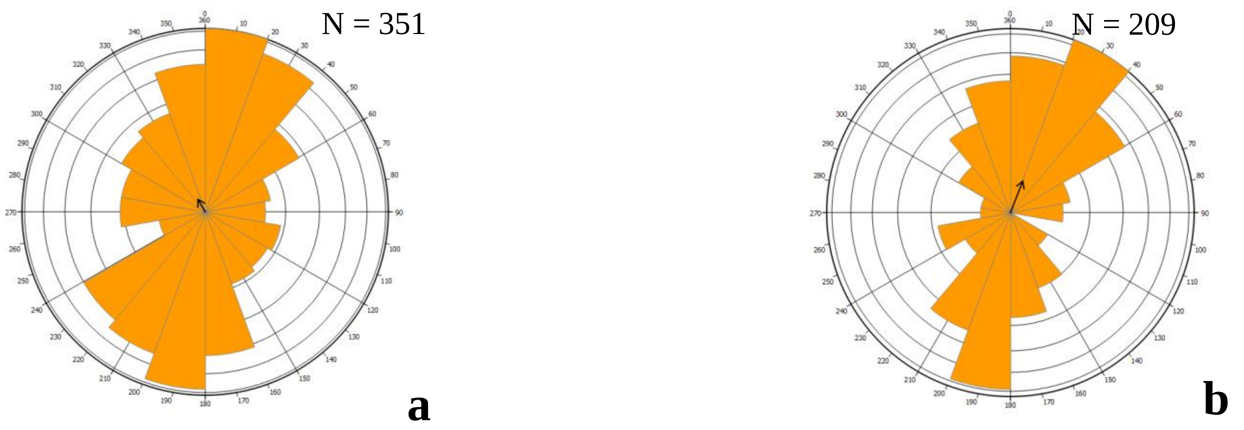

Figure 22. Rose plot of foliation plane strikes, every twentieth strike interval. **23a**: Strike in migmatite. **23b**: Strike in the mantling sequence. Data from Urai et al. (1990), Kruckenberg et al. (2010), Cao et al. (2013) and own data. Arrows indicate the attitude and amplitude of the mean.

Dip data used in the 3D model construction was divided in two ways. Two stereoplots were constructed dividing the dataset by the structural syncline trending NNE-SSW between subdomes (eg. Kruckenberg et al. 2011) in the middle of the migmatite dome complex (fig. 24). A second set of Stereonet plots encompassing all data from outside the migmatite dome (N = 248, demarcation was drawn at the edge of the migmatite using a DEM overlain with the geologic map from Cao et al. 2013) was analyzed in subsets according to its geographic quadrant (N, S, E and W) on the map as seen in figure 25. This was done to isolate and shed light on fold geometries prevalent in the different quadrants of the island and to check the overall fold geometry expected in the principal shortening direction as well as its concordance with the model.

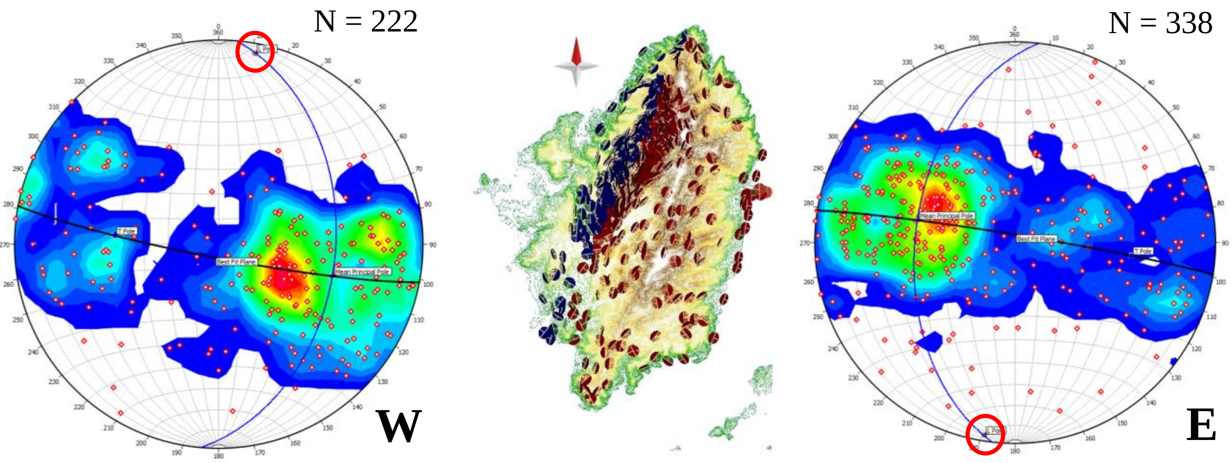

Figure 24. Equal area, lower hemisphere projection of poles to foliation planes for the western- (**W**) and the eastern (**E**) part of the island. Derived fold axis is circled in red, the blue great circle is the axial plane and the best fit great circle is black. 10% Terzahgi bias correction for azimuth has been applied to both plots. The map shows geographical selection criteria in color code **W** is **blue** and **E** is **red**. Data from Urai et al. (1990), Kruckenberg et al. (2010), Cao et al. (2013) and own data.

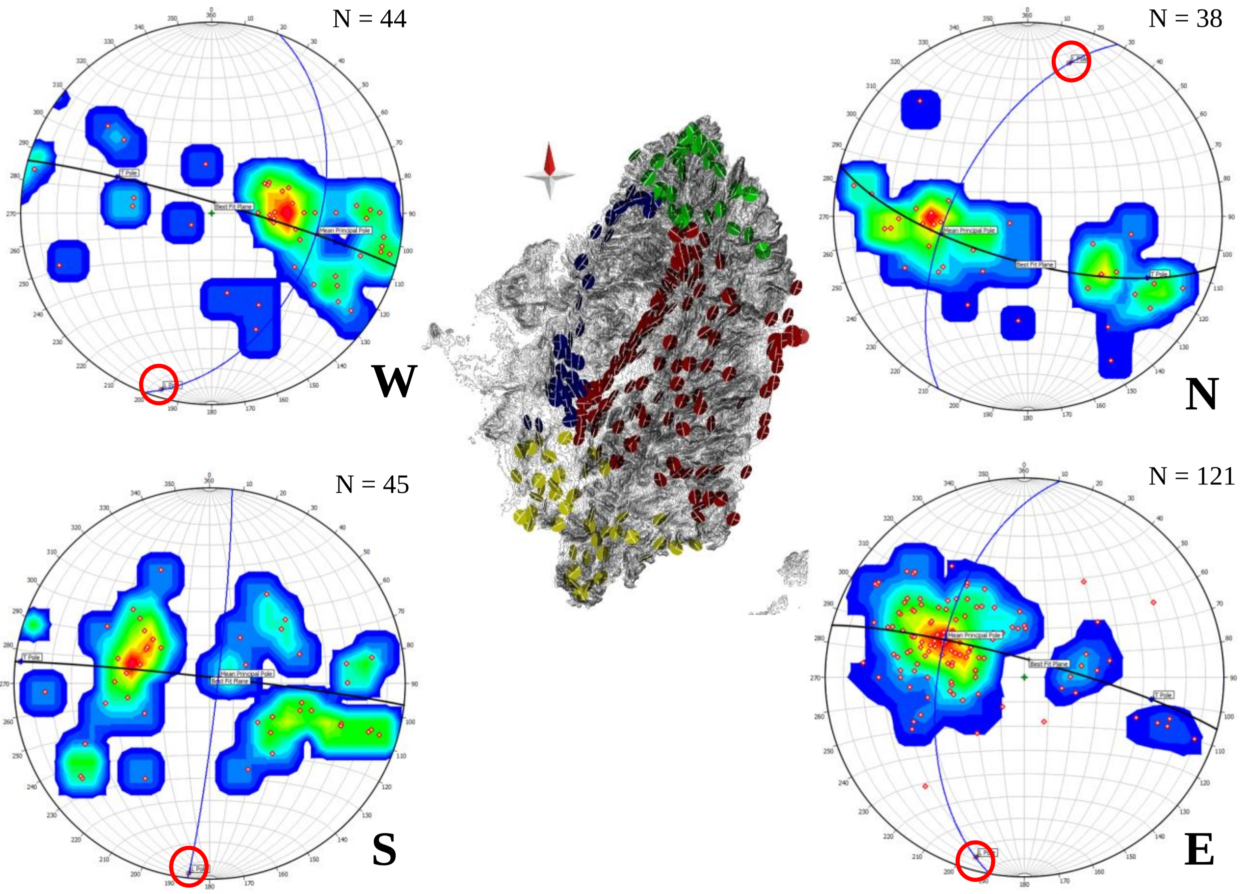

Figure 25. Equal area, lower hemisphere projection of poles to foliation planes of all dip-data outside the migmatite dome divided into color coded quadrants **N**, **S**, **W** and **E** (**green**, **yellow**, **blue** and **red** respectively) is shown on the map. Fold axis is circled in red, the blue great circle is the axial plane and the best fit great circle is black. Data from Urai et al. (1990), Kruckenberg et al. (2010), Cao et al. (2013) and own data.

All Stereonet plots agree with a NNE-SSW sub horizontal fold axis. Comparing the plots, the asymmetry seen in the E and W for figure 24 and 25 looks to be related to the fold geometry of the mantling rocks. The asymmetrical patterns indicate subhorizontal- to plunging inclined W-verging folds in the east and vice versa. This finding is corroborated by observations in the field (fig. 18), the initial 2D section interpretations (appendix 3) as well as in the literature (eg. Avigad et al. 2001).

The accepted 010° extensional direction, described by Kruckenberg et al. (2011) from lineations in the migmatite, seems to largely coincide with the fold axes of late E-W folds. Analyzing all available dip data with a 10% Terzaghi correction (not shown) indicate a ~014° fold axis would fit the structure of Naxos given the available dip data. Based on these analyses, a 282°-102° best-fit perpendicular to the foliation planes in the model was decided on as a good middle ground, thus resulting in an extensional direction of 012°-192°.

6.4. 3D Surfaces

The granodiorite and the S-type granite (orange layers, fig. 27) were not focused on and are largely constrained by where they are seen on the surface, some additional points are made about this in the discussion. Two versions were made of the principal rock layers in the model (fig. 28). Model one is the most thoroughly vetted and primary 3D representation of this work. The rock layers of model one and two were constrained horizontally by the detachment fault surface in all directions but south, where there are no constraints past the southern tip of the island. Model two was initially made to test the available tools within MOVE and as a way around unwanted geometries in fault displacement, essentially forward modeling the fault offset instead of manually editing it. This is probably the better approach as it minimizes the geometric artefacts that otherwise tend to make 3D layer unfolding and balancing an unpleasant experience in MOVE. While fault geometry results were more satisfying for model two, time constraints and lack of fault movement data made completion impossible. Model two was also made with a higher relief, mimicking the behavior of horizons on the geological map (eg. Cao et al. 2013) at the cost of not honoring dip data as closely as model one does. Model two has a more pronounced syncline in the middle of the MCC to account for what was seen of the vertically inclined marble in the field (eg. fig. 4). Views of the marble- and schist layers with dip angles color coded for visual clarity can be seen in figure 29.

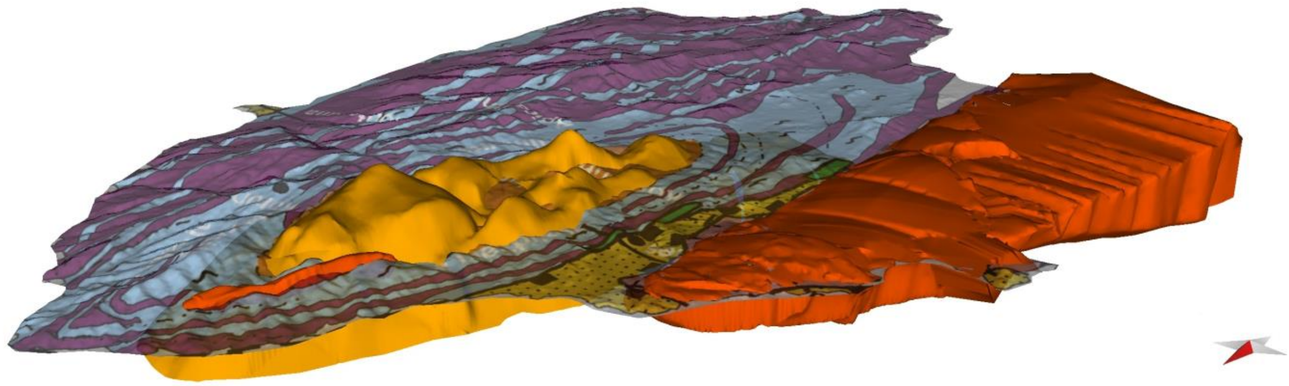

Figure 27. Geometry of the granodiorite (orange) in the west and the S-type granite (orange N-S cigar shaped body northwest of the migmatite) in relation to the migmatite dome (yellow) seen from the northwest. Semitransparent topographic DEM with geological map modified from Cao et al. 2013 shows marble (purple), schist (blue) and sedimentary infill (black dots on yellow). Note compass for heading. Scale of the island is ~32x22km.

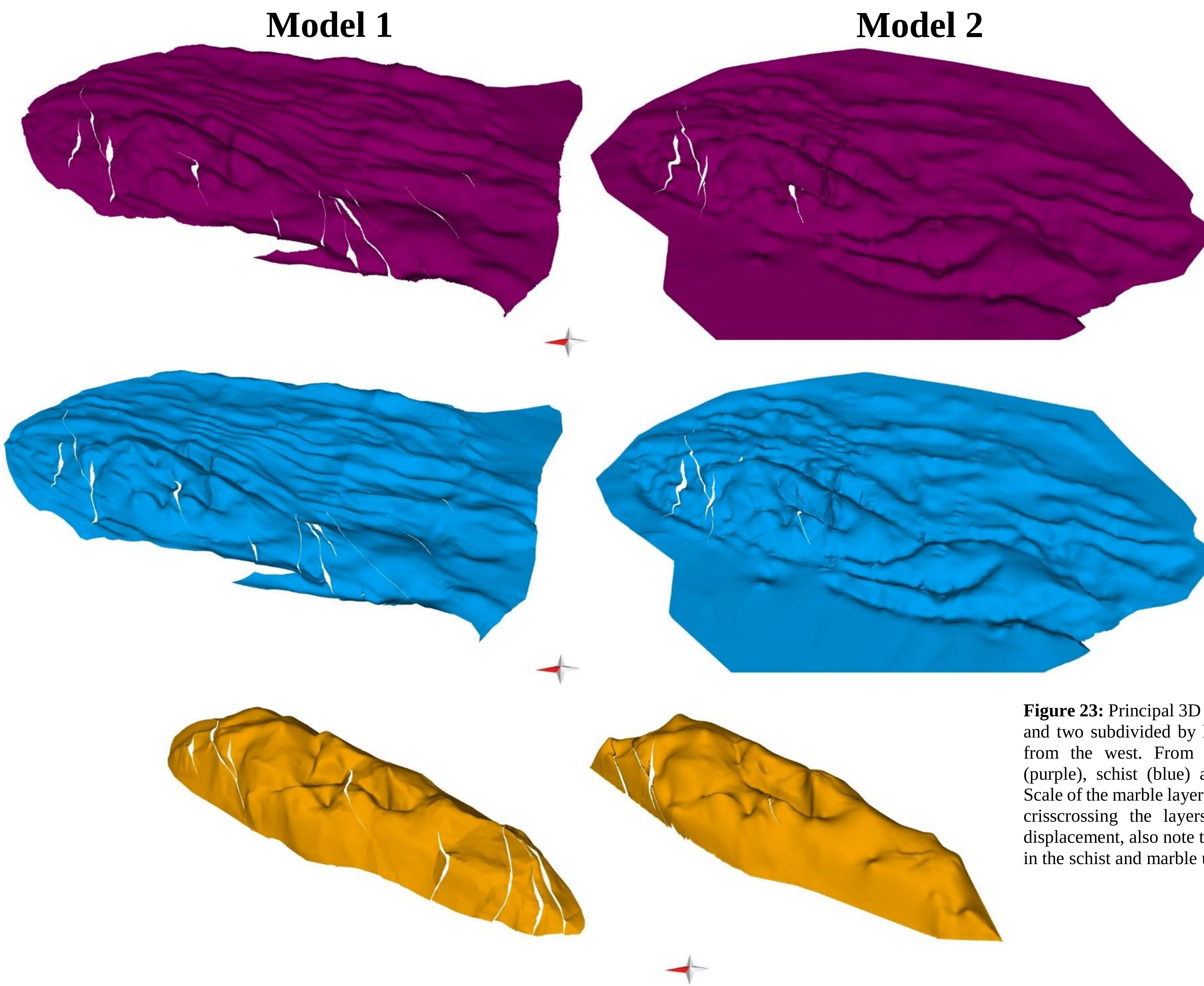

Figure 23: Principal 3D rock layers of model one and two subdivided by lithology seen top down from the west. From top to bottom; marble (purple), schist (blue) and migmatite (yellow). Scale of the marble layer is ~30x14km. The 'cuts' crisscrossing the layers are a result of fault displacement, also note the E-W folding apparent in the schist and marble units.

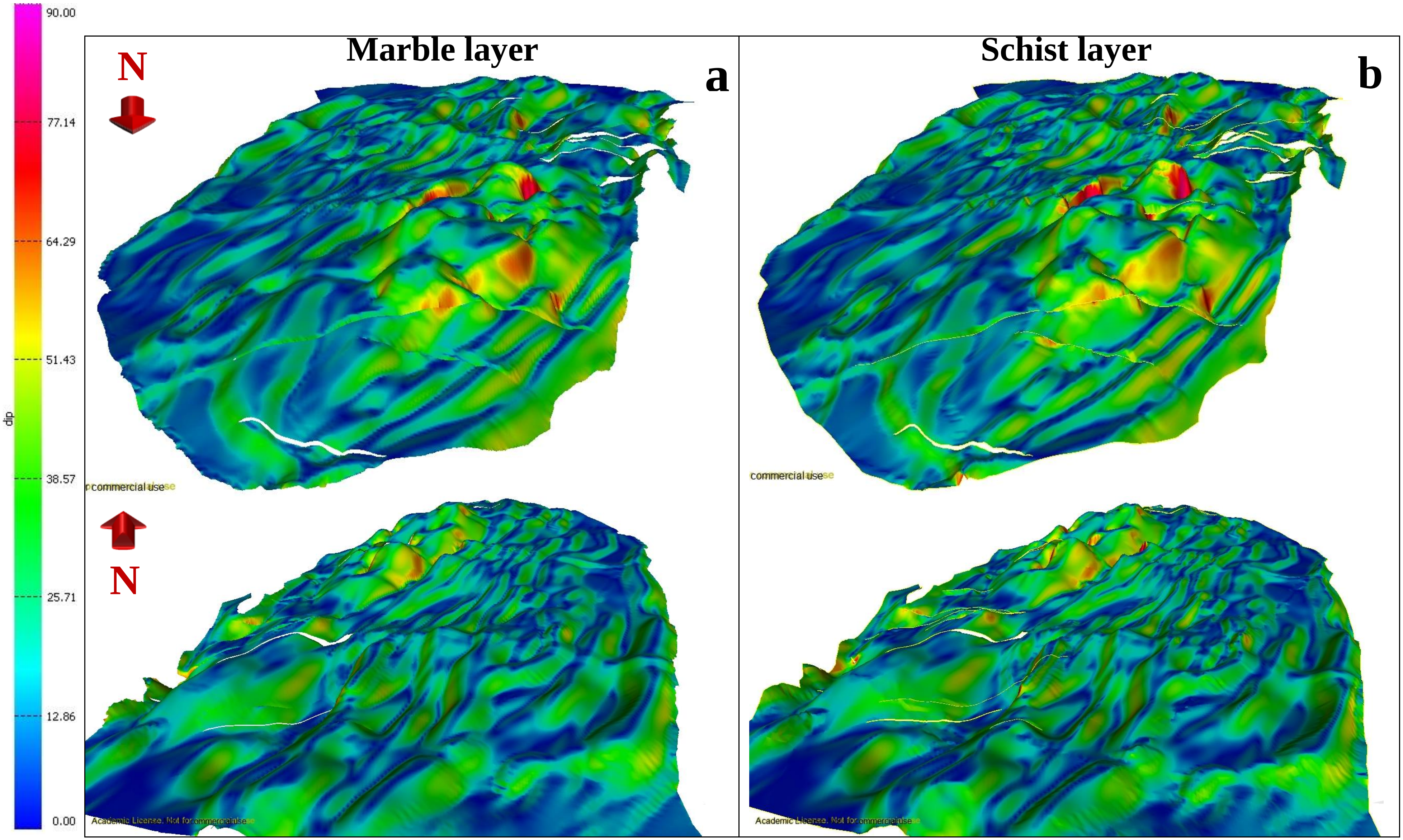

Figure 24. Dip map of marble and schist layers in model one seen from the north (above) and south (below). **29a**: Marble layer, upper and lower panel show different views of the same resultant dips. **29b**: Different views of the resultant dips for the schist layer. Color scale to the left denotes dip angle from 0° (blue) to 90° (purple). Dimensions are ~30x14km.

6.5. Naxos/Paros detachment fault

The reconstructed 3D geometry of the Naxos/Paros detachment fault shown in figures 31-33 highlight the shape of the Naxos/Paros detachment layer as well as the constraints used in its construction. In a profile seen from the north (fig. 30), the synclinal geometry of detachment in relation to the migmatite dome and topography of the island is shown. Figure 31 is a N-S profile of the relationship between the detachment surface and the principal rock layers of the model seen from the west, note the dotted green line indicating the horizontal N-S extent of the island Figure 32 shows the elevation and dip angles of the reconstructed 3D detachment. Most of the northwest, north, northeast, east and southwest extents of the model have around 30°-40° seaward plunge. The top, south and southwest of the surface have a much gentler <15° plunge, mostly to the north. The hanging wall is visible in the detachment syncline (fig. 32a:1), on the western tip of the island (fig. 32a: 2) and at the conglomerates east of Moutsounas (eg. fig. 2b and fig 15a) on the east coast (fig. 32a:3).

These areas constitute the only concrete constraints on the detachment plane. There is also an inferred detachment plane running parallel to the island off the coast to the NW, N, NE and SE (Jansen 1973, Gautier & Brun 1994) constraining the 3D detachment surface horizontally at sea level, this is shown in figure 32b (dashed red line). While termination in the southern parts is more speculative it is believed that a syncline will be forming south of where the 3D models detachment surface ends (eg. Lister & Davis 1989, Brun et al. 1994, Gautier & Brun 1994, Thomson et al. 2009, Mizera & Behrmann 2015) west of Iraklia and north of the Ios MCC. Late E-W folding on the detachment surface, supported by the work of Avigad et al. (2001) and findings in similar constrictional extensional regimes (Jolivet et al. 2004b and sources therein), is highlighted by the dip map in figure 32b.

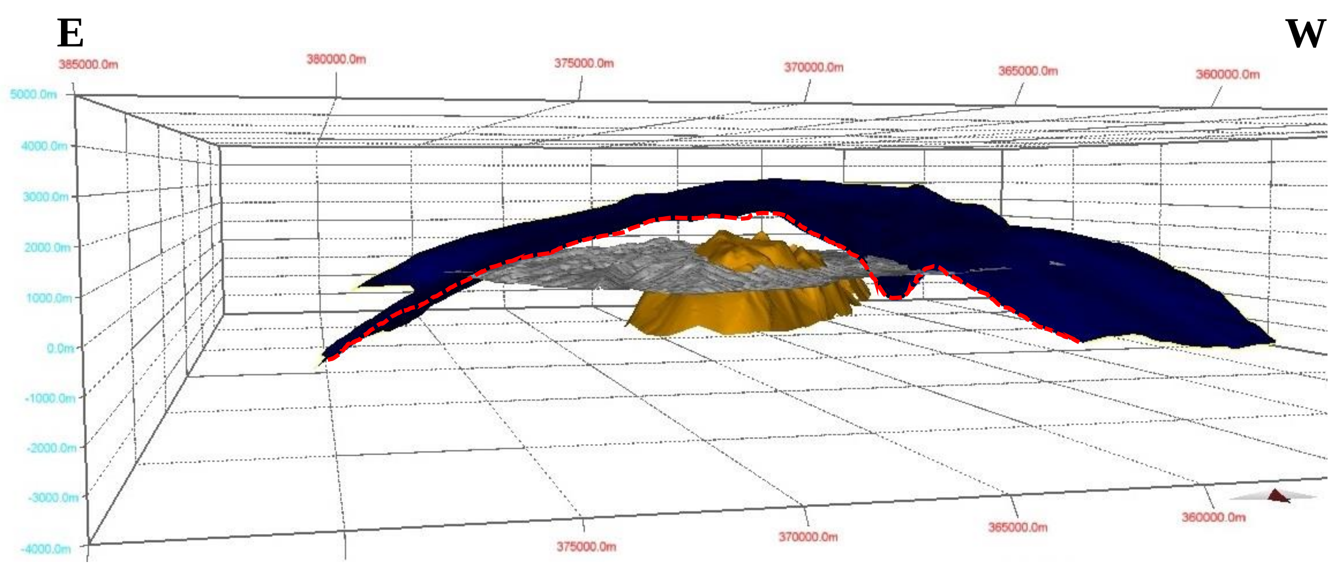

Figure 30. The Naxos/Paros detachment 3D layer in a 282°-102° profile with a topographic DEM (white layer) and the migmatite dome (yellow layer) superimposed. Detachment surface cut by the viewing plane is marked by dashed red line. Bounding box is 45x35x9km.

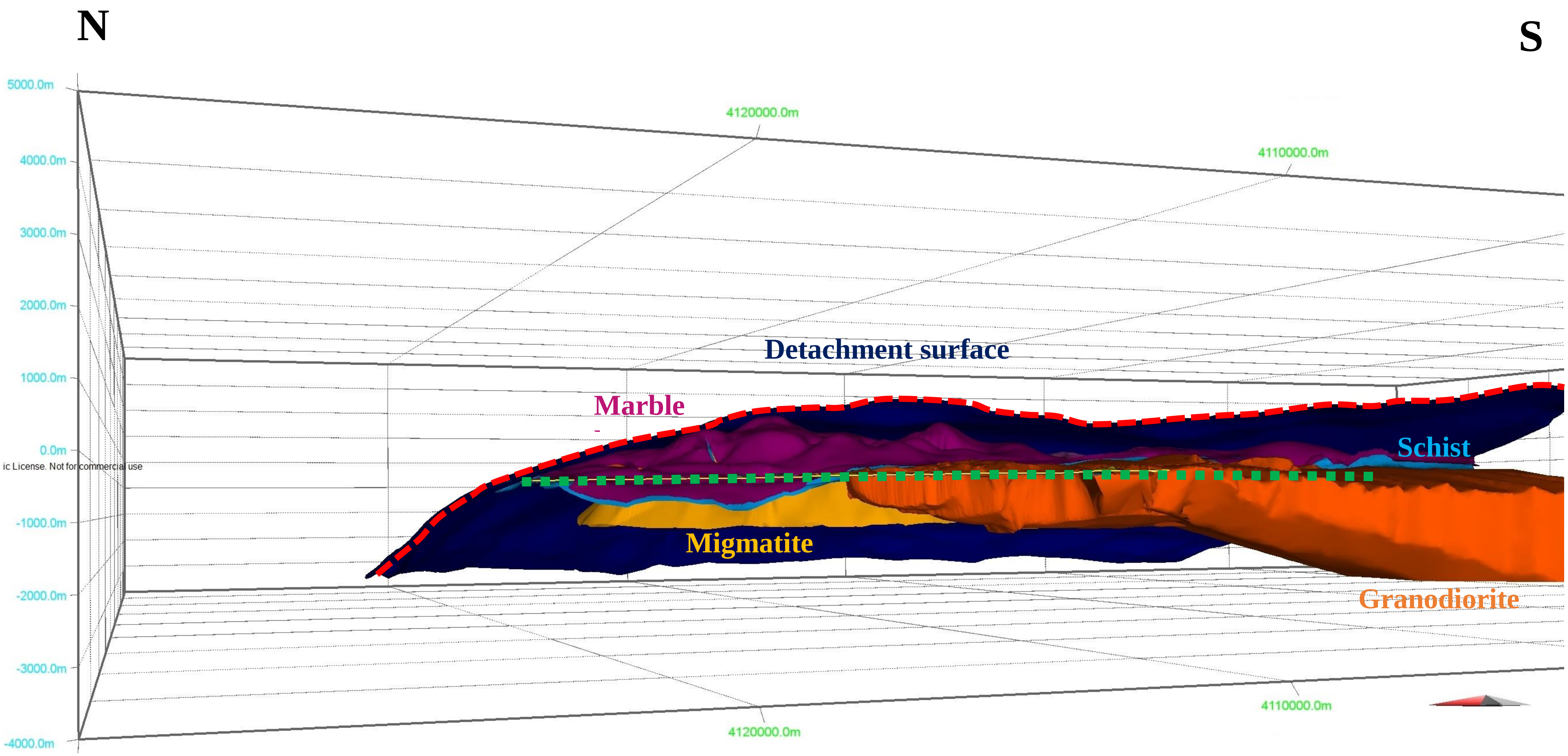

Figure 31. The Naxos/Paros detachment 3D layer seen from the west in a 012°-192° profile with the 3D rock layers (names color coded in figure). Dotted green line denotes horizontal extent and location of the island. The detachment section cut by the viewing plane is shown with a dashed red line. Rock layers extend to -1500 meters, the granodiorite body is cut off at -3000 meters and the detachment layer extends to a maximum of -3532 meters. Bounding box is 45x35x9km.

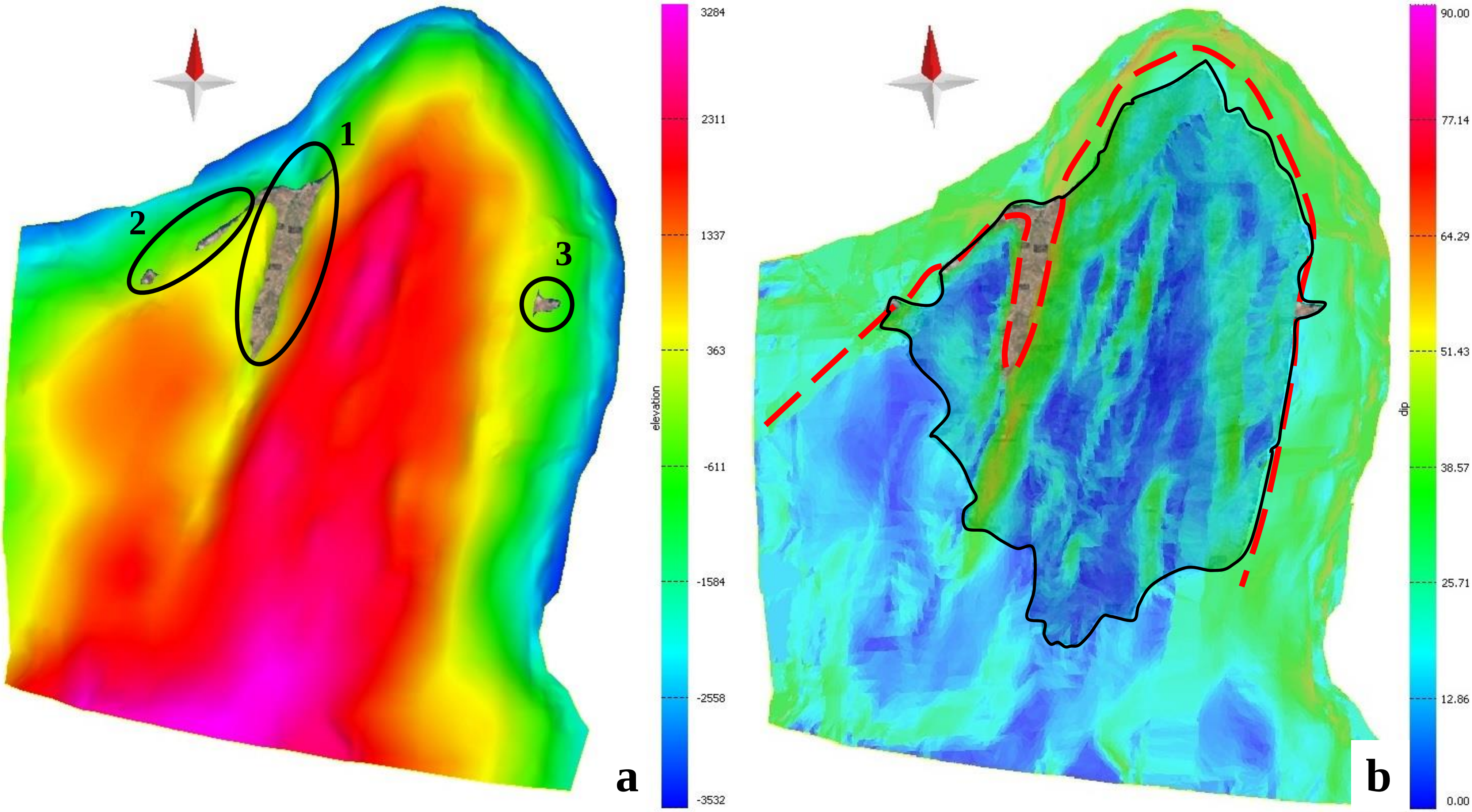

Figure 32a. Color map shows elevation of the 3D detachment layer. Hanging wall is circled in black at **1:** detachment syncline, **2:** western coast, **3:** Moutsounas at the east coast. Scale to the right denotes elevation from a depth of 3532 meters (blue) to an elevation of 3284 meters (purple). Sediments in the hanging wall were deposited syntectonically and are not part of the original hanging wall in these locations. **32b.** Dip map of the 3D detachment layer, note the E-W folding primarily in the center above the island. Dashed red line shows inferred detachment plane used in constraining the model and black line outlines the island. Scale to the right denotes dip angle and goes from 0° (blue) to 90° (purple). Scale of the 3D detachment layer is ~43x33km. Note compasses in the top of the image.

6.6. Metamorphic isograds

The metamorphic 3D isograds (fig. 33) were horizontally constrained by the petrologic map in Jansen & Schuiling (1976) and modifications by Kruckenberg et al. (2010) were also taken into consideration. Besides the 3D interpretation of the migmatite dome, a cross section in Gautier et al. (1993) served as a starting point for the 3D shape of the isograds (transect in fig. 33, dotted black line). The isograds are interpreted as asymmetrical ellipses on account of the the horizontal metamorphic boun-daries showing a closer spacing in the west. Dip data spatially associated with these boun-daries were analysed in MOVE to corroborate this interpreta-tion. Construction was done under the assumption that geometry and attitude is similar to that of the migmatite dome. Sample data for the original interpretation of the isograds, that have influenced all subsequent interpretations, are from Jansen & Schuiling (1976). Folding in these surfaces follow the general folding behaviour of present rock layers as the isograds froze in during extension (Wijbrans & McDougall 1988) and has probably seen some of the same E-W folding as the MCC. The 3D isograds extend from a depth of 1500 meters into the air where they are cut by the Naxos/Paros detachment surface (fig. 34). 2D sections of the metamorphic zones are presented below, one N-S (fig. 35) and one E-W (fig. 36). Figure 36a and 37a show the principal rock layers superimposed on the metamorphic sections to give an idea of their spatial relationship. Transects for these sections can be found in appendix 7. An image giving a better view of the inner isograds together with the migmatite dome is seen in appendix 9.

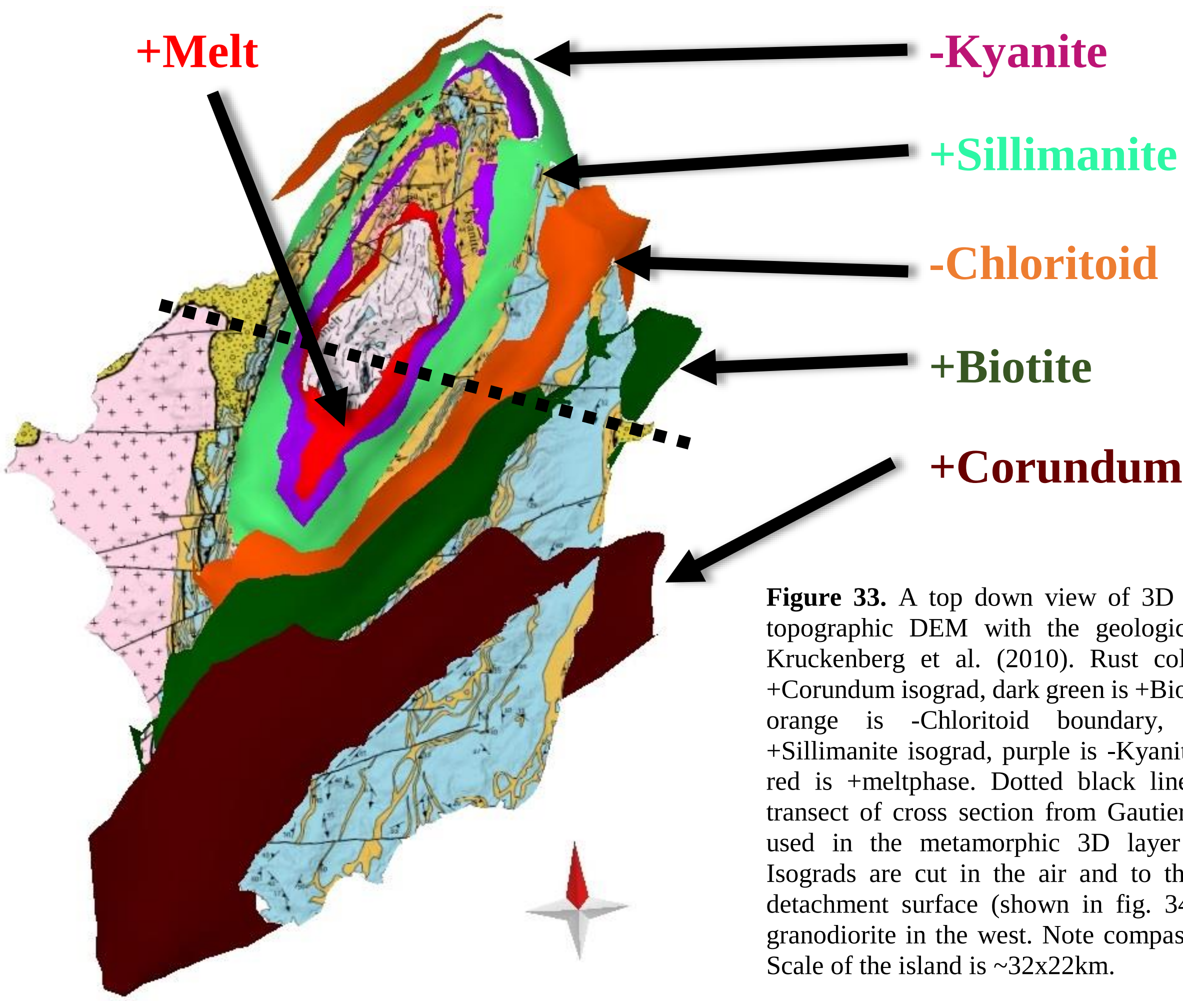

Figure 33. A top down view of 3D isograds on a topographic DEM with the geological map from Kruckenberg et al. (2010). Rust colored layer is +Corundum isograd, dark green is +Biotite boundary, orange is -Chloritoid boundary, turquoise is +Sillimanite isograd, purple is -Kyanite isograd and red is +meltphase. Dotted black line indicate the transect of cross section from Gautier et al. (1993) used in the metamorphic 3D layer construction. Isograds are cut in the air and to the east by the detachment surface (shown in fig. 34) and by the granodiorite in the west. Note compass for heading. Scale of the island is ~32x22km.

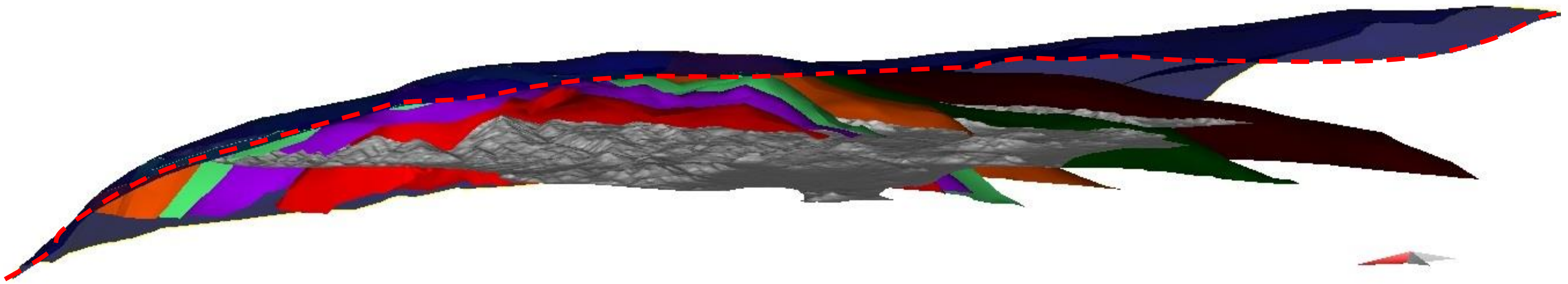

Figure 34. Metamorphic isograds cut by the detachment surface (dark blue) seen from the west, perspective is slightly top down. Dashed red line shows where the detachment is clipped by the section viewing plane. For additional information on layers refer to figure 33 above. Scale of the topographic DEM (white layer with shape of the island) is ~32x22km. Note compass in the bottom right for heading.

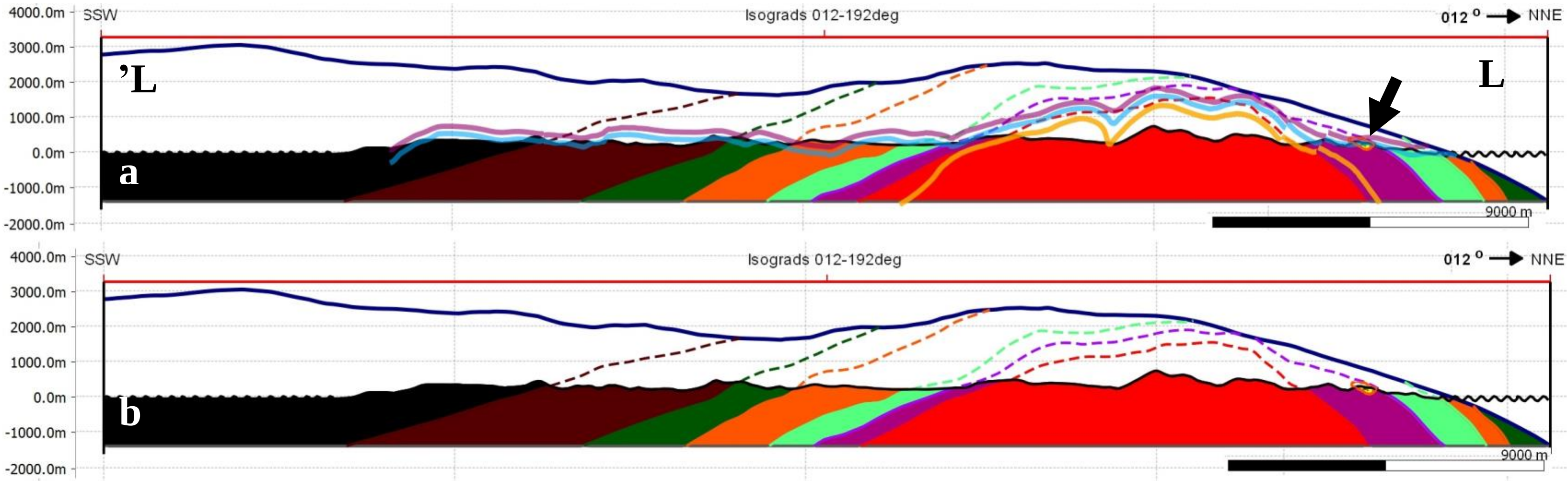

Figure 35a. S-N profile of isograds extending to the detachment plane (dark blue line) in 2D, constructed from the 3D model. Rock layer top boundary lines have been superimposed to show relationship between strata and metamorphic grade. Wavy horizontal line denotes sea surface. Black arrow points to the S-type granite. **35b.** Same S-N profile without the rock layers for clarity. Black unit is outside of Corundum isograd, for information on what the other colors represent refer to figure 33.

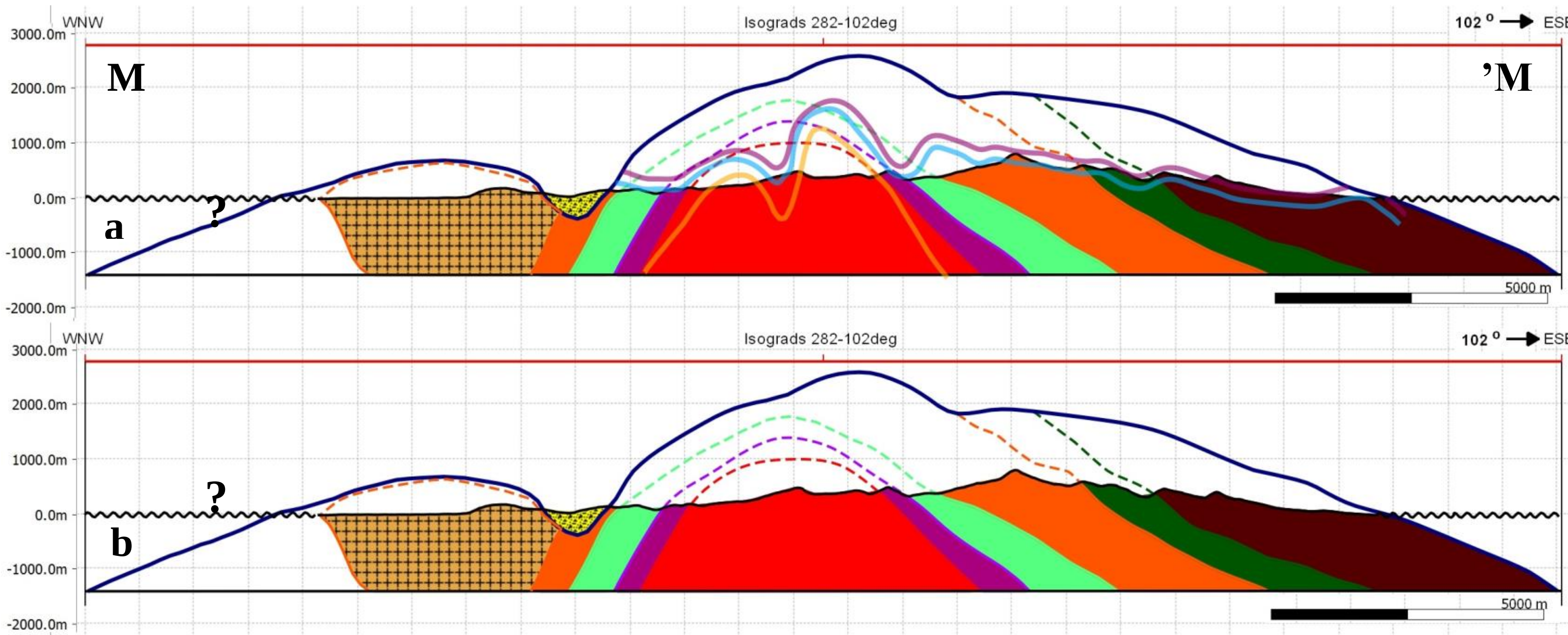

Figure 36a. W-E profile of isograds extending to the detachment plane (dark blue line) in 2D, constructed from the 3D model. Rock layer surface lines have been superimposed to show relationship between strata and metamorphic grade. Granodiorite (light brown) in the west cuts the -Chloritoid boundary below the detachment syncline. Late sediments (yellow) in the detachment hanging wall. Wavy horizontal line denotes sea surface. **36b.** Same W-E profile without the rock layers for clarity, for color coding information on the isograds refer to figure 33. Transects for sections in figures 35-36 are in appendix 7.

6.7. N-S extension and E-W shortening evaluation

Table 1 below lists the results for the calculations on finite extension/shortening made on the two separate 3D models with the units: Migmatite dome, Marble and Schist. Since there have been multiple phases of deformation and the migmatite formed during D_2, these results cannot be relied on to give exact numbers. Due to the difference in magnitude between N-S extension and E-W shortening (eg. Brichau et al 2006), and that there have been at least one N-S shortening event of unknown local magnitude prior to the N-S extension and E-W shortening it was not possible to constrain the geometrical starting point for calculating the Miocene extension from this model. Subsequently only the E-W shortening was successfully computed. The numbers are for average line length of the marble and schist horizons taken together and should only be considered a rough approximation. Sections used for the shortening estimation are shown in appendix 10-11 for model one and appendix 12-13 for model two. A graph illustrating shortening by section is presented in figure 37a. Transects and a 3D view of the sections in table 1 can be seen in figure 37b and 37c.

Table 1. Calculation of section shortening for 3D models one and two. L_f is the deformed length and L_0 is the unfolded line length. Section transects in figure 37b, complete sections in appendix 10-13.

Model-/ Section nr.	**Marble [m]**	**Schist [m]**	**L_f [m]**	**Average L_0 [m]**	**Extension/Shortening [%]**
Model1_section 1	16162	16047	16104.5	14784	-8.2
Model1_section 2	16553	16493	16523	15100	-8.6
Model1_section 3	16762	16548	16655	14959	-10.2
Model1_section 4	16007	15949	15978	14567	-8.8
Model1_section 5	17252	17189	17220.5	14270	-17.1
Model1_section 6	15788	15753	15770.5	13719	-12.6
Model1_section 7	15628	15612	15620	13646	-12.6
Model1_section 8	13333	13252	13292.5	11827	-11.0
Model1_section 9	7957	7925	7941	7508	-5.5
Model 1 Average					**-10.6**
Model2_section 1	15918	15822	15870	14784	-6.8
Model2_section 2	16021	15943	15982	15100	-5.5
Model2_section 3	15644	15562	15603	14671	-6.0
Model2_section 4	16275	16069	16172	14567	-9.9
Model2_section 5	17499	17366	17432.5	14270	-18.1
Model2_section 6	15829	15619	15724	13719	-12.8
Model2_section 7	16953	16740	16846.5	14682	-12.9
Model2_section 8	13208	13042	13125	11827	-9.9
Model2_section 9	8174	8085	8129.5	7508	-7.6
Model 2 Average					**-9.9**
Average shortening					**-10.3**

Average shortening at an axis perpendicular to the stretching direction is estimated at ~10%. Shortening was calculated to 10.6% for model one and 9.9% for model two. Taking all sections (N = 18) into account the results were 10.3% E-W shortening. The highest amount of shortening was achieved on sections 5-7 where the folding of the mantling rocks around the migmatite is very steep, as illustrated by figure 37a. The 2D and 3D interpretations in this work are believed to be conservative in respect to the wavelength and intensity of the E-W folds seen on Naxos. The 3D generated 2D sections above can be seen in appendix 10-11 to have the topographic surface sometimes lying above the upper boundary of the marble unit. This is an effect of the two layer model needing the marble to be of a consistent thickness to solve the island wide geometry and honor the data available. An attempt to address this was made in 3D model two and comparing the sections in appendix 10-11 (model one) to those in 12-13 (model two) a marked improvement can be seen in this respect.

Both models were used in the shortening calculations as they have different strengths and weaknesses. Numbers for individual models suggest no great difference in the shortening results but it is thought an average will provide some mitigation to interpretative error. Pre-extensional Cycladic crust is currently not well constrained and crustal stretching rate estimates for D_2 has ranged from 1.36 (eg. Faccenna et al. 2003) to 2 (eg. McKenzie 1978, Tirel et al. 2004) depending on the initial crustal thickness assumed and the mode of lithospheric extension. 320km total N-S Aegean extension over a NE-SW transect of 1200 km, calculated by Faccenna et al. (2003) produces extension on a factor of 1.36 (transect in fig. 38a). Interestingly section B-'B in Faccenna et al. (2003) ends at where the red line cuts the transect in figure 38a while the yellow line is exactly 1200 km long.

From exhumation rates and thermobarometry (Keay et al. 2001, Brichau et al. 2006, Seward et al. 2009, Ring et al. 2010) and on account of present crustal thickness beneath central Anatolia (Zhu et al. 2006) a pre-extensional Cycladic crustal thickness in the early Miocene of ~35 km can be assumed. A current crustal thickness of ~26 km, inferred from geophysical evidence (Tirel et al. 2004, Zhu et al. 2006, Sodoudi et al. 2006), gives a vertical crustal shortening of 9 km. This, assuming plane-strain and volume-constant deformation, equates to an extension of 1.35 (~35%) and vertical shortening of ~26%. It is however believed that local extension exceeds this factor, as indicated by movement on the Naxos /Paros extensional fault system (eg. Brichau et al. 2006). A 60 km section was made to coincide with the Naxos/Paros-Ios thermal anomaly on a NNE-SSW transect (fig. 38b) in the area of the Naxos/Paros detachment fault system.

Location and extent was decided on the grounds that weak, hot crust associated with the formation of MCC's could have facilitated a greater localized stretching here as has been shown for the Basin and Range province (eg. Gans 1978). Results from the simplified plane-strain equation for the Naxos transect using the 50 km extension from Brichau et al. (2006) gives an extensional factor of 1.83 and a shortening of ~45%.

Figure 37a. Data from table 1 presented as a diagram showing the sections in order, from south to north from both models. Model one is represented by blue diamonds and sections from model two are the orange squares.

37b. 3D view of the sections from model one used in the shortening calculations. Geologic map in b and c is modified from Cao et al. (2013). Note compass for heading.

37c. Transects (yellow lines) with the section numbers corresponding to those in the diagram shown on semi-transparent marble-, schist- and migmatite layers from model one.

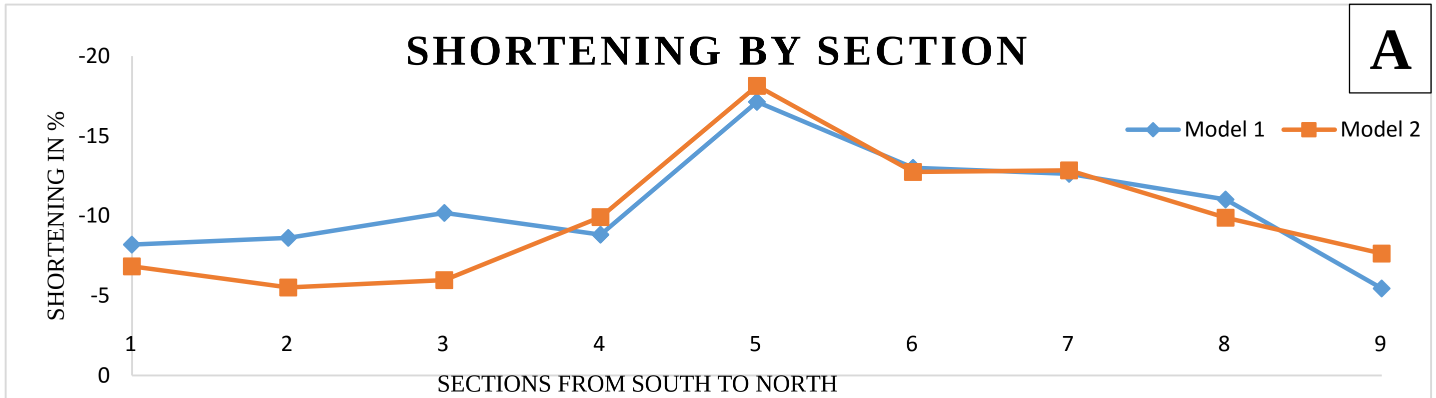

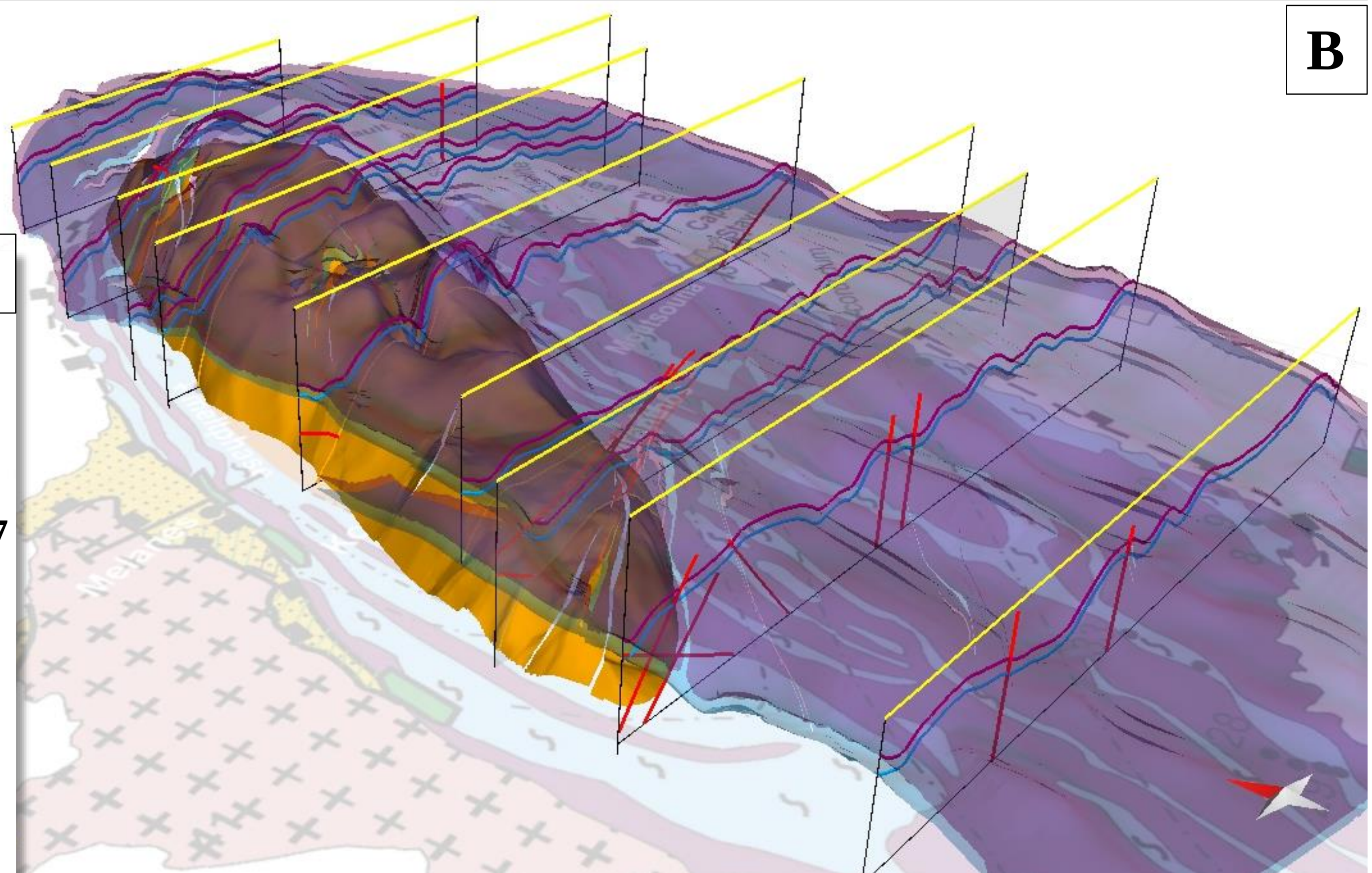

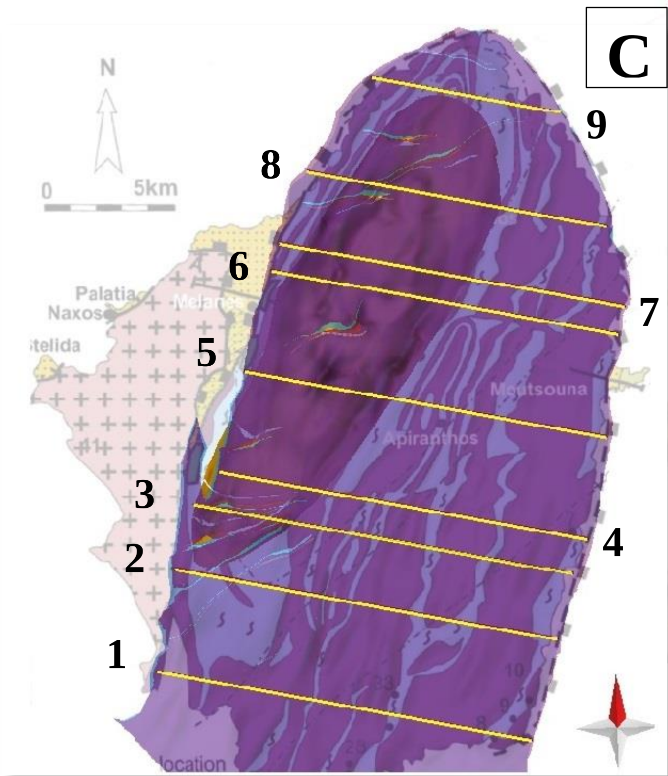

Figure 38a. 1200 km transect from Faccenna et al. (2003) superimposed on a satellite image modified from Google Earth. Red square denotes location of Naxos. Red line shows N-extent of section B-‘B in Faccenna et al. (2003). **38b.** Satellite image of Naxos modified from Google Earth. Yellow line shows the 60 km transect used in calculating the extension with displacement from Brichau et al. (2006). Dotted red line shows the Naxos/Paros-Ios thermal anomaly from Ring et al. (2010).

7. Discussion

7.1. Metamorphic isograds in relation to the detachment and E-W shortening

The metamorphic isograds on the geological map have largely the same asymmetrical shape as the migmatite dome (eg. fig. 33) but there are some differences. An area just north of the Melt-in isograd, the Kyanite-out isograd (fig. 39, dotted circle) follow the northernmost mantling folds (fig. 39, red lines). Since the isograds would originally be shaped by the local heat source (the migmatite) the geometry of the isograds should not follow folding in the mantling rocks, as they were not undisturbed before M_2. Looking at the 3D interpretation (fig. 27) its subsurface shape does not suggest the migmatite is the reason for the E-W folding of the isograd here. This leads to the same conclusion made by Urai et al. (1990), Buick et al. (1991), Forster in Lister & Forster (1997) and Avigad et al. (2001), that the isograds have been influenced by E-W shortening.

If indeed the isograds formed at ~16-15 Ma (Wijbrans & McDougall 1988) and the results of Brichau et al. (2006) that the brunt of extension was achieved between 16 and 8 Ma, holds true this indicates E-W shortening was coeval with N-S extension since at least 15 Ma. This has previously been cautiously suggested by Avigad et al. (2001). Due to the similar geometric behavior of the isograds and the mantling rocks the interpretation herein, for the purpose of constructing 3D surfaces, assumes they have the same general 'dip' to 'foliation'. Looking at the stereonet plot with data from outside the dome (fig. 25) the asymmetry seen is represented in the model by the gentler folding in the east in both rock layers and isograds. One definite way to test the 3D interpretation of metamorphic zonations would be to drill in the detachment syncline for the mantling sequence (fig. 36). This model predicts such a core would be found to be within the Chloritoid-out isograd and have a steep dip of the foliation plane to the west.

The small ellipsoidal Kyanite-out zonation to the east in figure 39 could belong to an underlying subdome of the same migmatite dome. While the asymmetry of the smaller Kyanite-out zonation could vary slightly due to a lack of data on its western boundary, the dataset from Jansen & Schuiling (1976) strongly suggest there is a separate zonation here on account of Kyanite having been found between the main- and northeastern zonations. Subdomes in the migmatite (eg. Kruckenberg et al. 2011) were a natural result of the conversion from 2D to 3D and it is unlikely that we see the full extent of the dome at the surface today, it could also be the effect of denudation on the exposed stratigraphy.

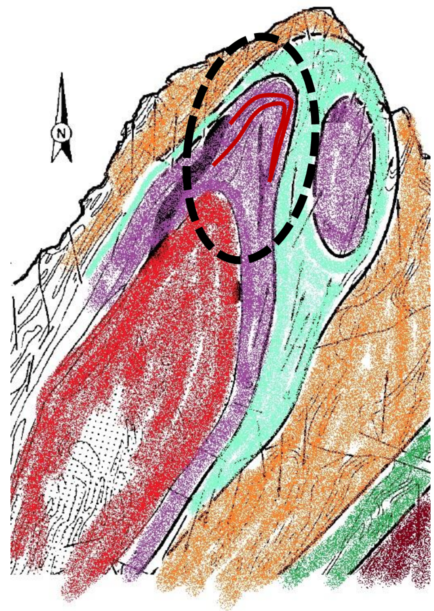

Figure 39. Metamorphic isograds on the northern part of Naxos, modified from Jansen & Schuiling (1976). Melt-in is red, Kyanite-out is purple, Sillimanite-in is turquoise. For additional information on zonations refer to figure 33.

It appears the detachment surface (N-S section in fig. 34, 35) cuts down section into the metamorphic isograds down profile seen from south to north, in the hanging wall transport direction of the detachment. This feature is concluded by Lister & Davis (1989) to be associated with the formation of mylonitic gneisses at depth in shallow-dipping ductile shear zones and typical for Metamorphic Core Complexes exhumed along detachment faults. Interestingly the conclusion by Lister & Davis (1989) was not reflected upon until after the 3D modeling was done and thus did not influence the making of the model.

It also looks as if the spacing of the zonations decreases toward the north, not entirely due to the migmatite (fig. 35a). This could simply be an effect of the section chosen or can perhaps be explained by the more rapid cooling during exhumation experienced near or at the detachment (Lister et al. 1984, Gautier et al. 1993). The age relationship between the static state of the isograds and the formation and propagation of the detachment is a crosscutting one, the brittle manifestation of the detachment is thus younger than the freezing in of the isograds. This conclusion strengthens the interpretation of E-W folds on the detachment surface, as the isograds themselves are affected by the E-W shortening component.

7.2. The role of NNE-striking strike slip- and E-W striking normal faults

Despite not finding evidence for any strike slip component to the fault in figure 11 it is likely that, due to its location, it is part of a swarm of dextral strike slip faults. These faults are crosscutting the southernmost part of the migmatite and surrounding mantling rocks (fig 9). With regional NNE-SSW extension with WNW-ESE shortening (Avigad et al. 2001) kinematics in the brittle regime, it is entirely possible that most faults on Naxos have an oblique sense of shear because of the transtensional strain regime the alignment of the faults seem to indicate (fig. 21, inset). Key faults are accounted for in the model (appendix 8) and apart from the detachment there seems to be no evidence of large scale displacement looking at where the NNE-SSW strike slip- and E-W normal faults pinch out on geologic maps. Seward et al. (2009) presented fission track ages for faults on Naxos described by Siebenaller (2008) and concluded that the vertical displacement for these faults was not statistically offsetting the age estimates for foot- and hanging wall. This speaks against any significant vertical component for these faults.

7.3. Detachment geometry, E-W shortening and tectonic implications

It has been shown that N-S extension surpassed E-W shortening by at least a factor of 4. It is inviting to suggest that a substantial part of the E-W shortening seen on Naxos is connected to the formation of the migmatite, itself thought to be a consequence of the N-S extension (Vanderhaeghe et al. 2007). Continuing this line of thought one could perhaps isolate the E-W shortening more likely to be associated with the constrictional component to extension by looking at the numbers for sections 1-3 and 9 in figure 37a. It seems ~7% is a reasonable estimate when the central, more highly deformed sections are filtered away.

There are two main models of extension related to detachment faulting: Simple shear (eg. Wernicke 1981, 1985) and Flexural rotation or Rolling hinge (eg. Buck 1988). These models have different implications for the initial formation and geometry of detachment faults and require wholly different crustal structures (Zhu et al. 2006). The southern termination of the Naxos/Paros detachment discussed below is one such feature. There is support for both models as the low angle geometry of said detachment indicates simple shear while decaying Moho topography (Zhu et al. 2006) suggests a rolling hinge model as the Aegean Moho is elevated beneath several large scale normal faults (Makris & Stobbe 1984).

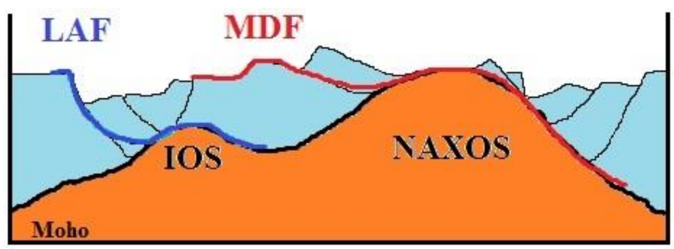

Figure 40. S-N profile of Naxos and Ios, freely after Brun et al. (1994). The main detachment fault (MDF) in red, listric accommodation fault (LAF) in blue.

In reconstructing the 3D geometry of the Naxos/Paros detachment, outside of the established constraints in the east and west, some assumptions made will be clarified. The continuation of the surface in a north-south profile was, as mentioned in the method section, based initially on how Gautier & Brun (1994) envisioned the propagation and gradual decrease in angle of main detachment faults. Additionally, the work of Mizera & Behrmann (2015) on the Ios detachment helped visualize how the Naxos/Paros detachment folds N-S into the 'Ios-Naxos structural synclinal' south of Naxos, although their interpretation would mean the very south of this models detachment surface should be dipping south.

Utilizing the analogue modeling of Brun et al. (1994) granted another solution. The illustration seen in figure 40 visualizes one possible explanation for the detachment geometry in this model. It could be that the detachment on Ios is in fact a listric accommodation fault.

The general N-S profile of the detachment on Naxos (MDF in fig. 40) is supported by the interpretation in Jolivet et al. (2004b), which is based on the work of Gautier et al. (1993). Another explanation, originally envisioned by Lister & Davis (1989), is that of multiple detachment faults forming from the same 'master detachment fault' during the temporal evolution of extension and MCC formation. Applied to this scenario the Naxos/Paros detachment (MDF in fig. 40) would be a younger fault propagating from the basement culmination (Naxos dome in fig. 40) as the older master fault surface (LAF in fig. 40) becomes progressively more bowed (eg. Buck 1988). This would also produce much the same detachment geometry as has been modeled in this work. The hanging wall transport direction on Ios is however described by Vandenberg & Lister (1996) as south to southwest. Structural work by Grütter (1993) and Thomson et al. (2009) however, found evidence for alternating top-N and top-S shear bands on the northern part of the island. Thomson et al. (2009) goes on to suggest that Ios hosts a bivergent, antithetic fault system to the dominant Naxos/Paros detachment. This interpretation does not contradict the 3D detachment geometry achieved in this work and serves to put the southern termination of the detachment in context.

Given the comparatively low angle of the Naxos/Paros detachment as it enters the seabed surrounding the northwest, north and the entire east coast of Naxos, seismic imaging would probably yield extensive information about the geometry of the fault system and how it propagates in the southeast. Data of this kind would greatly constrain future modeling of the detachment as in this work the main geometric shape of the 3D detachment was envisioned to have influenced and been influenced by the rising migmatite dome, displayed in the similar geometry. This would also provide valuable constraints on future local N-S extensional estimates based on the Naxos/Paros detachment.

Assessment of N-S extension is problematic at best as proper constraints for the crustal thickness and lithospheric mode of extension in the early Miocene are lacking. Results presented in this work favor the approach in where a large part of the extension is localized to where the MCC's are formed (eg. Ring et al. 2010), an environment where high heat flow produces an elevated and weak ductile crust that can accommodate more stretching. It is evident from studying the diagram in figure 37a that E-W shortening amplitude correlates with the metamorphic grade of the exposed rocks (fig. 33 for reference). It follows logic that the same should apply to the N-S extension.

High grade conditions in the migmatite reported by many authors and the high topography surrounding the migmatite on Naxos supports this weak/thin upper crust scenario (eg. Wernicke 1990). This is reflected in the choice of end points for the N-S extension assessment in figure 38b as it coincides with the Naxos/Paros thermal anomaly argued by Ring et al. (2010) to be at the center of maximum Cycladic-wide extension. The stretching results for the Naxos transect is therefore suggested to be viewed as the maximum localized extension to have taken place in the Cyclades.

It was important not to overextend the transect so as not to impinge on the Mykonos/Tinos detachment system (eg. Avigad et al. 1998) nor come too close to Ios. On the other hand too short a section would produce an exorbitant amount of estimated crustal thinning. It will be stated that the results are completely dependent on these choices and bear any shortcomings of the arguments backing them.

Previous extension rates supporting the calculated local extension of 83%, from Tirel et al. (2004) and McKenzie (1978), are based on the assumption of whole crust simple shear and an initial vertical thickness of ~50 km, inferred from that of continental Greece and estimated for the entire region. Small regional estimates on a factor of ~1.4 (eg. Angelier et al. 1982, Faccenna et al. 2003, Zhu et al. 2006) are close to the regional estimate calculated in this work (1.35). As previously stated, pre-extension constraints are missing for all these estimates making them unreliable. To become meaningful, extension rates can provide a framework for the E-W shortening component. With an extension of a factor of 1.35, ~26% shortening is needed to prevent crustal thinning. Assuming the Naxos transect (fig. 38b) is not too far off and the data from Brichau et al. (2006) is robust, a shortening of ~45% is required to maintain local crustal thickness. E-W shortening results presented in this work (~7-10%) thus suggest crustal thinning due to N-S extension cannot have been balanced by E-W shortening. This statement stands in contrast to the conclusion in Avigad et al. (2001), that E-W folding balanced Cycladic crustal thinning related to N-S extension in the Miocene. The shortening results herein could of course be too conservative but the difference between 10% (highest shortening estimate from the 3D models) and 26% (resultant shortening from smallest estimated regional extension) is substantial.

It becomes obvious that constant volume cannot be assumed. The question then becomes one of exploring where the local crust not accounted for by ~7-10% shortening comes from. Although it was stated by Zhu et al. (2006) that current crustal viscosity in the Cyclades is three times that of the Basin and Range province (eg. Gans 1978), by itself this does not exclude the possibility that ductile crust facilitated the mass transfer and compensated crustal thinning in the Miocene. Conceivably the geodynamic difference to the Basin and Range of the western United States lies in that the whole (ductile) crust was not uniformly stretched in the Cyclades. This would in part explain the Moho topography observed by Zhu et al. (2006). A thin and weak crust beneath the MCCs could have accommodated this localized extension and Wernicke (1990) suggested mass inflow be facilitated by less viscous crust in such a scenario. Alternately crustal delamination, in much the same way as was envisioned by Gans (1978) for the Basin and Range, would have led to lateral extrusion of the lower crust from surrounding areas in a hot, delaminated region (eg. Bird 1991).

Solving the mass balance of the Cyclades is far beyond the scope of this thesis and the same must be said of the cause for E-W shortening. Perhaps it was simply the concave geometry of the migrating subduction zone that provided the seed. Gravity spreading experiments by Gautier et al. (1999) produced similar kinematics as seen in the Aegean and coupled with an elevated geothermal gradient due to crustal thinning, the interplay between tectonic stress and plate geometry could have provided the impetus for E-W folding on Naxos during extension in the Miocene.

7.4. Stratigraphy

The Attic Cycladic Massif formed as a fore arc accretionary thrust in the Eocene and Oligocene (Ring et al. 1999, Ring & Layer 2003, Ring et al. 2010) and what was seen at the southeast coast (fig 13-15), could well be traces of this event (D_1). Thrusting between the lower units in a N-S compressional regime might have resulted in what looks like duplexes or an imbricate fan. E-W shortening (fig 15) in the SE was interpreted as part of the extensional D_2 event. Being able to date these sub units would greatly aid in the interpretation.

After having been in the field it was evident that the marble and schist horizons, modeled in 2- and 3D as two separate massive units, are in reality a complex metasedimentary sequence with frequently occurring interlayering. To get the folding geometries right as well as accuracy in fault displacement, identification of specific stratigraphic layers within this succession seems the logical next step. One way to achieve this could be Rb/Sr dating of the carbonate layers. While extremely work-intensive, since samples need to cover most of the exposed carbonates island wide, this method is not particularly sensitive to metamorphism in carbonates. The method should work assuming the depositional timing, in relation to the established seawater curve for $^{87}Sr/^{86}Sr$ (eg. McArthur et al. 2001), of the Naxos carbonates are favorable and that no element exchange has occurred between the carbonates and the clastics (Johannes Glodny pers comm.). Gaertner et al. (2011) had limited success using this method in the Cyclades (including Naxos) and also described Oxygen and Carbon dating with the same aim done in previous studies. Their conclusion seemed to be that at present, Rb/Sr-, O- and Carbon dating of individual marble horizons does not give unequivocal evidence for their stratigraphic relationship.

7.5. Closing thoughts on structural trends and the granodiorite

Of the complete dataset in figure 32, 63% is from the migmatite dome and these measurements are overrepresented in the more steeply dipping clusters. While the reversal in trend from north to south of the fold axis between stereonet plots (fig. 10, 24 and 25) can look confusing it is important to take into account the main fold axis of the entire set (~013°/05°). Considering the ~30° N-plunge of the fold axis in the north to a ~04° N-plunge in the outer central parts of the island (fig. 25), the alternating N-S plunge of the fold axis between plots is probably just an effect of the doming structure of the island being reflected in the main fold axis through the axial plane depending on data subset. E-W folding in the model agrees well with what was seen in the field.

The MCC plots somewhat like a narrow hinge fold. This is possibly due to the less competent meta-sediment sequence getting squeezed into overturned to recumbent folding patterns E and W of the migmatite, indicated by Avigad et al. (2001) to be associated with a deeper crustal level, which seems likely considering the island is host to rocks that have been at 10-15 Kbar (Gautier et al. 1993 and sources therein, Duchêne et al. 2006).

As a structural 3D model on a scale of ~45x30x6km there is only so much that can be done with surface measurements alone. Fieldwork helped constrain the model but more time would be needed for a comprehensive fault analysis study and across profile structural mapping with the stated goal of producing data for 3D modeling. Given the terrain, fenced off private property and infrastructure on Naxos this could prove time consuming. Reliable quantification of both strike slip and normal faults on the island as well as dating of marble horizons, seismic surveying and actual drill core data would benefit future 3D modeling of Naxos. It is important to remember that the shortening values from the geological interpretation in this work is exactly that. This is true of all such calculations based on interpretive data, a fact perhaps mitigated but not fundamentally altered by additional data.

Brun et al. (1990) observed that analyzing the shape of plutons gives clues as to the regional tectonics when they are syntectonically emplaced. Looking at the local crustal thickness (eg. Tirel et al. 2004) it seems possible that the Naxos granodiorite is the northeastern tip of a deeply rooted batholith to the southwest, south of Naxos and Paros. This could well be what the northward younging of the granodiorite in apatite- and zircon fission tracks (Seward et al. 2009) indicate. Perhaps greater knowledge of the granodiorites large scale geometry could shed light on the interaction between N-S extension and E-W shortening in middle-late Miocene. Because of time constraints and the granodiorite not being the focus of modeling this could not be explored further. The 3D granodiorite layer does however display a deepening to the southwest to reflect on this line of reasoning.

8. Conclusion

The most important conclusion to this work is the calculated, presumably D_2 related, E-W shortening of ~7-10%. These findings should be taken in the context of localized extension on a factor of ~1.83, mainly achieved by movement on the Naxos/Paros detachment fault within a regional Cycladic stretching of ~1.35 between ~16-8 Ma (Brichau et al. 2006). The shortening results contradict part of the conclusion in Avigad et al. (2001) that E-W shortening compensated for crustal thinning during N-S extension in the Miocene. It is concluded that constant volume assumptions cannot be made for the Cycladic crust since the early Miocene on account of ≥26% shortening needed to maintain crustal thickness and that the contribution of E-W shortening in mitigating crustal thinning is small.

Additionally the results indicate a Cycladic-wide maximum local N-S extension was achieved in the Naxos/Paros thermal anomaly (eg. Ring et al. 2010), mainly on the Naxos/Paros detachment system. If this localized extensional mode can be confirmed the similarities with the Basin and Range province of the United States (eg. Gans 1978) give clues as to how mass transfer can be accounted for (eg. inflow of ductile lower crust from surrounding areas), providing an explanation for the anomalously thick crust despite extensional thinning in the Miocene.

Given the assumption the 3D model produced is a reasonably accurate approximation of the geology on Naxos, another progress worth noting is the geometric relationship between the migmatite, mantling rocks, Naxos/Paros detachment and the metamorphic zonations which seem to indicate that E-W shortening was coeval to N-S extension at least since 15 Ma.

A more complex model is needed to increase accuracy, something not possible within the timeframe of this project. It is doubtful if a more highly resolved model can be achieved without extensive fieldwork and a better understanding of the meso-scale stratigraphy of the island. As it stands this work will hopefully help give a clearer picture of how the Cyclades has been evolving structurally.

9. Acknowledgements

The field study was partly funded by Stockholm University. I would like to thank my supervisor, Prof. Uwe Ring for giving me this opportunity to work with him, for sharing his knowledge of the region, helping clear up misconceptions on my part and for his constructive input and reviews of my manuscript. Acknowledgement is due to my co-supervisor Reuben Hansman, for his tireless efforts to answer my many questions about the software and insightful advice given from the early stages through the field excursion to the very end. I would have been lost without you. Thanks to Johannes Glodny for the discussion on Rb/Sr dating and other insights in the field. Alexandre Peillod is thanked for sharing his geological knowledge of Naxos, driving like a Frenchman and for obtaining literature otherwise hard to come by. I would also like to mention my wife Jessica for supporting me in this endeavor and my children, for reminding me there is more to life than Geology.

10. References

Allmendinger, R. W., Cardozo, N. C., and Fisher, D., 2013, Structural Geology Algorithms: Vectors & Tensors: Cambridge, England, Cambridge University Press, 289 pp.

Andriessen, P. A. M., Boelrijk, N. A. I. M., Hebeda, E. H., Priem, H. N. A., Verdurnen, E. T., & Verschure, R. H. (1979). Dating the events of metamorphism and granitic magmatism in the Alpine Orogen of Naxos (Cyclades, Greece). *Contributions to Mineralogy and Petrology*, *69*(3), 215-225.

Avigad, D. (1998). High-pressure metamorphism and cooling on SE Naxos (Cyclades, Greece). *European Journal of Mineralogy*, *10*(6), 1309-1319.

Avigad, D., Ziv, A., & Garfunkel, Z. (2001). Ductile and brittle shortening, extension-parallel folds and maintenance of crustal thickness in the central Aegean (Cyclades, Greece). *Tectonics*, *20*(2), 277-287.

Bird, P. (1991). Lateral extrusion of lower crust from under high topography in the isostatic limit. *Journal of Geophysical Research: Solid Earth (1978–2012)*, *96*(B6), 10275-10286.

Bolhar, R., Ring, U., & Allen, C. M. (2010). An integrated zircon geochronological and geochemical investigation into the Miocene plutonic evolution of the Cyclades, Aegean Sea, Greece: Part 1: Geochronology. *Contributions to Mineralogy and Petrology*, *160*(5), 719-742.

Brichau, S., Ring, U., Ketcham, R. A., Carter, A., Stockli, D., & Brunel, M. (2006). Constraining the long-term evolution of the slip rate for a major extensional fault system in the central Aegean, Greece, using thermochronology. *Earth and Planetary Science Letters*, *241*(1), 293-306.

Brun, J. P., Gapais, D., Cogne, J. P., Ledru, P., & Vigneresse, J. L. (1990). The Flamanville granite (northwest France): an unequivocal example of a syntectonically expanding pluton. *Geological Journal*, *25*(3-4), 271-286.

Buck, W. R. (1988). Flexural rotation of normal faults. *Tectonics*, *7*(5), 959-973.

Buick, I. S. (1991). Mylonite fabric development on Naxos, Greece. *Journal of Structural Geology*, *13*(6), 643-655.

Cao, S., Neubauer, F., Bernroider, M., & Liu, J. (2013). The lateral boundary of a metamorphic core complex: The Moutsounas shear zone on Naxos, Cyclades, Greece. *Journal of Structural Geology*, *54*, 103-128.

Cardozo, N., and Allmendinger, R. W., 2013, Spherical projections with OSXStereonet: Computers & Geosciences, v. 51, no. 0, p. 193 - 205, doi: 10.1016/j.cageo.2012.07.021

Duchêne, S., Aissa, R., & Vanderhaeghe, O. (2006). Pressure-temperature-time evolution of metamorphic rocks from Naxos (Cyclades, Greece): constraints from thermobarometry and Rb/Sr dating. *Geodinamica Acta*, *19(5)*, 301-321.

Dürr, S., Altherr, R., Keller, J., Okrusch, M., & Seidel, E. (1978). The median Aegean crystalline belt: stratigraphy, structure, metamorphism, magmatism. *Alps, Apennines, Hellenides*, *38*, 455-476.

Faccenna, C., Jolivet, L., Piromallo, C., & Morelli, A. (2003). Subduction and the depth of convection in the Mediterranean mantle. *Journal of Geophysical Research: Solid Earth (1978–2012)*, *108*(B2).

Gaertner, C., Broecker, M., Strauss, H., & Farber, K. (2011). Strontium-, carbon-and oxygen-isotope compositions of marbles from the Cycladic blueschist belt, Greece. *Geological Magazine*, *148*(04), 511-528.

Gans, P. B. (1987). An open-system, two-layer crustal stretching model for the Eastern Great Basin. *Tectonics*, *6*(1), 1-12.

Gautier, P., Brun, J. P., & Jolivet, L. (1993). Structure and kinematics of Upper Cenozoic extensional detachment on Naxos and Paros (Cyclades Islands, Greece). *Tectonics*, *12*, 1180-1194.

Grütter, H. S. (1993). *Structural and metamorphic studies on Ios, Cyclades, Greece* (Doctoral dissertation, University of Cambridge).

Huet, B., Labrousse, L., & Jolivet, L. (2009). Thrust or detachment? Exhumation processes in the Aegean: insight from a field study on Ios (Cyclades, Greece). *Tectonics*, *28*(3).

Jansen, J. B. H. (1973). Geological Map of Greece, Island of Naxos (1:50,000). *Institute for Geology and Mineral Resources, Athens*.

Jansen, J. B. H., & Schuiling, R. D. (1976). Metamorphism on Naxos; petrology and geothermal gradients. *American Journal of Science*, *276*(10), 1225-1253.

Jansen, J. B. H. (1977). *The geology of Naxos* (Vol. 19, No. 1-3). Institute of geological and mining research.

Jolivet, L., Rimmelé, G., Oberhänsli, R., Goffé, B., & Candan, O. (2004). Correlation of syn-orogenic tectonic and metamorphic events in the Cyclades, the Lycian nappes and the Menderes massif. Geodynamic implications. *Bulletin de la Société Géologique de France*, *175*(3), 217-238.

Jolivet, L., Famin, V., Mehl, C., Parra, T., Aubourg, C., Hébert, R., & Philippot, P. (2004b). Strain localization during crustal-scale boudinage to form extensional metamorphic domes in the Aegean Sea. *Geological Society of America Special Papers*, *380*, 185-210.

Jolivet, L., & Brun, J. P. (2010). Cenozoic geodynamic evolution of the Aegean. *International Journal of Earth Sciences*, *99*(1), 109-138.

Jolivet, L., Lecomte, E., Huet, B., Denèle, Y., Lacombe, O., Labrousse, L. & Mehl, C. (2010b). The north cycladic detachment system. *Earth and Planetary Science Letters*, *289*(1), 87-104.

Keay, S., Lister, G., & Buick, I. (2001). The timing of partial melting, Barrovian metamorphism and granite intrusion in the Naxos metamorphic core complex, Cyclades, Aegean Sea, Greece. *Tectonophysics*, *342*(3), 275-312.

Kruckenberg, S. C., Ferré, E. C., Teyssier, C., Vanderhaeghe, O., Whitney, D. L., Seaton, N. C., & Skord, J. A. (2010). Viscoplastic flow in migmatites deduced from fabric anisotropy: An example from the Naxos dome, Greece. *Journal of Geophysical Research: Solid Earth (1978–2012)*, *115*(B9).

Kruckenberg, S. C., Vanderhaeghe, O., Ferré, E. C., Teyssier, C., & Whitney, D. L. (2011). Flow of partially molten crust and the internal dynamics of a migmatite dome, Naxos, Greece. *Tectonics*, *30*(3).

Lister, G. S., Banga, G., & Feenstra, A. (1984). Metamorphic core complexes of Cordilleran type in the Cyclades, Aegean Sea, Greece. *Geology*, *12*(4), 221-225.

Lister, G. S., & Davis, G. A. (1989). The origin of metamorphic core complexes and detachment faults formed during Tertiary continental extension in the northern Colorado River region, USA. *Journal of Structural Geology*, *11*(1), 65-94.

Lister, G. S., & Forster, M. (Eds.). (1997). *Inside the Aegean metamorphic core complexes*: a field trip guide illustrating the geology of the Aegean metamorphic core complexes: Thera, Ios, Naxos and Paros (Vol. 45). Australian Crustal Research Centre.

Makris, J., & Stobbe, C. (1984). Physical properties and state of the crust and upper mantle of the Eastern Mediterranean Sea deduced from geophysical data. *Marine Geology*, *55*(3), 347-363.

McArthur, J. M., Howarth, R. J., & Bailey, T. R. (2001). Strontium isotope stratigraphy: LOWESS version 3: best fit to the marine Sr-isotope curve for 0–509 Ma and accompanying look-up table for deriving numerical age. *The Journal of Geology*, *109*(2), 155-170.

McKenzie, D. (1978). Active tectonics of the Alpine—Himalayan belt: the Aegean Sea and surrounding regions. *Geophysical Journal International*, *55*(1), 217-254.

Mizera, M., & Behrmann, J. H. (2015). Strain and flow in the metamorphic core complex of Ios Island (Cyclades, Greece). *International Journal of Earth Sciences*, 1-14.

Philippon, M., Brun, J. P., & Gueydan, F. (2012). Deciphering subduction from exhumation in the segmented Cycladic Blueschist unit (Central Aegean, Greece). *Tectonophysics*, *524*, 116-134.

Ramsay, J. G., & Huber, M. I. (1987). *The techniques of modern structural geology: Folds and fractures* (Vol. 2). Academic press.

Ring, U., Laws, S., & Bernet, M. (1999). Structural analysis of a complex nappe sequence and late-orogenic basins from the Aegean Island of Samos, Greece. *Journal of Structural Geology*, *21*(11), 1575-1601.

Ring, U., & Layer, P. W. (2003). High-pressure metamorphism in the Aegean, eastern Mediterranean: Underplating and exhumation from the Late Cretaceous until the Miocene to Recent above the retreating Hellenic subduction zone. *Tectonics*, *22*(3).

Ring, U., Thomson, S. N., & Bröcker, M. (2003). Fast extension but little exhumation: the Vari detachment in the Cyclades, Greece. *Geological Magazine*, *140*(03), 245-252.

Ring, U., Glodny, J., Will, T., & Thomson, S. (2010). The Hellenic subduction system: high-pressure metamorphism, exhumation, normal faulting, and large-scale extension. *Annual Review of Earth and Planetary Sciences*, *38*, 45-76.

Schellart, W. P. (2005). Influence of the subducting plate velocity on the geometry of the slab and migration of the subduction hinge. *Earth and Planetary Science Letters*, *231*(3), 197-219.

Seward, D., Vanderhaeghe, O., Siebenaller, L., Thomson, S., Hibsch, C., Zingg, A. & Duchêne, S. (2009). Cenozoic tectonic evolution of Naxos Island through a multi-faceted approach of fission-track analysis. *Geological Society, London, Special Publications*, *321*(1), 179-196.

Sodoudi, F., Kind, R., Hatzfeld, D., Priestley, K., Hanka, W., Wylegalla, K., ... & Bohnhoff, M. (2006). Lithospheric structure of the Aegean obtained from P and S receiver functions. *Journal of Geophysical Research: Solid Earth (1978–2012)*, *111*(B12).

Siebenaller, L. (2008). Circulations fluides au cours de l'effondrement d'un prisme d'accrétion crustal: l'exemple du" Metamorphic Core Complex" de l'île de Naxos (Cyclades, Grèce) (Doctoral dissertation, Nancy 1).

Tirel, C., Gueydan, F., Tiberi, C., & Brun, J. P. (2004). Aegean crustal thickness inferred from gravity inversion. Geodynamical implications. *Earth and Planetary Science Letters*, *228*(3), 267-280.

Thomson, S. N., Ring, U., Brichau, S., Glodny, J., & Will, T. M. (2009). Timing and nature of formation of the Ios metamorphic core complex, southern Cyclades, Greece. *Geological Society, London, Special Publications*, *321*(1), 139-167.

Urai, J. L., Schuiling, R. D., & Jansen, J. B. H. (1990). Alpine deformation on Naxos (Greece). *Geological Society, London, Special Publications*, *54*(1), 509-522.

Vandenberg, L. C., & Lister, G. S. (1996). Structural analysis of basement tectonites from the Aegean metamorphic core complex of Ios, Cyclades, Greece. *Journal of Structural Geology*, *18*(12), 1437-1454.

Vanderhaeghe, O. (2004). Structural development of the Naxos migmatite dome. *Geological Society of America Special Papers*, *380*, 211-227.

Vanderhaeghe, O., Hibsch, C., Siebenaller, L., Martin, L., Duchêne, S., de St Blanquat, M., Kruckenberg, S., Fotiadis, A. (2007) Penrose Conference - Extending a Continent, Naxos Field Guide. *Journal of the Virtual Explorer.* DOI: 10.3809/jvirtex.2007.00175

Wernicke, B. (1981). Low-angle normal faults in the Basin and Range Province: nappe tectonics in an extending orogen. *Nature*, *291*, 645-648.

Wernicke, B. (1985). Uniform-sense normal simple shear of the continental lithosphere. *Canadian Journal of Earth Sciences*, *22*(1), 108-125.

Wernicke, B. (1990). The fluid crustal layer and its implications for continental dynamics. In *Exposed cross-sections of the continental crust* (pp. 509-544). Springer Netherlands.

Wijbrans, J. R., & McDougall, I. (1988). Metamorphic evolution of the Attic Cycladic Metamorphic Belt on Naxos (Cyclades, Greece) utilizing 40Ar/39Ar age spectrum measurements. *Journal of Metamorphic Geology*, *6*(5), 571-594.

Zhu, L., Mitchell, B. J., Akyol, N., Cemen, I., & Kekovali, K. (2006). Crustal thickness variations in the Aegean region and implications for the extension of continental crust. *Journal of Geophysical Research: Solid Earth (1978–2012)*, *111*(B1).

11. Appendix

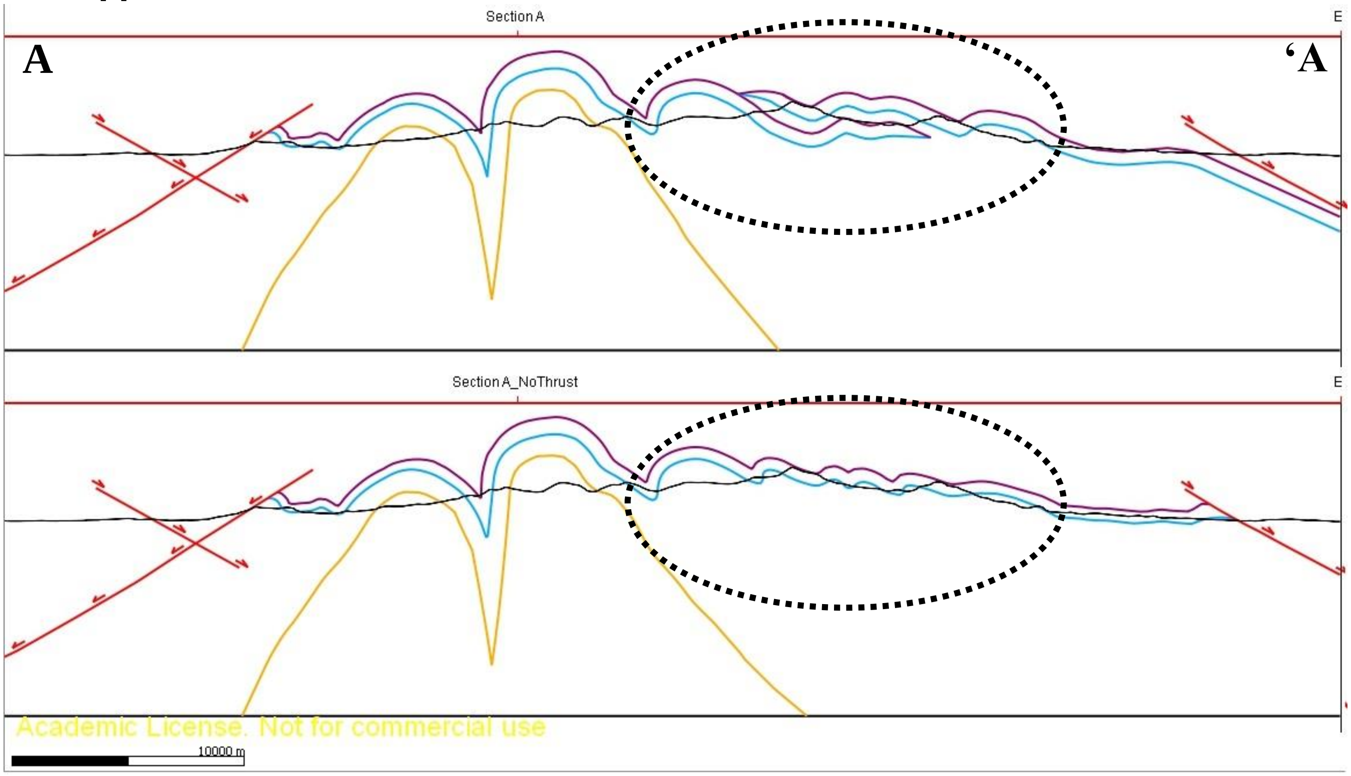

Appendix 1. Section A-'A with interpreted thrust (top) and final interpretation (bottom). Dotted black circle shows the difference in interpretations. Purple is the marble layer, blue is schist and yellow is the migmatite. Red lines are faults and the black line is the topographic relief.

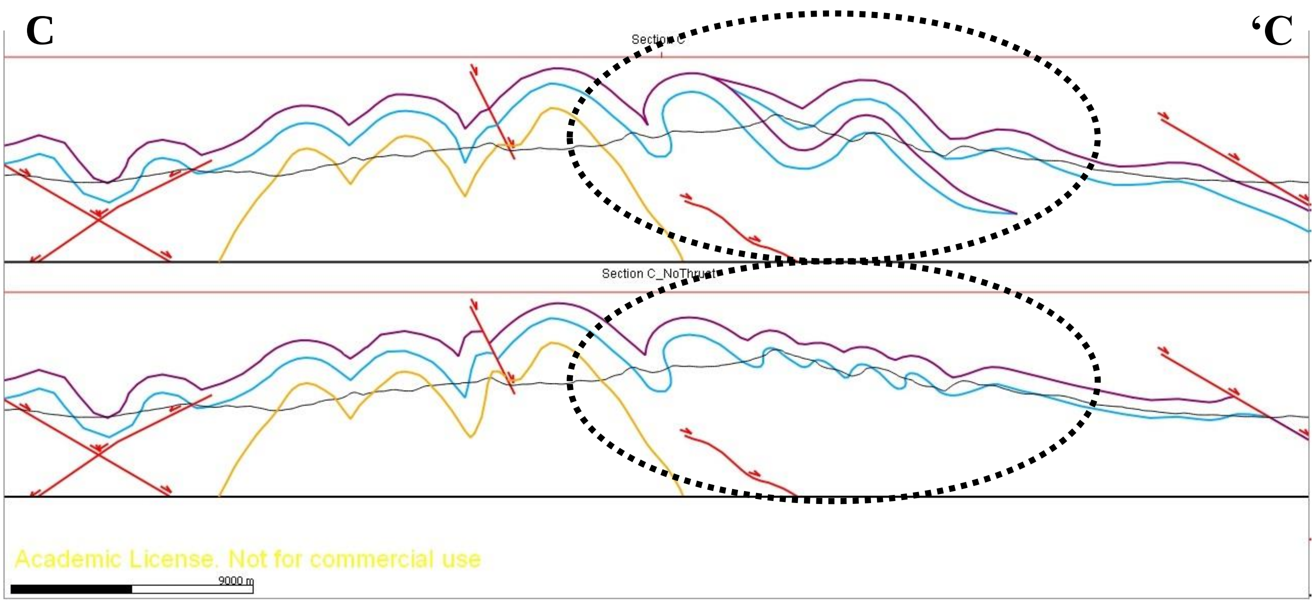

Appendix 2. Section C-'C with interpreted thrust (top) and final interpretation (bottom). Dotted black circle shows the difference in interpretations. Purple is the marble layer, blue is schist and yellow is the migmatite. Red lines are faults and the black line is the topographic relief.

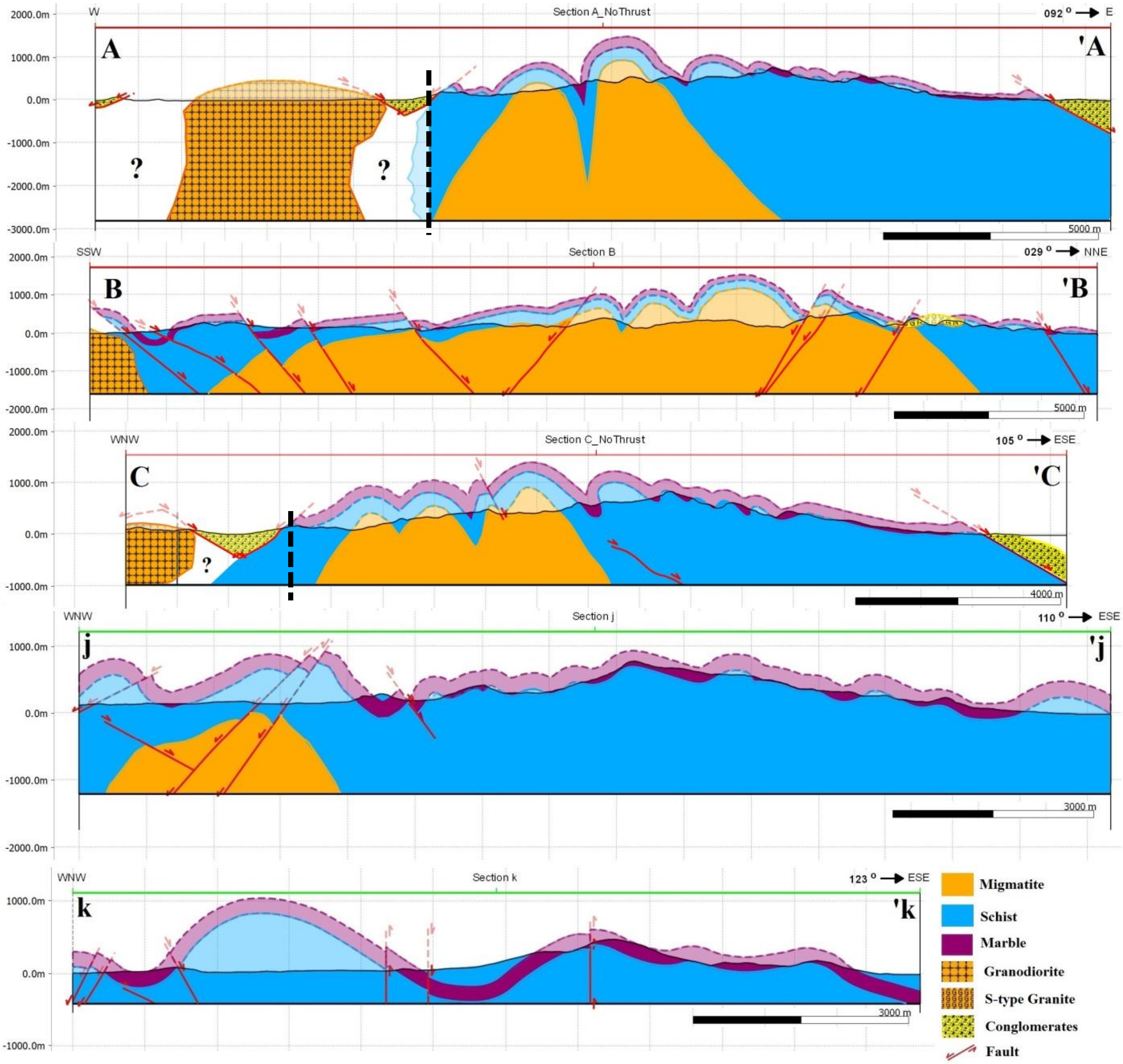

Appendix 3. Sections A-'A, C-'C, j-'j and k-'k after 2D balancing. Black line is the topographic relief. Dashed black line in A-'A and C-'C shows to what point the sections were balanced, left of this line there was only conglomerates (excluded from the model) and granodiorite at the surface. The profile of the detachment syncline in A-'A and C-'C are derived from the 3D model. Transects can be found in appendix 6a.

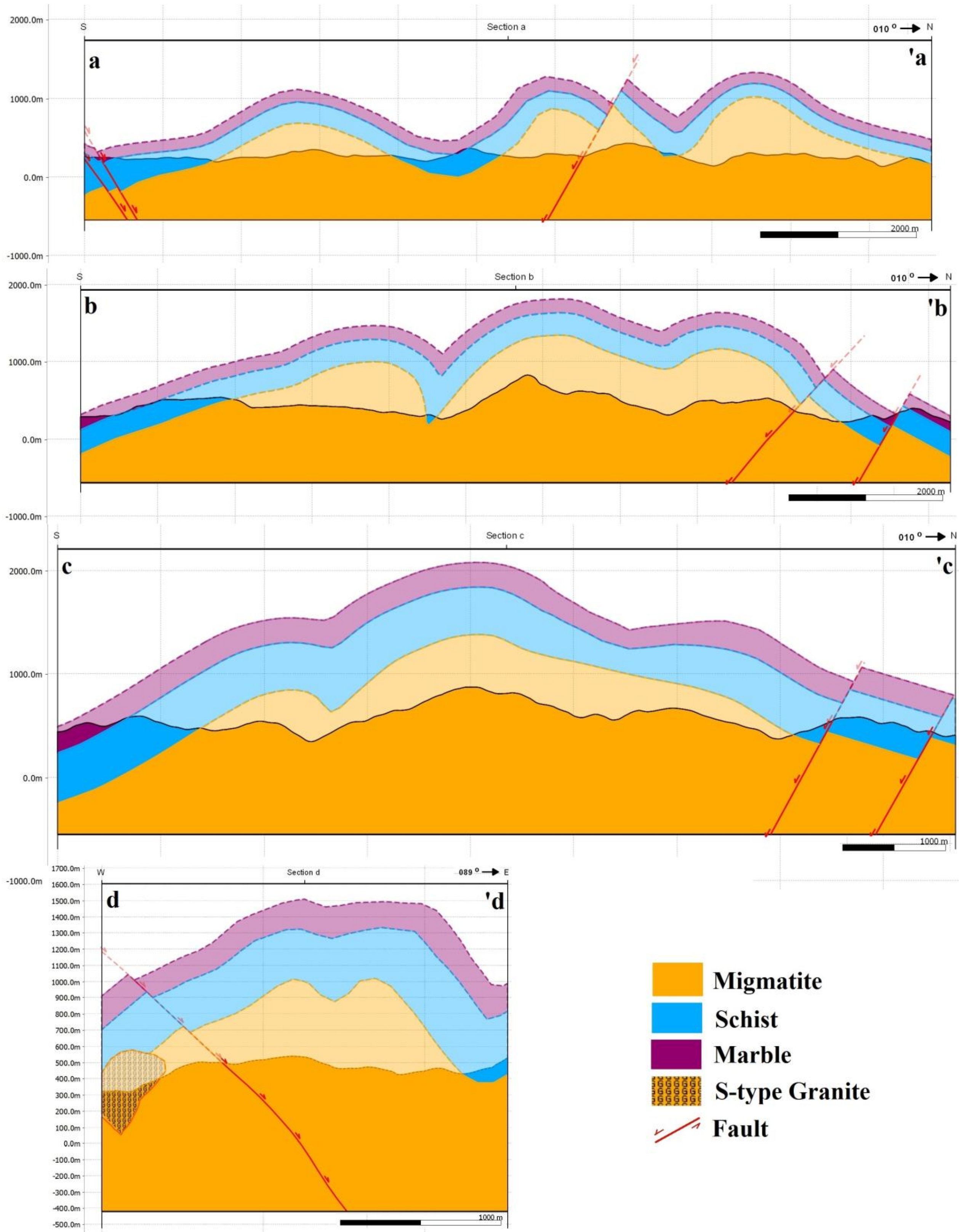

Appendix 4. Sections a-'a to d-'d. Black line is the topographic relief, the S-type granite in d-'d is derived from the 3D model and was not part of the section balancing. Transects in appendix 6b.

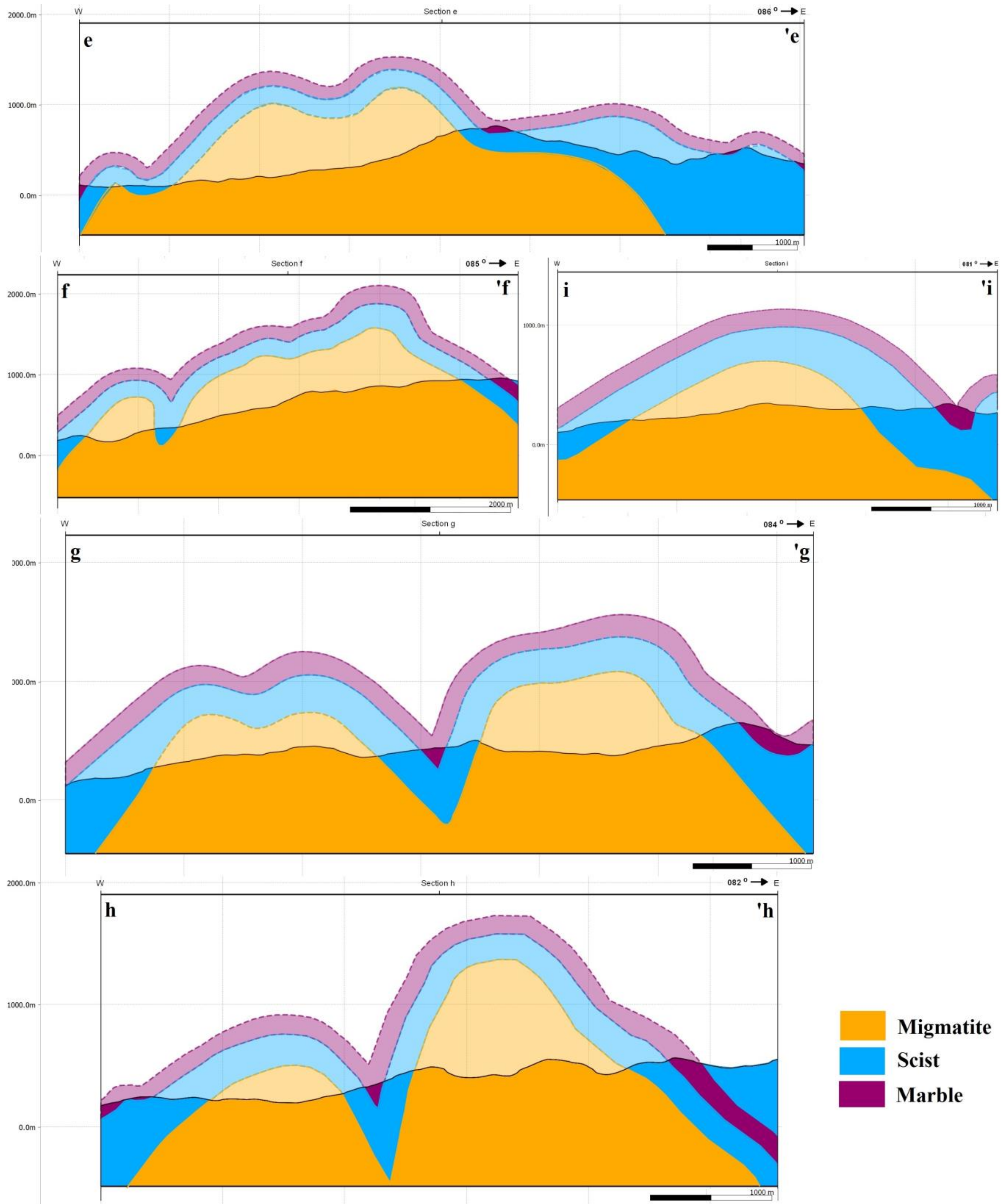

Appendix 5. Sections e-'e to i-'i. Black line is the topographic relief. Transects can be found in appendix 6b.

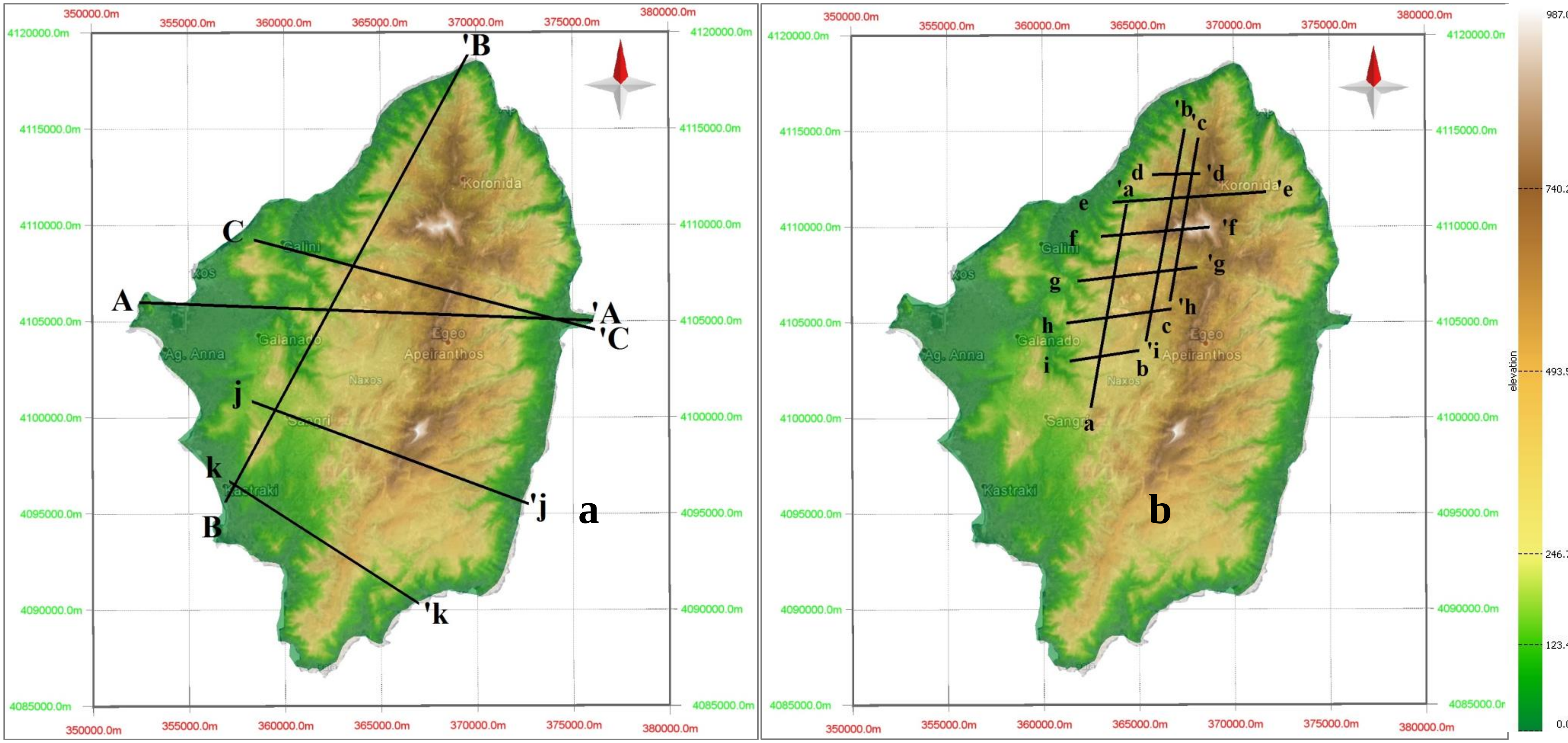

Appendix 6a. Transects for sections A-'A to C-'C and j-'j to k-'k. **6b**. Transects for sections a-'a to i-'i. Color scale left of appendix 6b shows topographic elevation for both maps in meters from 0 (green) to 987 (white). Compass for heading and UTM grid for coordinates (UTM zone 35).

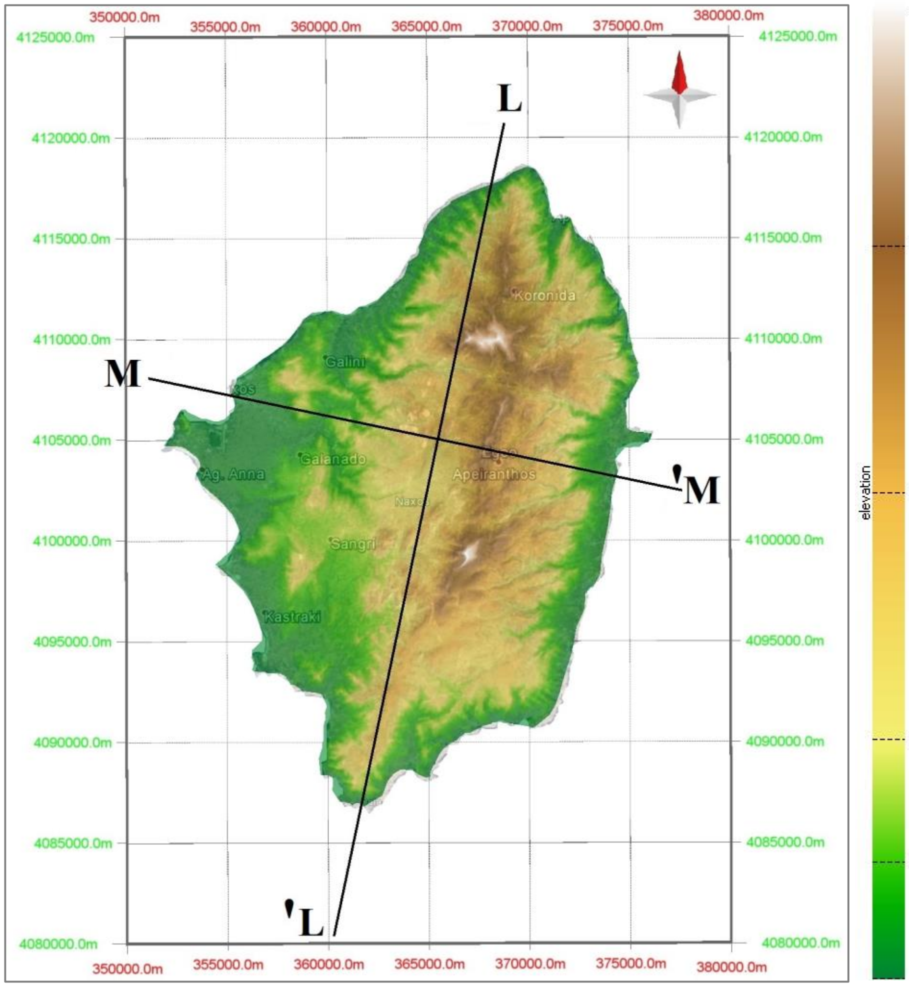

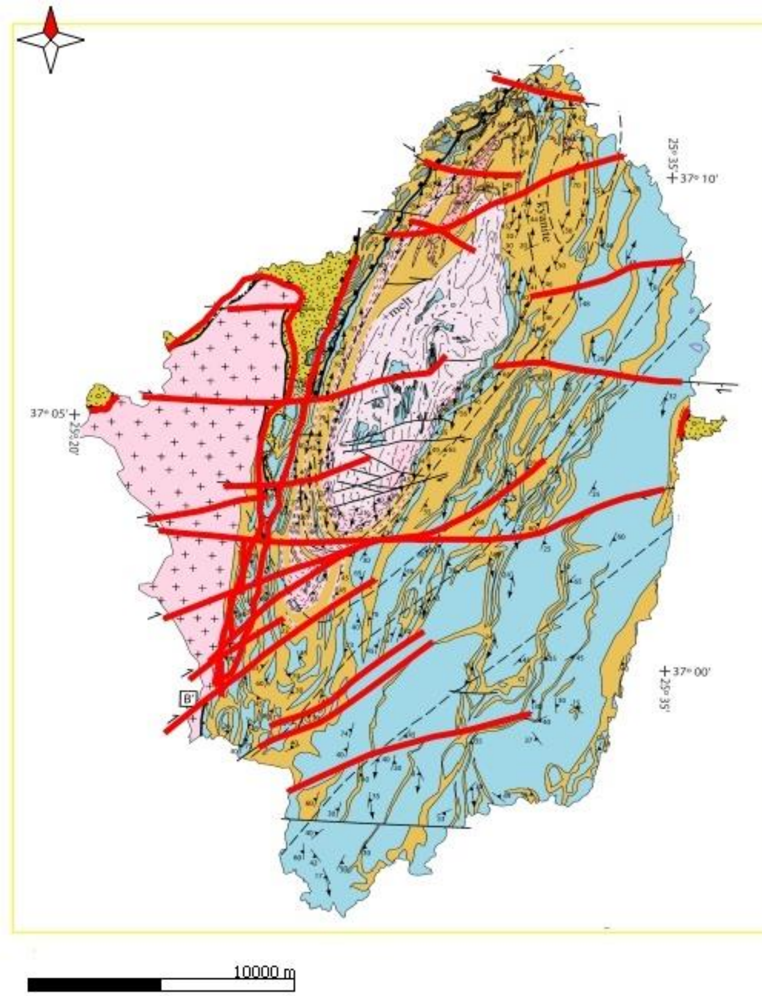

Appendix 7. Transects for metamorphic isograd sections L-'L and M-'M. Color scale on the right shows topographic elevation in meters from 0 (green) to 987 (white). Compass for heading and UTM grid for coordinates (UTM zone 35).

Appendix 8. Topographic trace of the faults modeled in 2D and 3D. Map overlay is modified from Kruckenberg et al. (2010).

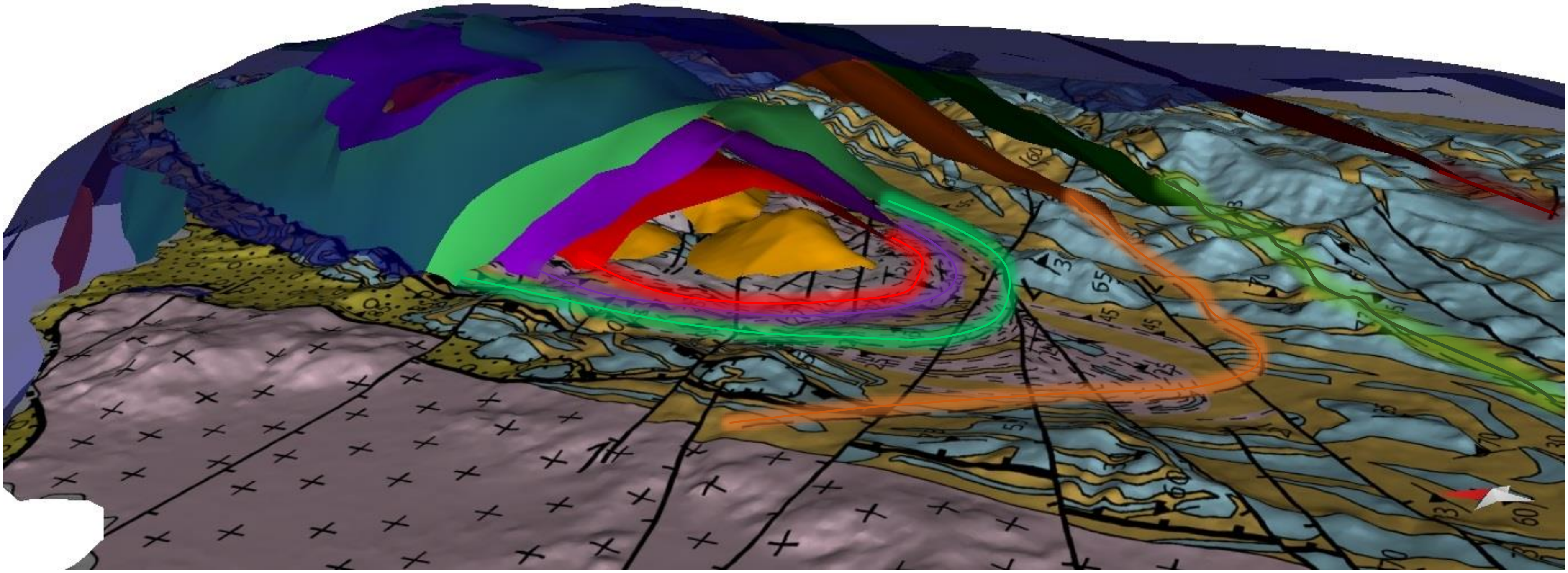

Appendix 9. 3D Metamorphic isograd layers seen from the WSW illustrating the concordance with the isograds on a geologic map modified from Kruckenberg et al. (2010). Colored lines are boundaries on the map. Rust colored layer in the top right is +Corundum isograd, dark green top center is Corundum/Biotite boundary, orange is Biotite/Chloritoid boundary, turquoise is Chloritoid/Kyanite-Sillimanite transition zone boundary, purple is +Sillimanite isograd and red is +melt. The Naxos/Paros detachment surface is represented by the dark blue semitransparent layer on top, cutting the isograd layers.

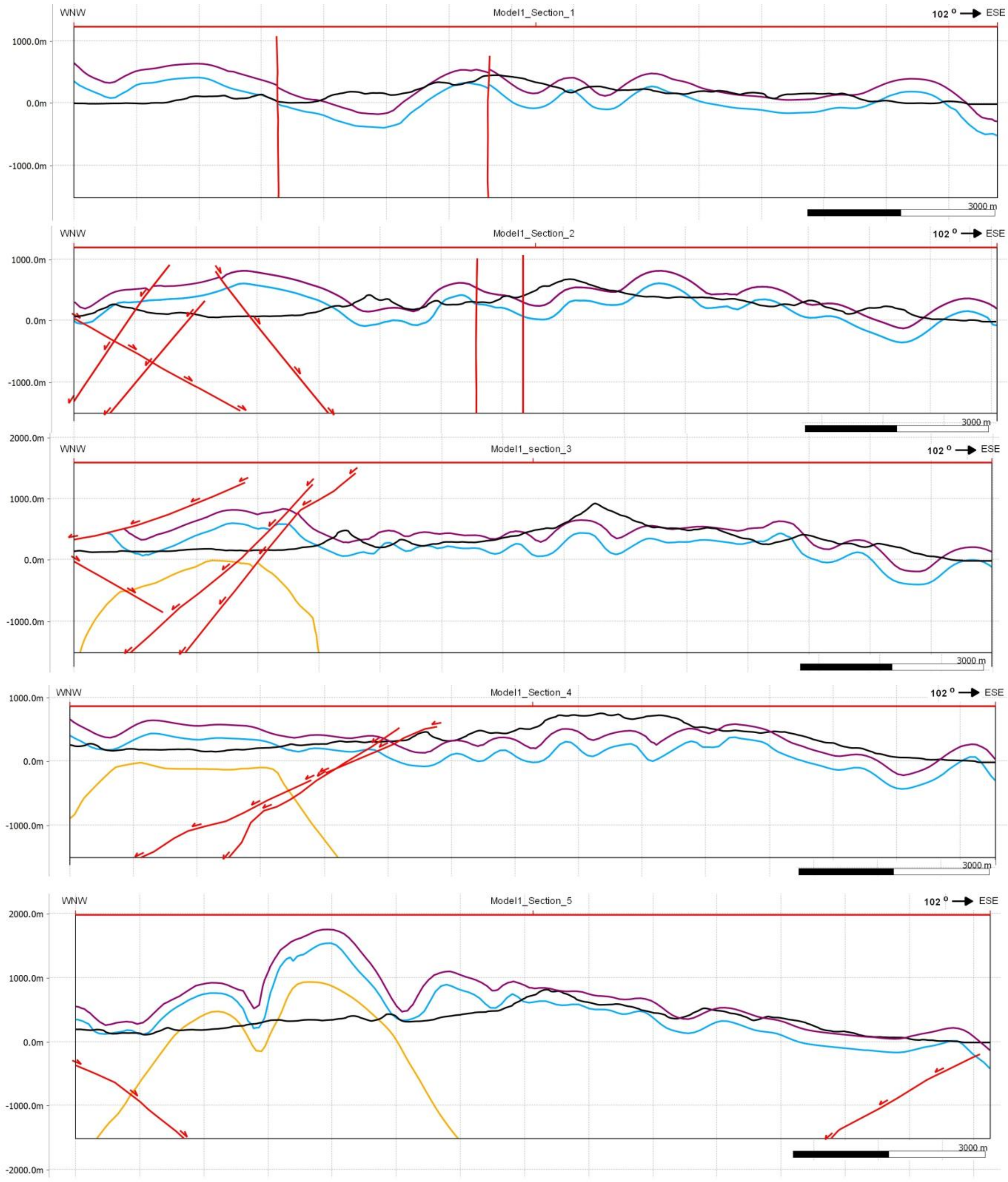

Appendix 10. From top to bottom; Sections 1-5 from model one, used in shortening calculations in table 1. Purple line is the marble surface, blue is the schist and yellow is the migmatite, orange is S-type granite. Red lines are faults and the black line is the topographic relief.

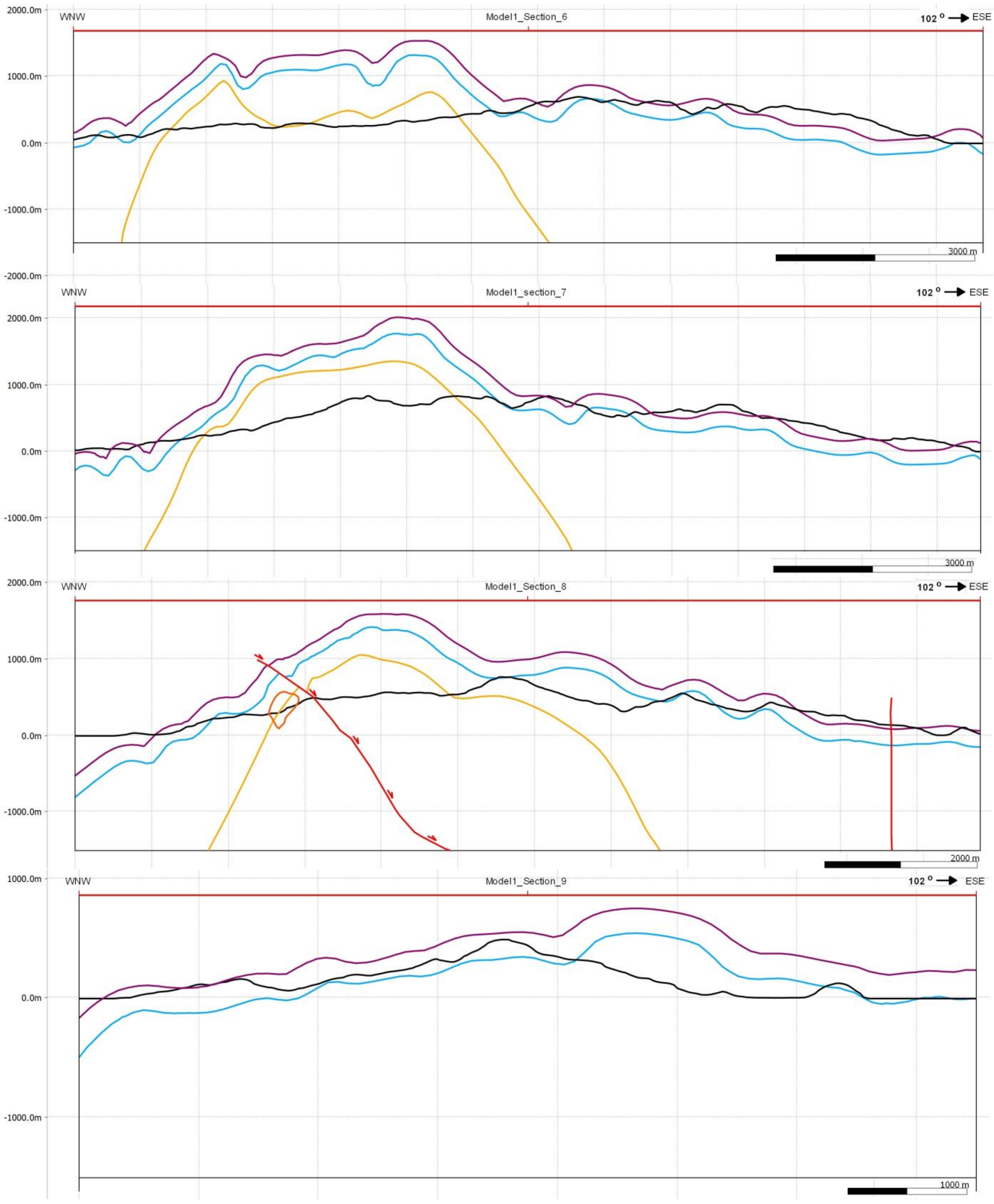

Appendix 11. From top to bottom; Sections 6-9 from model one, used in shortening calculations in table 1. Purple line is the marble surface, blue is the schist and yellow is the migmatite. Red lines are faults and the black line is the topographic relief.

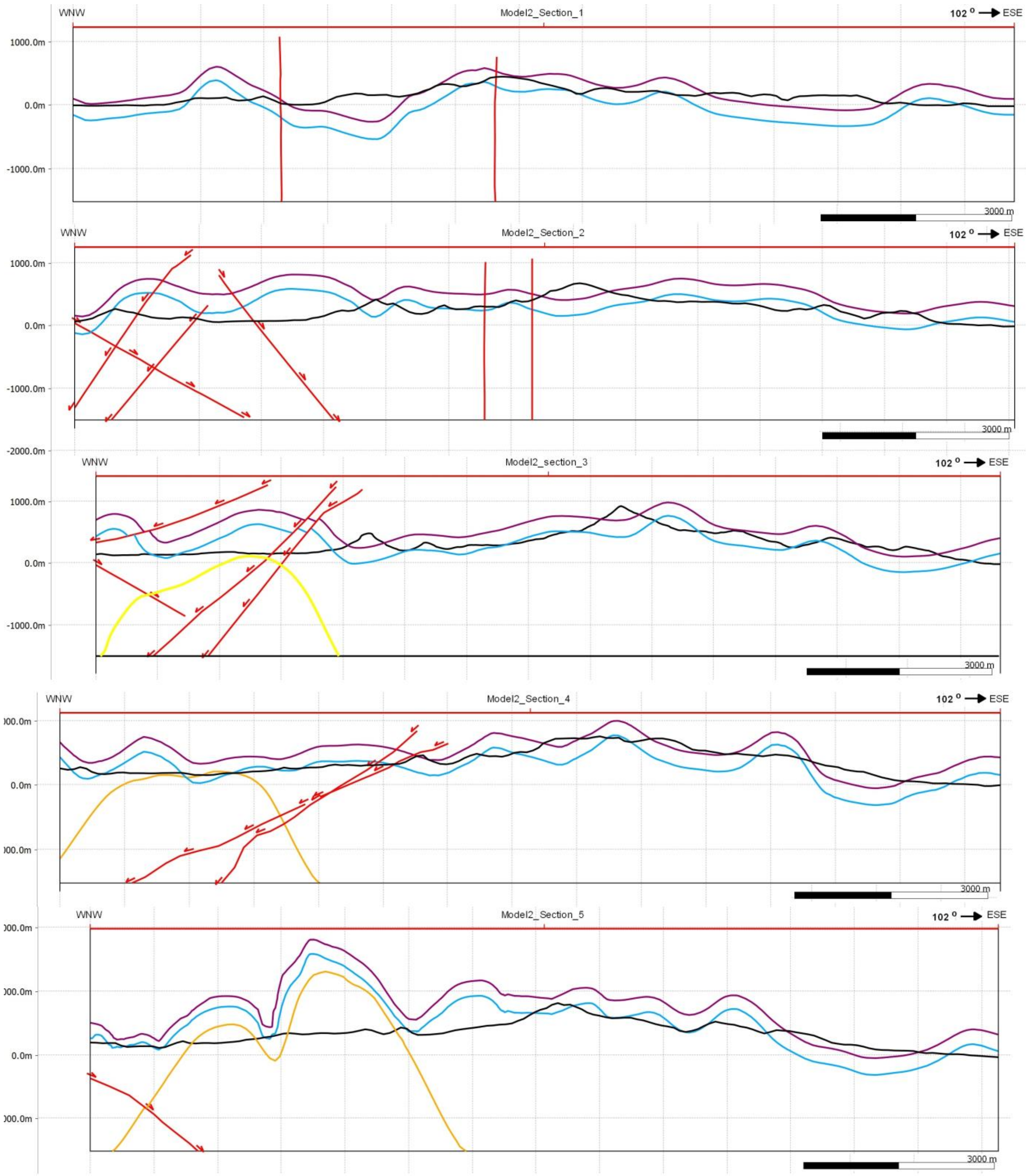

Appendix 12. From top to bottom; Sections 1-5 from model two, used in shortening calculations in table 1. Purple line is the marble surface, blue is the schist and yellow is the migmatite, orange is S-type granite. Red lines are faults and the black line is the topographic relief.

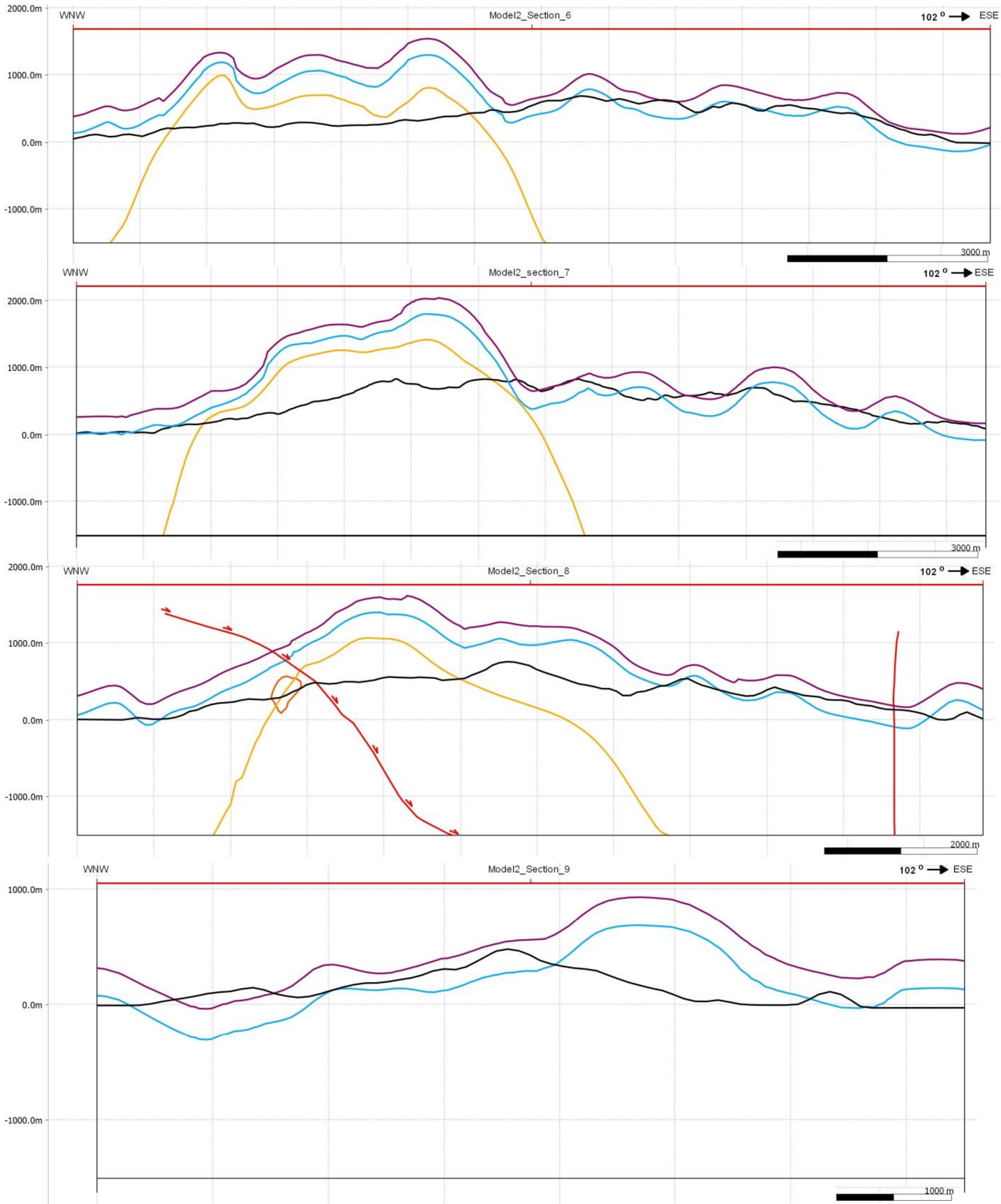

Appendix 13. From top to bottom; Sections 6-9 from model two, used in shortening calculations in table 1. Purple line is the marble surface, blue is the schist and yellow is the migmatite. Red lines are faults and the black line is the topographic relief.